Study and detection of the dissolution-recrystallization phase conversion of biogenic carbonates

by

© **Brian Espinosa Acosta**

A thesis submitted to the School of Graduate Studies in partial fulfillment of the requirements for the degree of Master of Science.

Department of Chemistry

Memorial University

August 2024

St. John's, Newfoundland and Labrador, Canada

Abstract

Aragonite and calcite, the most common $CaCO_3$ polymorphs, are among the most abundant minerals in the ocean. Both are slightly soluble, yet aragonite dissolves narrowly more than calcite. Therefore, an aragonitic suspension will be supersaturated with respect to calcite, which, consequently, should precipitate. Thus, an aqueous co-suspension of aragonite and calcite powders should transform into a calcite suspension. Since most $CaCO_3$ in the ocean is of biogenic origin, using them to study this transformation has applicability to understanding the carbonate marine mineral cycle. This work focuses on several biogenic sources of aragonite and calcite. We examined whether biogenic carbonate mixtures alone trigger conversion or if composition differences from lab-synthesized carbonates affect dissolution-recrystallization behaviour.

We first explored different parameters and configurations, such as mechanically removed organics, preheated samples, different shell parts, and shell composition. Our results show that butter clams are aragonitic shells with less than a few percent calcite, and blue mussels are mixtures of calcite and aragonite. Elemental content showed less than 0.5 wt% impurities in clams. Heating reduced its organic carbon and nitrogen by 60% each. Then, we prepared ultrapure water suspensions of either single aragonitic material or mixtures of polymorphs and monitored the phase conversion before and after suspension. None of the starting biogenic carbonate with or without organics showed reconversion after one week of stirred water suspension, whereas our synthetic aragonite does. Small amounts of biogenic calcite in the biogenic aragonite structure or the addition of biogenic calcite does not accelerate the transformation in these timeframes. However, adding pure reagent-grade calcite triggers detectable aragonite dissolution and recrystallization as calcite in every case. We used Attenuated Total Reflectance-Fourier Transform Infrared spectroscopy to track polymorph

changes before and after water treatment. Powder X-ray diffraction is complementary for assigning crystal structure differences. Inductively coupled plasma-optical emission spectrometry gives insight into the elemental composition of selected samples. Total organic carbon helps us to assess the organic content before and after heating treatments.

These results indicate that there are variabilities across biogenic carbonates that will make them undergo aragonite-to-calcite transformation at different paces and, in many cases, at a slower conversion rate when compared to lab-synthesized carbonates. Removing organic material (by heating or scraping) does not qualitatively change the polymorphic phase transformation within our monitored time frames. These experiments suggest that solubility differences are insufficient when explaining biogenic polymorphs' dissolution-recrystallization. Future oceanic carbonate minerals studies could evaluate if biogenic carbonate-dependent conversion rates are more suitable than those for lab-synthesized carbonates.

For my family

Lay summary

Carbon dioxide (CO_2) has rapidly increased in the atmosphere due to human activities. The ocean absorbs a big part of the CO_2, leading to ocean acidification. One of the most common ocean sediments, calcium carbonate ($CaCO_3$), dissolves to counter this acidification. $CaCO_3$ is commonly found in sea organisms' shells and skeletons. Recent studies have predicted that the most soluble form of $CaCO_3$, aragonite, sacrifices to delay the dissolution of the less soluble form, calcite. Subsequently, the net effect is that aragonite should transform into a more stable calcite. Lab experiments by others have agreed with the models by mimicking and indirectly tracking this interplay. However, they have recognized that a bigger scope of samples and more direct measurements should be pursued. We also emulated this aragonite-calcite interaction by suspending them together in the water. We used a wide range of $CaCO_3$ sources to study if the expected behaviour applied equally to every scenario. We observed that the amount of phase transformation during a set period of time was not exactly the same for all carbonate sources. In some situations, an aragonite-to-calcite transformation is undetectable and, in others, can be easily tracked. This means that future models will not only need to include $CaCO_3$ forms but also will need to reevaluate their applicability with different biogenic carbonate kinetics.

Acknowledgements

I want to start by expressing my deepest gratitude to my advisor, Dr. Kristin M. Poduska, for her absolute support, patience and guidance during the length of this research and thesis writing.

I wish to recognize the valuable feedback of my Supervisory Committee: Dr. Lindsay Cahill and Dr. Chris Kozak. I would like to highlight the insightful comments, encouragement and constructive critique of my examiners.

I am honoured to be part of Memorial University family and am thankful for their financial support. Also, praise to Dr. Liqin Chen and NSERC for the monetary aid.

Shout out to my collaborators, Prof. Meghan Burchell, Jake J. Breen and others, for their contribution. Special recognition to technicians Dr. J. B. Lin and Dr. S. Kommenscher for their help with characterizations.

Thanks to the Department of Chemistry, their staff and especially to Debbie Hickey.

Finally, I would like to express my profound gratitude to my family for being there for me.

Statement of contribution

This thesis contains a chapter (Chapter 3) manuscript coauthored with Dr. Kristin M. Poduska (Department of Physics & Physical Oceanography), Dr. Meghan Burchell (Department of Archaeology), and undergraduate student Jake J. Breen (Department of Chemistry). In this thesis, all experiments, data analysis, plotted graphs and paper drafting were conducted by me. Dr. Kristin M. Podosuka, my supervisor, provided theoretical background, experimental guidance and thesis draft revisions. Dr. Meghan Burchell procured the samples and theoretical insights about clams' structure and biology. Undergraduate student Jake J. Breen provided perspective about his crab samples' characteristics and behaviours and collaborated with Chapter 3 drafting. Live-collected butter clam samples were obtained in ancestral land and with the recognition of the Tsleil Waututh Nation. Coral samples were obtained thanks to Dr. K. C. K. Ma (Department of Ocean Sciences). "Biogenic and geogenic carbonates aqueous suspensions" Chapter 4 is a broader survey of samples from which many results could be part of the database information of the "Biogenic calcium carbonate: phase conversion in aqueous suspension" Chapter 3 manuscript, which targets butter clam as the main case study.

Attenuated Total Reflectance-Fourier Transform Infrared Spectroscopy (ATR-FTIR) characterization technique was conducted by me. Capillary Powder X-ray Diffraction (PXRD) analysis was conducted by Dr. J. B. Lin, and Inductively Coupled Plasma-Optical Emission Spectroscopy (ICP-OES) by Dr. S. Kommescher at the Centre for Chemical Research and Training through Memorial University's Core Research Equipment and Instrumental Training (CREAIT) network. Large microscope high-definition images were obtained with the help of Meghan Burchell's PhD student, Sarah Kuehn.

Table of contents

List of tables

List of figures

List of abbreviations

ACC	Amorphous Calcium Carbonate
ATR-FTIR	Attenuated Total Reflectance-Fourier Transform Infrared Spectroscopy
$CaCl_2$	Calcium Chloride
$CaCO_3$	Calcium Carbonate
CO_2	Carbon Dioxide
dis-rec	dissolution-recrystallization
DOM	Dissolved Organic Matter
FTIR	Fourier-Transform Infrared
GHG	Greenhouse Gases
IAP	Ion Activity Product
ICP-OES	Inductively Coupled Plasma-Optical Emission Spectroscopy
IRE	Internal Reflectance Element
IR	Infrared
Na_2CO_3	Sodium Carbonate
PXRD	Powder X-ray Diffraction
PDF-2	Powder Diffraction File Database
WPF	Whole Pattern Fitting

Chapter 1

Introduction

1.1 Research inspiration

Calcium carbonate ($CaCO_3$) has three typical polymorphic phases: vaterite, aragonite and calcite, determined by the structural arrangement of the Ca^{2+} and CO_3^{2-} ions. Each carbonate compound has been thoroughly studied individually, but more recent papers focus on the interaction of carbonate minerals with the medium and within them, delving into their dissolution-recrystallization (dis-rec) interactions [11, 12]. This recent interest came from the role $CaCO_3$ dissolution plays as the ultimate fate of anthropogenic carbon dioxide (CO_2) [13].

Today, there is a public and scientific consensus over the main factors that harm the delicate climate equilibrium on Earth. Greenhouse gases (GHG) are one of those factors that have been targeted because of their role in climate change. CO_2, the most recognized GHG, is produced by natural processes and human industrialization; therefore, many researchers are focused on everything related to CO_2 chemistry, physics and, by extension, its natural behaviour [14].

The ocean plays a substantial role in withdrawing CO_2 from the atmosphere, for which it is known to be the second largest carbon sink and one of the many natural

CO_2 regulators. In water-based environments, the equilibrium of carbonate species participates in the exchange of carbon between atmospheric CO_2, carbonic acid, carbonate ions, and carbonate mineral solids [14]. The Atlantic Ocean provides about 60% of the global ocean CO_2 uptake [15] where most of the intake flux is concentrated in the cold regions of the north, especially Labrador Sea [16]. Biomineralized calcium carbonates are a key part of this cycle process [17] since they constitute an extensive amount of the ocean [18, 19]. Those biominerals generally come from marine organisms, including oysters, crabs, clams, mussels, and corals, among other hard tissues [20, 21, 22]. Many of them are either calcite, aragonite or a mixture. Biogenic samples are not only comprised of $CaCO_3$, but they also have a complex mineral composition and a species-specific organic matrix [23, 24, 25, 26].

Aragonite and calcite have low solubility constants, for which they are barely soluble in water solutions [27]. Since calcite is the more stable (less soluble), its suspensions will rapidly saturate and reach equilibrium. However, pure synthetic aragonite will transform to calcite in aqueous suspension due to the slightly higher solubility of aragonite over calcite. This means that an aragonite suspension will dissolve until it reaches equilibrium and, at that point, will be supersaturated with respect to calcite, which subsequently will precipitate. Nevertheless, well-ordered and pure aragonite dissolution and recrystallization might take long periods of time unless this transformation is fastened by temperature, diffusion, or the presence of structural defects [28]. If both phases are present in water, then the presence of calcite growing sites should translate into a faster transformation. This process will be further explained in this chapter and has been well-described experimentally [28, 11, 12].

Commonly, biogeochemical models use calcite kinetics to predict solution-solid equilibriums and step back in oceanic carbon cycles [29, 30]. However, recent $CaCO_3$ polymorphs dissolution-recrystallization simulation studies indicate that the symbiotic relationship between the two most common crystal structures, where aragonite dissolution may protect calcite at the bottom of the sea, must be included in the

models [31]. These simulations clearly state that these models have several limitations and simplifications, such as using parameters from the abiotic polymorphs to model biogenic samples and omitting shell structure and composition. Recent studies tried to track this aragonite-calcite interaction using pH and alkalinity as their process tracking measurements [32]. Although their results indicate that aragonite dissolution can inhibit calcite dissolution and provoke its precipitation within one day, their pH measurements were not able to track this process directly. Hence, they suggest testing this polymorphic interaction with other types of measurements to address the limitations of their experiments. Additionally, they discuss the necessity of widening biogenic carbonate sources to obtain a better sense of this behaviour across different $CaCO_3$ sources.

Most aragonite-to-calcite conversion studies have been performed in seawater-simulated solutions [26, 32]. Since open ocean processes carry considerable complexity, far-from-natural or simulated marine solutions are a trade-off to a more straightforward setup to understand the stability of these polymorphs. Therefore, there is value in studying the dis-rec behaviour of aragonite-calcite biogenic suspension mixtures from a simplified lab setup, aiming to describe the individual effect of different variables like inorganic minerals, organic matrix, pH, suspension time or mass transport. A better understanding of this polymorphic interaction could help in carbon budget modelling, future ocean alkalinity enhancers, and following complex interactions of biogenic-originated ocean sediments.

1.2 Physical and chemical properties influencing biogenic calcium carbonates dissolution and re-crystallization

The focus of this thesis is to study biogenic carbonates' water-suspension interactions as a further step compared to pure synthesized $CaCO_3$ suspended mixtures studied before [33, 11]. Even though biogenic carbonates are a big component of ocean sediments [20], only calcite, Mg-calcite and aragonite are widely found on the seafloor. Other carbonated minerals like vaterite, ikaite (hydrated $CaCO_3$), dolomite ($CaMg(CO_3)_2$), magnesite ($MgCO_3$), siderite ($FeCO_3$) and others are virtually nonexistent or only found under "irregular" conditions (low temperatures, high-pressures, reducing environments) in seawater [20]. Therefore, the thesis will mainly describe the properties of calcite and aragonite, along with the influence that inorganic and organic compounds may have on their structure, precipitation, and dissolution.

1.2.1 Calcium carbonates ($CaCO_3$)

Calcite possesses a trigonal crystal structure, space group $R\,\bar{3}\,c$, which can be visualized using a hexagonal unit cell where with the c-axis oriented upwards, Ca^{2+} cations are placed in horizontal layers divided by planar $CO_3{}^{2-}$ (See Figure 1.1a). Aragonite crystallizes as an orthorhombic cell, space group $P\,m\,c\,n$, showing a staggered orientation and resulting in a denser structure than calcite (See Figure 1.1b). Calcite's rhombohedral structure has a lower calculated surface energy than aragonite, making the earlier more metastable [34].
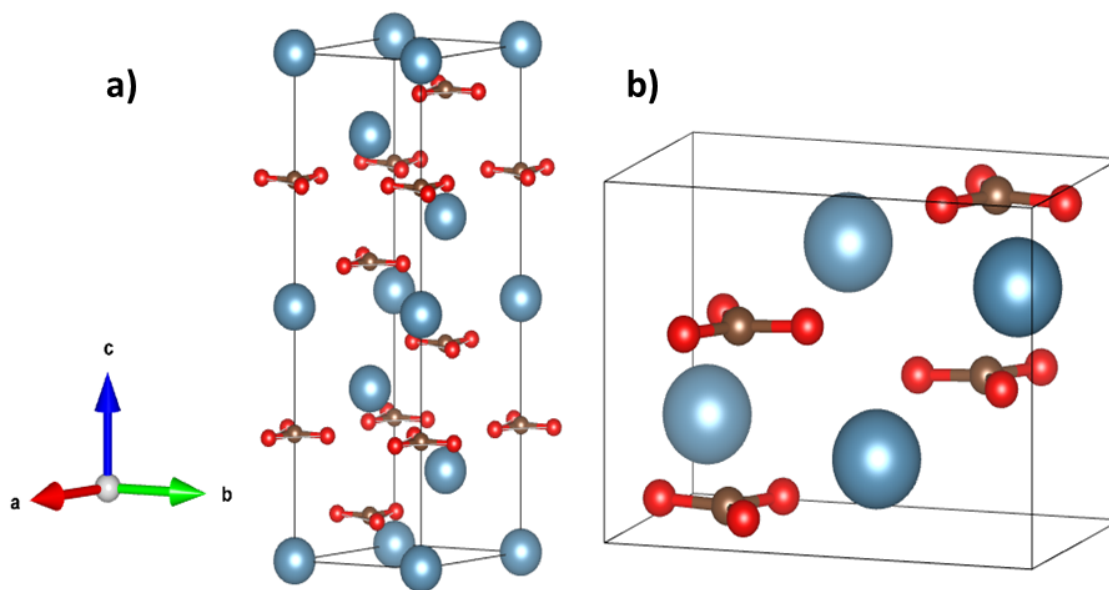
Figure 1.1: Rhombohedric calcite (a) and orthorhombic aragonite (b) crystal structures. Ca atoms are in light blue, C atoms are in brown, and O atoms are in red. These unit cell representations were created using VESTA software [2] from calcite and aragonite (PDF-2 98-000-0141 and 98-000-0098 database) [3].

Dissolution

$CaCO_3$ dissolution and recrystallization reactions are opposite processes that reach thermodynamic equilibrium. The dissolution occurs when Ca^{2+} and CO_3^{2-} ions are released into the solution. This process is spontaneous when the solution is undersaturated with respect to the ions in the solution. On the contrary, crystallization happens when these ions recombine to form a precipitate. Usually, this takes place when the ions are supersaturated in solution. The solution is saturated when both process rates are equivalent and is said to be in equilibrium [35]. Equation 1.1 represents this dissolution and recrystallization equilibrium. The thermodynamic equilibrium constant for this reaction is called the solubility constant (K_{sp}) and expresses the activities (a_i for component i) of the ions when the solution has reached equilibrium (Equation 1.2) [36]. Note that the $CaCO_3$ activity is not included since the activity of solids is considered to be one. The K_{sp} is most commonly expressed in terms of activities to

account for the temperature, pressure and composition (Gibbs free energy (ΔG) of the solid/polymorph) influence in the K_{sp}.

$$CaCO_{3(s)} \rightleftharpoons Ca^{2+}_{(aq)} + CO^{2-}_{3(aq)} \tag{1.1}$$
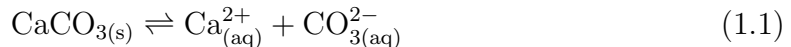
$$K_{sp} = a_{Ca^{2+}} \cdot a_{CO_3^{2-}} \tag{1.2}$$

It is common to represent solubility constants as a logarithm $pK_{sp} = -log(K_{sp})$ so that the higher the value, the more stable or less soluble the solid. Experimental solubility constants prove that calcite is the most stable polymorph of $CaCO_3$ in standard conditions with a $pK_{sp\,Cal} = 8.48$, followed by aragonite $pK_{sp\,Ara} = 8.336$, vaterite $pK_{sp\,Vat} = 7.913$ and amorphous calcium carbonate (ACC) $pK_{sp\,ACC} = 6.39$ [27, 37, 34]. The solubility constants are higher (lower pK_{sp}) under 35% salinity, which is close to seawater salinity, giving a $pK_{sp\,Cal} = 6.36$ for calcite and a $pK_{sp\,Ara} = 6.18$ for aragonite [38]. This indicates higher solubility for both polymorphs in ocean conditions. This behaviour can also be seen at low NaCl concentrations [39]. The effect of temperature in $CaCO_3$ dissolution is opposite to what is commonly seen in other solids. An increase in solution temperature decreases calcite, aragonite and vaterite solubility [27, 39]. Pressure, on the other hand, makes calcite more soluble [40].

Under standard temperature and pressure conditions, without free H^+ and dissolved CO_2 Equation 1.1 carries forward to CO_3^{2-} consumption through speciation (Equation 1.3). The formation of bicarbonate ions HCO_3^- and OH^- leads to a basic pH between 8 and 10. The dissolution $CaCO_3$ proceeds as in Equation 1.4 when it is dependent on the H^+ ion activity and as in Equation 1.5 when the P_{CO_2} is taken into account [41]. Notice that in Equation 1.5, H_2CO_3 results from CO_2 dissolution in water. In a natural context, these three processes occur simultaneously, and pH and P_{CO_2} are inversely correlated since pH decreases when P_{CO_2} increases. From this, it

can be easily derived that $CaCO_3$ is more soluble with pH decrease and P_{CO_2} increase, which it has also been proved experimentally [39].

$$CaCO_{3(s)} + H_2O_{(l)} \rightleftharpoons Ca^{2+}_{(aq)} + HCO^-_{3(aq)} + OH^-_{(aq)} \tag{1.3}$$

$$CaCO_{3(s)} + H^+_{(aq)} \rightleftharpoons Ca^{2+}_{(aq)} + HCO^-_{3(aq)} \tag{1.4}$$

$$CaCO_{3(s)} + H_2CO_{3(aq)} \rightleftharpoons Ca^{2+}_{(aq)} + 2HCO^-_{3(aq)} \tag{1.5}$$
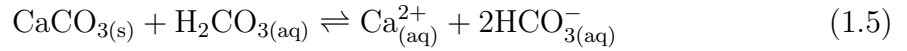
Dissolution kinetics are another factor that influences the behaviour of $CaCO_3$ when it is in solution. From a kinetics standpoint, dissolution starts with the first ions being released into the bulk fluid. The relation between the ionic activity product (IAP) and the solubility constant (K_{sp}) at any given time is called the saturation index (Ω). As seen in Equation 1.6, when the IAP is lower than the K_{sp} ($\Omega < 1$), we can say that the solution is undersaturated. The solution is in equilibrium when they are equal ($\Omega = 1$). Finally, when there is an excess of ions in the solution ($\Omega > 1$), it is supersaturated. The relationship of $CaCO_3$'s surface area-normalized dissolution rate ($\mathbf{r}$) to the saturation index (Ω) has been found to slow down to 0 as saturation reaches equilibrium (Equation 1.7). In this equation, $\mathbf{k}$ is the rate constant and $\mathbf{n}$ is the overall reaction order [42, 20, 4].

$$\Omega = \frac{IAP}{K_{sp}} = \frac{a_{Ca^{2+}} \cdot a_{CO_3^{2-}}}{K_{sp}} \tag{1.6}$$

$$r = k(1 - \Omega)^n \tag{1.7}$$

From a mechanistic standpoint, dissolution follows several steps: (1) diffusion of

solvents to the solid surface, (2) adsorption on the solid surface, (3) movement of re-
actants to active sites (point defects, terraces, vacancies), (4) reaction with the ions in
the solid, (5) motion of products (solvated ions) out of the active sites, (6) desorption
and (7) mass transport of the solvated ions to the bulk solution [42, 20]. The rate of
this chain of reactions will be controlled by the slowest step. In the case of carbonate
minerals, it is influenced by the pH and temperature of the solution bath. Normally,
an increase in temperature makes diffusion control processes be enhanced, although
the total rate of dissolution decreases (see Equation 1.8 where **A**: chemical affinity, **R**:
ideal gas constant, **T**: temperature) [4, 20]. On the other hand, the pH increase makes
the slowest controlling step pass through three stages. In acidic pH up to 5, there
is a direct relation between free H^+ and dissolution rate with a negative slope (rate
decrease at higher pH); hence, the reaction is said to be diffusion controlled. In the
neutral pH region, it follows complex transition kinetics. Commonly for carbonates
at higher pH (like seawater), the step implicating the attachment and detachment of
these ions from the surface dislocations becomes the controlling reaction. Because
of this, $CaCO_3$ dissolution and recrystallization in a natural context is typically a
surface-controlled reaction, and a bigger number of imperfections on the solid surface
will lead to higher dissolution rates [42, 20]. This can also be explained in terms of the
crystal surface texture and morphology, which increases during the dissolution reac-
tion as the roughness of the crystal surface area increases. For the same reason, if the
particle radius increases (volume increase and surface area decrease), the dissolution
rate will decrease [43].

$$r = k(1 - exp(-A/RT))^n \tag{1.8}$$

Although the overall trend of the dissolution rate tends to ease as the reaction
reaches equilibrium, the slope at which this happens is not equivalent for $CaCO_3$
polymorphs. Geometric surface area-normalized solubility rate (r_{gsa}) equations for

geogenic calcite (1 from 1.9) and aragonites (2,3 from 1.9) have been obtained experimentally by Cubillas, et al. (2005) (Equation 1.9). Aragonite rate equation (2 from 1.9) was obtained only for geogenic source data, whereas aragonite rate equation (3 from 1.9) represents the fitting line of non-biogenic plus biogenic (clam and cockle shells) combined data [4]. Notice that, generally, at time 0, aragonite dissolution progresses faster than calcite dissolution. However, when the saturation index is approximating equilibrium, $0.85 < \Omega < 1$, geogenic calcite and aragonite dissolution rate are virtually equal (See Figure 1.2). Nonetheless, the geometric surface area-normalized dissolution rates of biogenic aragonitic bivalves closely correspond to those of their non-biological counterparts [4].

$$r_{gsa\ calcite} = 1.82 \cdot 10^{-10} \cdot (1 - \Omega)^{1.25} \qquad (1)$$

$$r_{gsa\ aragonite} = 2.63 \cdot 10^{-10} \cdot (1 - \Omega)^{1.45} \qquad (2) \qquad\qquad (1.9)$$

$$r_{gsa\ a-b-aragonite} = 2.69 \cdot 10^{-10} \cdot (1 - \Omega)^{0.86} \qquad (3)$$
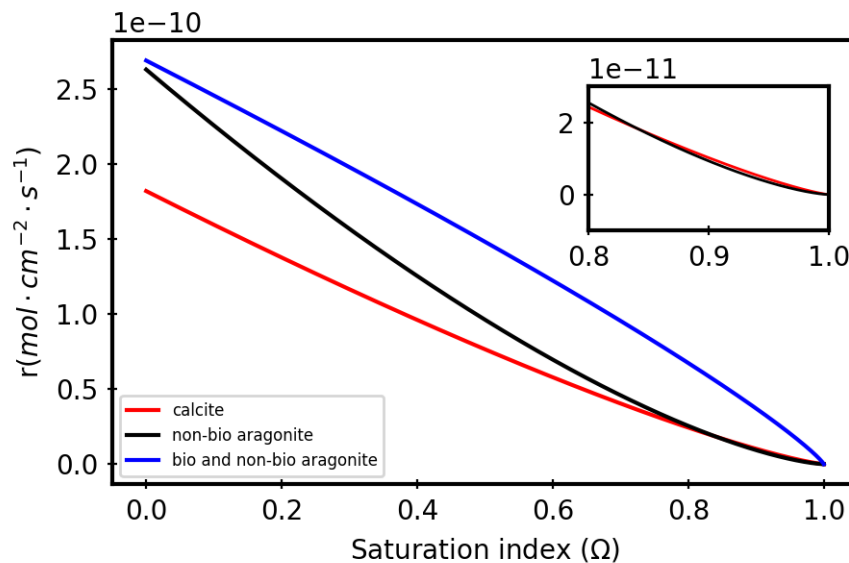
Figure 1.2: Simulated dissolution rate vs saturation index Ω using Cubillas (2005) equations [4].

Crystallization

CaCO$_3$ crystallization has a lot of similarities when analyzed as the inverse process of dissolution. However, some differences will be highlighted in this section. From a saturation point of view, the IAP will dictate the spontaneous precipitation from the solution when it reaches a state of supersaturation ($\Omega > 1$) with respect to CaCO$_3$ polymorphs (see Equation 1.6). Nonetheless, since the saturation index differs for each polymorph, the supersaturation state will be reached first for the less stable polymorph. Therefore, ACC precipitates immediately when the ion activities are higher than 0.004 M [44, 45]. After this first unstable stage, the recently formed carbonate will proceed with a dis-rec mechanism that will yield different polymorphs depending on the solution temperature and initial supersaturation state [45]. Generally, the unstable phase is followed by a metastable one that could be vaterite at median temperatures (50 °C) or aragonite at higher temperatures (above 75 °C). If the precipitate is filtered and dried at this temperature, the resulting solid will be the metastable phase. The stable calcite phase is generally achieved at lower temperatures (below 25 °C). IAP activity product below 0.004 M is the only condition where vaterite, aragonite, and calcite could nucleate following a direct and classical precipitation pathway. The supersaturation index and temperature pair can also control the morphology of the resulting polymorph [45].

Kinetically, crystallization occurs following a series of steps, as in the dissolution process. (1) Transport of the ions from the bulk solution to the forming mineral surface, (2) adsorption of those ions on the surface, (3) migration through the surface to the active site, and (4) reaction of the ions with the formation of the chemical bond, ion exchange or desolvation, are the steps involving crystallization of the first polymorph as stated previously. Again, as in the dissolution process, the slowest process is the formation reaction at the reactive site [20]. The next step is an iteration of the explained dis-rec mechanisms.

Dissolution-recrystallization

A conclusion derived from the previous analysis is the diagenetic transformation that occurs for the less stable $CaCO_3$ polymorph in an aqueous environment. Even when aragonite and calcite are both insoluble, aragonite is slightly more soluble than calcite. Pure lab-synthesized aragonite suspended in water will start dissolving and releasing Ca^{2+} and CO_3^{2-} to the medium. When this suspension gets to equilibrium ($\Omega_{\text{aragonite}} = 0$), the IAP will be such that the solution will be supersaturated with respect to calcite ($\Omega_{\text{calcite}} > 1$) due to the different K_{sp} (See Equation 1.6). Therefore, this supersaturation will be alleviated by calcite precipitation. This hypothetical scenario implies that aragonite diagenesis and transformation to calcite is a dis-rec phenomenon in most aqueous environments. Experimental measurements have proved this scenario [11, 46].

1.3 Chemical components influence

1.3.1 Magnesium (Mg)

Small Mg^{2+} ions usually take the place of Ca^{2+} in the 6-fold calcite structure, making Mg-Calcites a common calcitic mineral in natural environments [20]. In general, Mg^{2+}'s presence in calcite structure is addressed as a solid solution between calcite ($CaCO_3$) and magnesite ($MgCO_3$). Notice that 50% is dolomite. While the Mg% increases in the solid, the cell parameters of the calcitic orthorhombic crystal structures start contracting along the a and c axes, and consequently, its cell volume is smaller [47, 48].

The Mg^{2+} presence in the aragonite structure is more unlikely, energetically speaking, since substituting the 9-fold coordinated Ca^{2+} for Mg^{2+} is more difficult [34]. Despite that, Mg^{2+} containing aragonites has been reported either forming part of

the crystal structure in very low concentrations [49], as part of a secondary phase [50] or, in the case of aragonitic organisms, as a constituent of the organic matrix and the inorganic phase nanostructures [51, 52].

In the dis-rec process, many mechanisms occur simultaneously, but to simplify it, some facts must be stated as separate processes. Calcite dissolution highly depends on its Mg^{2+} content [34]. When there is Mg^{2+} in calcite's structure, the solid becomes more stable (less soluble) with up to 4 mole% of Mg^{2+} (Low Mg-Calcites), whereas if the Mg^{2+} content is >4 mole% (High Mg-Calcite) the solid is more soluble compared to calcite and passing the 15 mole%, it starts being less stable than aragonite [53, 54]. In the case of biogenic Mg-Calcites, the data shows that they become more soluble than aragonite with a lower Mg^{2+} content mainly because of the presence of organic compounds and small size particles that react faster [55, 56, 54]. Therefore, biogenic high Mg-calcite tends to stabilize either through Mg^{2+} loss, becoming a low Mg-calcite, or particle annealing and cleaning that reduces their solubility but not their Mg% [54]. Nevertheless, the presence of Mg^{2+} in sea organisms is not homogeneous, meaning that there is often a dispersion of high-Mg calcite nanoparticles in a low-Mg calcite matrix [23]. Aragonite bivalve shells' Mg/Ca ratio within the shell (mineral and organic matrix) during its growth is the highest in a 35% salinity environment [52].

In a medium with only Ca^{2+} and CO_3^{2-} precursors, temperature, pH and ion concentrations will dictate the precipitated polymorph, as explained earlier in this chapter. When Mg^{2+} is present in the solution, it controls the polymorph that will crystallize. If $Mg^{2+}/Ca^{2+} > 2$ in solution, the Mg uptake into the calcite structure will increase its surface energy, whereas aragonite surface energy is not affected by Mg, making aragonite nucleation a preference [34, 57]. When the Mg^{2+}/Ca^{2+} ratio is lower than 2, the precipitation from the solution always occurs through a Mg-ACC formation followed by a dis-rec that can produce different polymorphs. This one will depend on the $a_{Mg^{+2}}/a_{Ca^{+2}}$ (a: activities) ratios or the SI (supersaturation index) of the remanent ions after the Mg-ACC was formed. In general $5 \leq a_{Mg^{+2}}/a_{Ca^{2+}} \leq 8$

causes the Mg-ACC to Mg-Calcite transformation, while $8 \leq a_{\mathrm{Mg}^{+2}}/a_{\mathrm{Ca}^{2+}} \leq 12$ results in monohydrocalcite (Mhc) [58, 59, 60].

1.3.2   Strontium (Sr) and others

Ions of strontium (Sr^{2+}) are rarely found in pure calcite structure; however, they can precipitate along with Mg^{2+} when magnesium calcites are being formed in natural environments [61]. The arrangement of Sr^{2+} in the aragonite structure has been observed more commonly in natural environments than in calcite structure [46, 52, 20]. As for Mg^{2+}, Sr^{2+} also substitutes Ca^{2+}. Its properties are also described in terms of a solid solution between $CaCO_3$ and $SrCO_3$, where 0% represents aragonite and 100% represents strontianite. With increasing strontianite content in the aragonitic structure, the overall effect on the cell parameters and volume is a steady and linear increase [62]. Structurally speaking, Ba^{2+} and Pb^{2+} are two other atoms that can get into aragonite and provoke similar crystal distortions [63]. In theory, for strontianite concentrations of $\sim 1\%$ (commonly found in biogenic aragonites), a maximum of stabilities is reached, but the stability of excess-Sr^{2+} aragonitic phases remains a long debate [64, 20, 62]. Still, the effect of Sr^{2+} in the solubility of aragonite has been found experimentally to be less soluble with Sr^{2+} increase. The solubility of aragonite with a 26% $SrCO_3$ content ($pK_{sp\,26\%Sr-Ara} = 8.479$) closely matches the solubility of pure calcite ($pK_{sp\,Cal} = 8.48$) [64]. When Sr^{2+} is present in the solution, it will promote the precipitation of aragonitic phase $CaCO_3$ following a similar process to what Mg^{2+} does [44, 65].

Sulphate (SO_4^{2-}) and sodium (Na^+) ions as a pair are also found in the calcite and aragonite structures. The amounts of these ions that get into $CaCO_3$ is relatively less than the other elements mentioned above, and in comparison to calcite, biogenic aragonites have less than 6000 ppm SO_4^{2-}. They generally increase calcite unit cell sizes, mainly caused by Na^+. Although they are relatively lower in concentration in calcite

structure, they provoke a similar effect to Mg^{2+} in its solubility. Low mole percent concentrations first decrease the solubility constant, and around 4 mole% of SO_4^{2-} and Na^+ ions, calcite becomes more soluble than aragonite. During crystallization, increasing SO_4^{2-} tends to inhibit calcite precipitation [66].

1.4 Thesis outline

This thesis aims to study the dis-rec process of biogenic carbonates from different sources and specimens, their mixtures with purchased calcite and synthesized aragonite, and carbonates from other sources. We intended to study all the possible factors (mineral, organic, diffusion, heating) that could approach us to what occurs in nature from a simplified lab setup. This research builds on the discoveries of a predecessor labmate (Gao, B. [33, 11, 12]) but with samples beyond synthesized carbonates.

To accomplish the objectives of this research, this thesis is organized as follows:

- Chapter 2: Summarizes the characterization techniques principles, the general sample collection and preparation and the aqueous suspensions.

- Chapter 3: Does an in-depth dis-rec study focusing on only one species, butter clams. Different parameters are studied, such as organic removal, clam section, stirring and substitutional impurities.

- Chapter 4: Expands the scope to diverse biogenic and geogenic samples. It studies the stability of our synthesized and biogenic aragonites in water suspension. Finally, it examines the dis-rec of mixtures of biogenic aragonites with either pure purchased calcite, biogenic calcites or dolomite-like rocks.

- Chapter 5: This is a conclusion chapter where the main takeaways of this thesis are summarized.

Appendix A contains extra data and sample surveys from Chapter 4. The replication database for Chapters 3 and 4 can also be found in the Borealis database [67].

Chapter 2

Characterization methods

2.1   Characterization methods principles

This thesis and research work aim to track the dis-rec processes of a wide range of calcium carbonates when they are either alone or mixed with different counterparts and under diverse conditions. The main technique used during the entire research was Attenuated Total Reflectance-Fourier Transform Infrared spectroscopy (ATR-FTIR). Other techniques like capillary Powder X-ray Diffraction (PXRD), Inductively Coupled Plasma-Optical Emission Spectroscopy (ICP-OES), large microscope pictures, Total Organic Carbon (TOC), and pH measurements were used for specific case studies. In this chapter, I intend to briefly describe some of those techniques and the reason why I employed them. I also explain the general process of material selection and aqueous suspensions done throughout the course of the experiment. Chapter 3 has its own variation of the material and methods section since it was written as the manuscript for a peer-reviewed paper.

2.1.1 Attenuated total reflectance-Fourier transform infrared spectroscopy (ATR-FTIR)

ATR-FTIR spectroscopy is a technique that allows the characterization of samples that contain molecules where their dipole moment changes when vibrating (infrared active), and it is a rapid way of obtaining an exploratory view of the compound's structure [68]. In simple words, a beam of infrared (IR) light passes through an internal reflectance element (IRE) at a larger than the critical angle so that the IR internally reflects in the IRE. The sample is placed onto the surface of the IRE. Every internal reflection point (where the IRE is in contact with the sample) creates an evanescent wave that gets into and is absorbed by the sample. The IR wave has a limited penetration depth (pd) that is proportionally direct to the wavelength (λ) and inversely proportional to the IRE refraction index, the sample refraction index and the incident angle [69]. Typically, the penetration depth ranges from 0.5 to 5 μm. The detector measures the intensity decay of the outcoming beam compared to the incoming beam. The sample's absorption can be described by a slightly modified Beer-Lambert law. The equipment records an interferogram in real-time; thus, Fourier-transform mathematic processing converts the data into an absorbance vs wavenumber (cm^{-1}) spectrum. In our research, the ATR-FTIR spectrum spans from 4000 to 400 cm^{-1} (higher frequency/low wavelength to low frequency/long wavelength), corresponding to the mid-infrared region. Since pd $\propto \lambda$, the lower wavenumber IR beams get deeper in the sample.

The main reason for using ATR-FTIR as our principal characterization technique is that it allows us to qualitatively track aragonite to calcite polymorph changes before and after water suspension treatments. This has been backed up by several studies of our own research group that tracked the complete recrystallization of lab-synthesized aragonite to calcite in water and the inhibition of it by other molecules [33, 11, 12]. Also, our group has demonstrated that it allows us to qualitatively assess

other structural feature changes like particle size, scattering or strains [70, 48, 71]. Furthermore, we can detect the presence of organic and mineral impurities on the spectra. Unlike FTIR transmission sample preparation, ATR-FTIR does not need to make KBr pellets; it only needs grinding and tightly pressing the sample against the IRE window. Grinding is necessary to achieve homogeneity and the best information possible about the bulk solid. Finally, it is a relatively cheap and easy technique that can be employed in field experimentation.

There are some drawbacks of this technique that are worth mentioning. The penetration depth limits the information that can be obtained from the bulk solid, potentially hiding the secondary phases and impurities that might be present in the inner portion of the particle. There is difficulty quantifying phases and phase ratio changes across different sample sizes and characteristics. Although some authors have attempted to use ATR-FTIR to quantify polymorph proportions using calibration curves or internal standards [72, 73, 74], our collected sample sizes are not enough to spare in calibration curves and should not be contaminated with internal standards.

2.1.2 Capillary powder X-ray diffraction (PXRD)

PXRD is another technique that allows us to discern the crystal structure of the powdered solid. In principle, an X-ray beam is shot into a polycrystalline solid sample, and as a consequence of the crystal structure lattice spacing, the beam will scatter in all directions allowed by Bragg's law. The atom's arrangements in the crystal structure of a solid can be represented as a sequence of parallel lattice planes with specific spacing (d). Bragg's law ($2dsin\theta{=}n\lambda$) indicates that if an X-ray beam with wavelength λ and incident angle θ will diffract for a d spacing that complies with the equation. n is the diffraction order. As a result, a diffraction pattern where each line corresponds to a lattice plane is created. Each crystal structure has a set of lattice planes and intensities for which the diffraction pattern will function as a fingerprint.

With this, PXRD allows identifying different crystal phases in a solid [75]. Capillary PXRD refers to the holder in which this technique variation is done, where the sample is introduced in a capillary, and the X-ray is shot through it.

This technique was chosen to complement ATR-FTIR limitations since PXRD has a longer penetration depth (10-100 μm) [76], which will give us information about any hidden phase in the sample's bulk. PXRD can also give us details regarding cell parameters upon processing, from which we can assess lattice constraints and/or mineral impurities. Although PXRD is generally a strong quantification technique, we chose capillary PXRD. We decided to use a capillary to save as much sample as possible, and since carbonate polymorphs do not have spherical particles usually, there is a significant risk that a sample with a different morphology could pack with a preferred orientation inside the capillary. Hence, the intensities in the diffraction pattern may not correspond to the polymorph proportion phase ratios, making a possible false-positive quantification, which means quantifying phase proportions is less advisable for our samples' conditions [77]. However, since cell parameters depend on peak positions rather than intensities, some robust information can still be extracted from these experiments.

2.1.3   Inductively coupled plasma-optical emission spectrometry (ICP-OES)

ICP-OES is a powerful analytical technique that we used to determine the elemental composition of our samples. The procedure principle is: first to digest the sample using an acidic solution, then the sample is atomized in an extremely hot ($\sim$10,000 K) argon plasma, which ionizes the atoms. The electrons in the ions then retreat to lower energy states by recombination and emit energy as light at characteristic wavelengths for each element. A detector measures this emitted light, producing a spectrum that identifies the elements present. Calibration curves are necessary for each element that

is intended to be quantified. ICP-OES offers high sensitivity, detecting elements at parts per billion (ppb) to parts per million (ppm) levels [78]. Although this technique does not give molecular information, it provides the different mineral concentrations that could be present in our biogenic carbonates. Some of the limitations of this technique for our experiments are that it overlaps spectral lines and has issues preparing calibration curves of certain elements. Moreover, C and O cannot be quantified with this technique since there could be contamination with atmospheric CO_2 and O_2. It is also expensive and time-consuming.

Chapter 3

Biogenic calcium carbonate: phase conversion in aqueous suspensions

Abstract

Powdered biogenic calcium carbonate from butter clams shows variations in its tendency to convert from aragonite to calcite when suspended in water, depending on whether the suspension has additional calcite or not. Our investigations treat these biogenic samples as complex hierarchical materials, considering both their mineral and organic components. We assess the mineral composition from Attenuated Total Reflection Fourier Transform Infrared spectroscopy peak shifts, as well as quantitative assessments of lattice constant refinements (powder X-ray diffraction). To isolate the mineral portions, we compare results from samples where the periostracum is removed mechanically and samples that are heated to temperatures that are sufficient to remove organic material but well below the temperature for thermal phase conversion from aragonite to calcite. The results show that the total organic content does not play a significant role in the aqueous mineral phase conversion. These results have potential implications for understanding carbonate mineral interactions in ocean sediments.

3.1   Introduction

Calcium carbonate ($CaCO_3$), most commonly in the form of calcite or aragonite but also found as vaterite or amorphous calcium carbonate (ACC), is one of the most common biominerals in marine organism skeletons, including clams, oysters, crabs, mussels, and corals [20, 80, 81]. Each species has a different predisposition for forming a given polymorph, and it is not uncommon for one species to have different polymorphs in different parts of its hard tissue [82]. For this reason, it is important to acknowledge the individuality of each species when it comes to considering it as a biomaterial.

Between the two most common forms of $CaCO_3$, aragonite is known to have a

higher solubility constant than calcite, but both polymorphs have very low solubility in water (aragonite $K_{sp} = 10^{-8.34}$ and calcite $K_{sp} = 10^{-8.48}$ at ambient temperature and pressure [27, 83]). Recent studies by us and others [31, 12] have demonstrated that this small solubility difference can lead to a surprisingly effective dissolution–recrystallization process in which aragonite can dissolve completely—recrystallizing as calcite—when it is in close proximity to calcite. To describe this in another way, when either calcite or aragonite is present in water on its own, there is only slight solubility. However, when both phases are present, a solution that is in equilibrium with respect to calcite will be undersaturated relative to aragonite, triggering aragonite dissolution; on the other hand, when the solution is in equilibrium with respect to aragonite, it will be supersaturated relative to calcite, which can trigger calcite precipitation. This effect has been effectively modelled based on thermodynamic principles, being described as galvanic dissolution [31], a buffering effect [84], and a thermodynamic pump [12], since the overall result is to deplete the more soluble phase (aragonite) in favour of the less soluble phase (calcite). Our previous solid-state NMR experiments [12] provided evidence that this is indeed a dissolution–recrystallization process.

Although knowledge of this aragonite-to-calcite conversion process is not new [46, 85], the implications of this phase conversion have received more attention recently because of its potential relevance for the stability and preservation of marine minerals. In particular, the time scales and length scales over which this transformation occurs remain open questions, raising the possibility that this process could be important to consider for carbon cycling calculations that involve the ocean. Others have begun exploring these questions through simulations [31], as well as experiments [86, 84]. Other more foundational experiments [12] provided evidence that this phase transformation does indeed proceed through a dissolution–recrystallization reaction and that additives to the water (polyphosphate) can become surface-embedded during dissolution–recrystallization, thereby arresting the polymorphic pumping process.

Biogenic calcite and aragonite can have very different microstructures and textures compared to lab-synthesized calcite [87, 88, 89]. Bivalves, which are a group of calcium carbonate-shell-forming organisms, produce their shells in layers, where the oldest minerals produced by the organism are found in the inner layer of the shell, and the newest minerals are found in the outer layer of the shell [80, 89]. It is well known and documented that bivalves can produce a number of different microstructures of calcite and aragonite through biomineralization and that these possibilities may be different between species. Common microstructures include prismatic, lamellar, and nacreous motifs [81]. The outer and inner layers can have distinct microstructures and will typically vary by species [88]. Thus, an extremely broad range of calcium carbonate microstructures and compositions would exist in any kind of natural environment where powdered aragonite and powdered calcite might interact, such as in sediments.

In this experiment-focused work, we take a simplified model case to consider whether the polymorph composition of biogenic calcium carbonate (calcite, aragonite, or others) is well correlated with the polymorphs that exist when powders of these biomaterials are suspended in freshwater. We use the butter clam as a case study for biogenic calcium carbonate and compare what happens when different portions of the clam—with different pretreatments to remove organic components—are powdered and suspended in ultrapure water. A key aspect of this work is describing polymorph variations that appear in different parts of the clam shell, and unlike some recent work [84], we compare the results with and without the organic components removed. Our data show that some individuals exhibit polymorph behaviour that is similar to what we have observed with lab-synthesized specimens [33, 12] and what others have simulated [31] and observed with treated biogenic minerals in treated seawater [84]. We use structural and compositional analyses to assess some of the compositional differences between the lab-synthesized and biogenic materials and to assess under which conditions the biogenic samples exhibit this polymorphic conversion.

3.2 Materials and Methods

3.2.1 Overview of Butter Clam Microstructure

Bivalve shells, such as the butter clam, have growth rings that are much like trees, with the relevant layering visible on length scales that are appropriate for optical imaging (tens to hundreds of micrometres) [89]. Figure 3.1 shows representative views of a half-shell (valve) of the butter clam over different length scales (Zeiss Axiozoom (Oberkochen, Germany) under reflected light, with image enhancement using Adobe Photoshop (version 23, San Jose, CA, USA)). The top view of an entire valve (Figure 3.1a) shows a ridged surface topography, with the axis of maximum growth indicated with a red line. A cross-sectional view along this midline (Figure 3.1b) shows the growth rings as grey lines. Staining with Mutvei's solution [90] (Figure 3.1c,d) makes the growth layers easier to see because of the increased visual contrast between the mineral (lower uptake of the stain) and organic-rich layers in between (higher uptake of stain). The outer proteinaceous layer on the outer surface of the shell (periostracum) also has higher stain uptake.
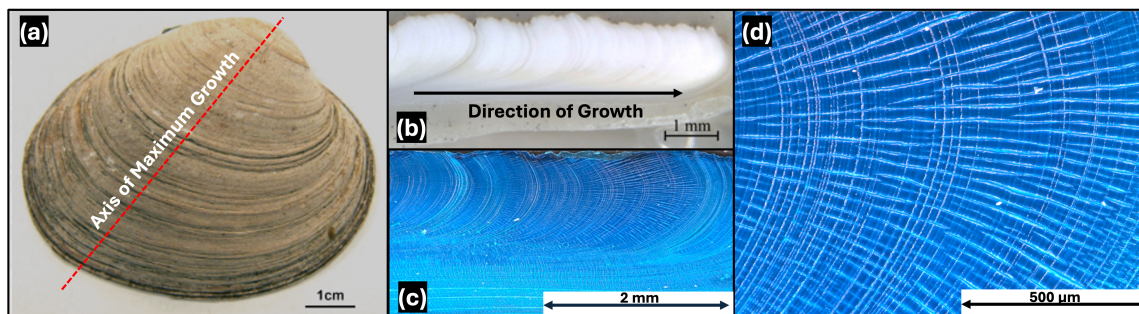
Figure 3.1: Representative photographs of (**a**) a butter clam valve (midline shown with a red line), (**b**) an unstained section through the valve midline, (**c**) a stained section through the valve midline, and (**d**) a zoom of the stained section through the valve midline. In (**c,d**), the organic material is stained darker than the mineral material, which provides better visual contrast for the growth lines.

Even though butter clams are a species of bivalve that is relatively well characterized [91, 92], there is still surprisingly little that is known about the specific organic

components that exist within the shells. This is an active area of research entailing the characterization of the specific organic proteins and molecules [17]. The mineral portion of butter clam shells has been studied by others. XRD analysis and minor-element composition studies show that butter clam shells are predominantly aragonite [91, 92]. The hinge has been more well characterized in the previous literature [93], so we focus our studies on the hinge portions.

3.2.2 Specimen Preparation

Live-collected, mature (2–6 years old) butter clams (Clams 1 and 2 from Sechelt Inlet, British Columbia, Canada) were sectioned according to Figure 3.2 and Table 3.1. The left and right valves were each divided into quarters, yielding four hinge portions and four non-hinge portions per individual. The organic-rich periostracum on the outer portion of the shell was removed mechanically using a hand drill with a 1 mm cylindrical diamond-coated bit (models 27304 and 835104010, Minitor Co. Ltd. (Tokyo, Japan)). Two different half valves (Clams 3 and 4) from dead-collected clams with intact periostracum were also ground and used as separate samples. Butter clams are very hard, and the shells can be crushed and ground only with considerable effort. The most efficient method was hand grinding to a powder (with particle sizes in the range of 40–120 μm) with an agate mortar and pestle; attempts to grind with stainless steel ball milling were abandoned because it introduced metallic debris to the samples.

As outlined in Table 3.1, selected samples were heated (alumina crucible in a Thermolyne 114300 furnace) to remove organic material. The heating profile was a ramp from 20 to 300 °C at 100 °C/h, holding at 300 °C for 1 h (except Clam 2 for 3 h), and then cooling to 150 °C before opening the furnace. Table 3.1 also reports the % mass changes after heating.

Left valve **Right valve**
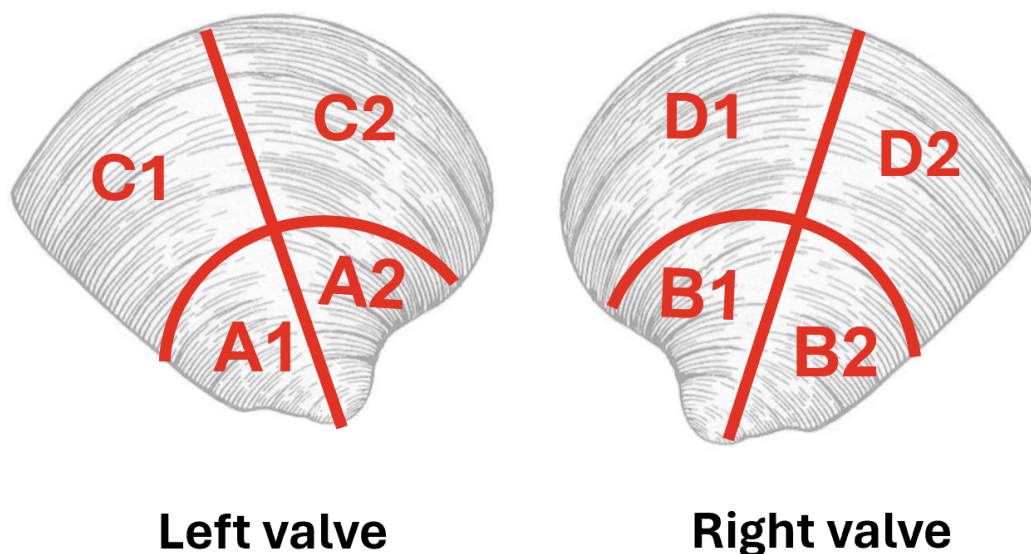
Figure 3.2: Schematic depiction of the sectioning and labels for different clam portions: A1, A2, B1, and B2 are hinges, while C1, C2, D1, and D2 are non-hinge portions. Adapted from a public domain image [5].

3.2.3 Aqueous Suspension Experiments

The powders described in Table 3.1 were tested individually for their polymorph stability in ultrapure water (Barnstead Nanopure, 18.2 MΩ·cm, initial pH 6.7–7.1), with the same mass-to-water ratio for all samples, all in an ambient atmosphere. The powder mass varied among different suspension experiments due to the fact that the different shell portions (Figure 3.2) did not have the same mass. Suspensions were sonicated for two minutes in capped glass vials and then stirred (Teflon-coated magnetic stir bar, 1000 rpm) for up to 1 week. After 1 week, the supernatants were removed and their pH measured, and the powder was left to dry overnight; the supernatant pH values were 8.3–8.6, which is consistent with trends from earlier studies [11] and is in a similar range to the ambient temperature activity product constants for aragonite (8.36) and calcite (8.52) [94]. We note that, for some heated clam powders, the supernatant pH after one week was slightly higher (9.7). After their suspension, the dried powders were still free-flowing and not densely hard-packed.

Table 3.1: Labels for different butter clam portions showing their subsequent treatments. Valve and hinge refer to different shell portions shown in Figure 3.2; a label with "W" indicates that a whole valve was powdered without sectioning. The organic-rich periostracum was manually removed from some samples before heating; the mass change after heating (ΔMass) is recorded in a separate column. Aqueous suspension experiments used either clam powder alone (clam mass/water volume) or mixtures (clam mass plus purchased calcite mass/water volume), with or without stirring.

Label	Valve	Hinge?	Periostracum?	ΔMass %	Alone (mg:mL)	Mix ((mg):mL)	Stir?
Clam 1							
1A1	left	yes	yes	–	50:5	(50+50):10	yes
1A2	left	yes	no	–	50:5	(50+50):10	yes
1C1	left	no	yes	–	100:10	(50+50):10	yes
1B1	right	yes	no	–	10:1	–	yes
			no	-2.9	50:5	(50+50):10	yes
1B2	right	yes	yes	–	–	–	yes
			yes	-2.4	50:5	(50+50):10	yes
Clam 2							
2B1	right	yes	no	-3.1	–	–	–
2B2	right	yes	yes	-2.6	–	–	–
Clam 3							
3W1	–	–	yes	–	100:10	(50+50):10	yes
3W2	–	–	yes	-2.1	100:10	(50+50):10	yes
Clam 4							
4W1	–	–	yes	–	–	(50+50):10	no
			yes	–	100:10	–	yes

In some experiments, after 2 days, 1 mL aliquots of the suspensions were removed by a micropipette and air-dried for further characterization. This allowed us to compare the results of experiments where the vial was opened periodically, exposing the contents to the air, with those where the vials remained capped for the entire experiment. We did not see any differences in the results between these two types of experiments.

A second set of aqueous suspension experiments followed the same procedure described above but involved a mixture of clam powder and purchased calcite. For these experiments, the total proportion of powder to water was the same as above,

but the composition of the powder was a 50%–50% mixture by mass of clam powder to purchased calcite (ACS reagent grade, Alfa Aesar, 99%).

3.2.4   Characterization

Powder X-ray diffraction (PXRD) data for the hand-ground starting powders were collected at room temperature using an XtaLAB Synergy-S, Dualflex, HyPix-6000HE diffractometer (Rigaku, The Woodlands, TX, USA) with Cu Kα radiation ($\lambda = 1.5406$ Å). The powder samples were loaded in a 0.5 mm borosilicate glass capillary (HR6-112, Hampton Research). The detector distance was set to 86.0 mm. Data acquisition involved a series of 360 ° ϕ-scans at ω angles of $-65.792°$, $-23.646°$, $23.802°$, and $65.948°$, with an exposure time of 300 s for each image. Data collection and extraction were performed within CrysAlisPro (version 38, Rigaku OD, Tokyo, Japan, 2024). We refined the lattice constants for each starting material using whole-pattern fitting (JADE 10 software [1]) and compared them with aragonite and calcite unit cells reported in the PDF-2 databases [3]. Additionally, we used Rietveld refinements on selected patterns to assess the phase composition of the starting materials. These results are described in more detail in the Supplementary Materials Table 3.2 and Figures 3.8− 3.12

To complement the PXRD data, polymorph identification (before and after suspending the powders) was facilitated by Attenuated Total Reflectance Fourier Transform Infrared (ATR-FTIR) spectroscopy (Bruker Alpha with OPUS software version 7.8, Bruker, Billerica, MA, USA), 2 cm^{-1} resolution, 36 scans, 4000–400 cm^{-1} range). Spectra were recorded in triplicate to account for heterogeneity within a given aliquot of powder; a representative subset of these data is shown here, with many dozens of other spectra provided as a dataset. Polymorph assignments were based on comparisons with ATR-FTIR spectral standards (RRUFF project [6]), since the different

measurement geometry for transmission FTIR data leads to slightly different peak positions, widths, and asymmetries for the same specimen. We note that Raman spectra are not helpful in these kinds of biogenic samples due to fluorescence interference.

For elemental analysis (Perkin-Elmer 5300 DV ICP-OES (Shelton, CT, USA)), a subset of powders that were used for the PXRD analyses (where there was sufficient mass remaining) were dissolved in acid (HNO_3:HCl 4:1) for 1 h and then diluted to 1%. These solutions were then analyzed for the following elements, which are commonly found in biogenic aragonite: Ca, Mg, Sr, Ba, and Fe.

We assessed the total organic carbon (TOC) data (Shimadzu TOC-L, Kyoto, Japan) before and after heat treatments. The instrument was calibrated with 99% recrystallized acetanilide standards and commercial reference standards from the Hansell consensus reference material program (RSMAS, University of Miami, Coral Gables, FL, USA). Samples were acidified with HCl and then purged with a CO_2-free gas before injection onto a platinum catalyst (at 720 °C). This converted the organic carbon to CO_2 and was quantified by a non-dispersive infrared detector.

3.3   Results

3.3.1   Clam Mineral Characterization

Our sample preparation strategy focused on isolating different portions of the clam shell (hinge and non-hinge), followed by different treatments to remove organic material. This gave us several replicates per individual so that we could explore how the mineral part of the shell behaves with and without the periostracum (removed manually), in combination with heating or without heating. We note that our sections give us an average bulk result for a distinct portion of each individual; even so, this sampling strategy glosses over many of the interesting microstructural and textural details of the biogenic specimens that we described earlier [80, 81], but it gives us

data that are arguably more representative of what a crushed shell might experience in a natural setting.

Representative ATR-FTIR spectra (Figure 3.3) show that butter clams are predominantly aragonite, with peaks at 1447–1460 cm^{-1} (ν_3), 1083 cm^{-1} (ν_1), 854–857 cm^{-1} (ν_2), and 712–713 and 700 cm^{-1} (both ν_4). These peak positions are consistent with those reported for aragonite standards, whose spectra were also collected using the ATR-FTIR measurement geometry (RRUFFID=R040078 [6]). There is no evidence of vaterite or amorphous calcium carbonate (ACC), nor is there any difference with or without the periostracum. Additional comparisons among different portions of different shells (listed in Table 3.1) are shown in Supplementary Materials Figures 3.13 and 3.14.
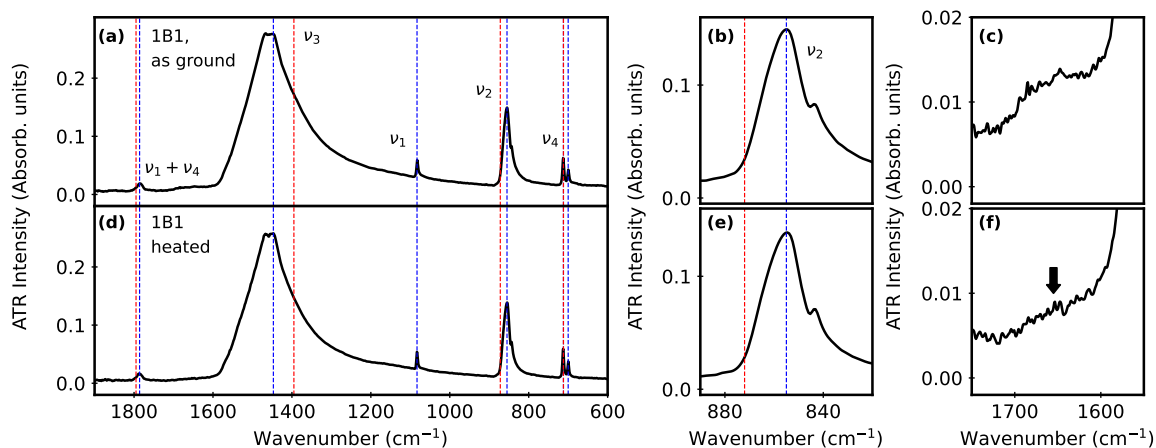
Figure 3.3: Representative ATR−FTIR spectra for butter clam powder before (**a**–**c**) and after (**d**–f) heating. Blue and red vertical lines show peak positions for standards of aragonite (RRUFFID R040078) and calcite (RRUFFID R040070), respectively [6]. Plots (**b**,**e**) focus on the ν_2 region; plots (**c**,**f**) highlight the region where weak protein-based amide and water peaks disappear after heating (1600–1700 cm^{-1}). The black arrow (f) highlights the reduction of the protein hump peak intensity after heating.

After heating, ATR-FTIR spectra show a decrease in the broad hump near 1600 cm^{-1} (Figure 3.3 c,f). Since this is a region where amide and water peaks appear [95, 96], this kind of change would be consistent with a reduction in protein content. We

note that this spectral change is also correlated with a small mass loss (2–3% in Table 3.1), which is a similar magnitude of change to that observed after heating other related types of biogenic aragonite (such as Arctica Islandica [97]). The TOC analysis of Clam 3 showed a 60% organic carbon reduction after heating (leaving 0.14% by mass) and a total nitrogen reduction of 60% (leaving <0.02% by mass). Examples of this change in other samples after heating are shown in Supplementary Materials Figure 3.15.

In PXRD data (Figure 3.4), we also find that aragonite dominates in all butter clam specimens; Figure 3.5 summarizes the lattice constant refinement results. Heating decreases the aragonite cell parameters consistently, which is an effect that has been reported by others and is attributed to relaxation and reordering in biogenic aragonite [8, 7]. After heating, a new PXRD peak appears (Figure 3.4b,d) in a region where the strongest calcite diffraction peak (104) would appear. We note that this intensity change is very small, corresponding to less than a few % of the total sample. Additional PXRD spectra are included in Supplementary Materials Figures 3.17 and 3.18.

Since we noticed that the aragonite lattice constants for our clams are consistently smaller than the PDF standard, we also looked at elemental analysis data (ICP-OES) for the sample that had enough remaining powder for this measurement (Clam 4). These results show very low amounts of common substitutional impurities that are possible in calcium carbonate (Mg: 0.010(1), Sr: 0.19(3), Fe: 0.007(3), Ba: 0.01(6), all values in wt%). For comparison, the literature data referenced in Figure 3.5 also have very low impurity levels. Conch had impurities measured below 0.1 wt% [7], while geogenic aragonite was reported to have atomic wt% of Sr: 0.25, Al: 0.06, Na: 0.03, and Mg: 0.02 [7, 8, 9].

To summarize, the mineral content of butter clams is predominantly aragonite, with trace amounts of calcite appearing in PXRD data after heating, along with lower-intensity protein-related peaks in ATR-FTIR and some mass loss. We note
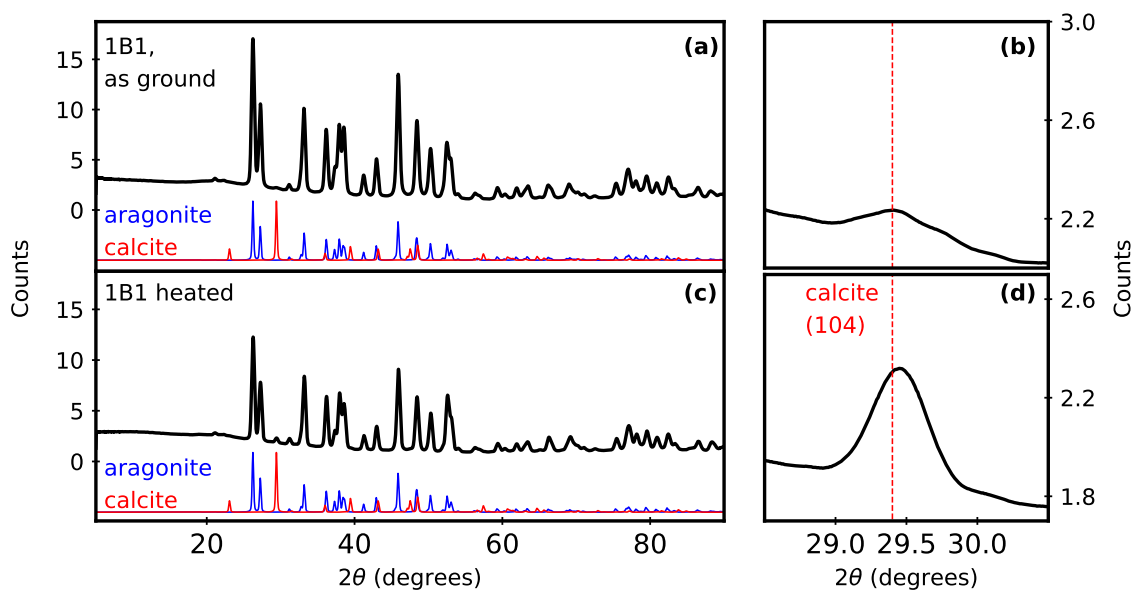
Figure 3.4: Representative PXRD data of butter clam powder (black lines) before (**a**) and after (**c**) heating. The blue and red patterns show data for standards of aragonite (PDF 980000098) and calcite (PDF 980000141), respectively [3]. Plots (**b,d**) show an intensity increase for the strongest calcite line (104) after heating; the dotted red vertical line shows the peak position for the calcite standard pattern.

that leaving the periostracum intact does not lead to any difference in the ATR-FTIR or PXRD data, nor does it change the % mass loss after heating. This suggests that most of the mass loss in these powdered samples is related to either water loss or the elimination of organic material that exists between mineral layers in the shell.

3.3.2 Monitoring Polymorphs after Aqueous Suspension

In order to track polymorphic phase conversion, we compared the ATR-FTIR spectra of powders before and after they were stirred in water (ultrapure, 18.2 MΩ·cm) for 1 week. A detailed comparison of representative spectra is shown in Figure 3.6, including a single powder alone (Figure 3.6a–d,i–l) or mixtures of clam powder with purchased calcite (Figure 3.6e–h,m–p). Additional spectra are provided in Supplementary Materials Figures 3.14 and 3.16.
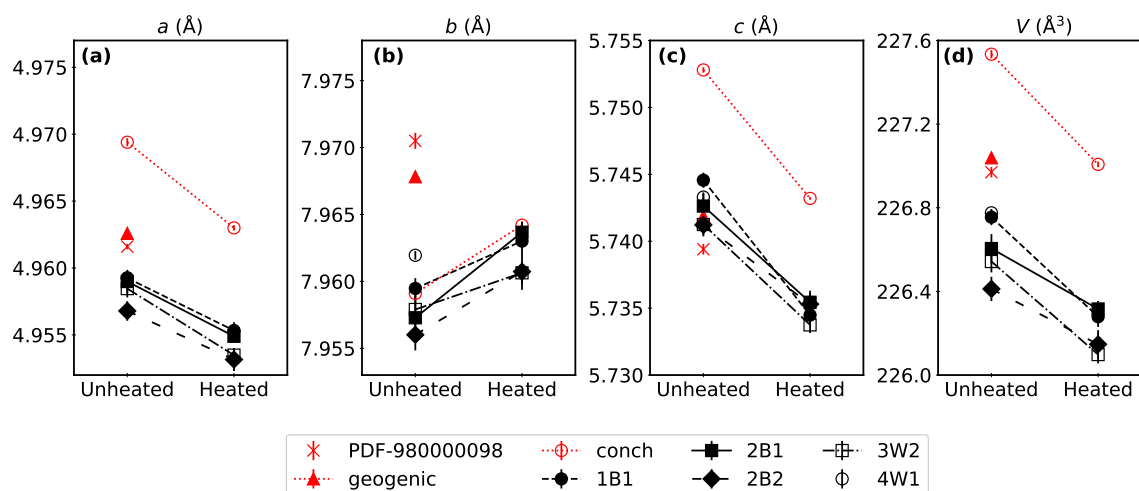
Figure 3.5: A comparison of aragonite cell parameters a, b, c (in Å) (panels **a**–**c**) and V (volume in Å^3) (panel **d**), for different clam samples before and after heating (where possible), all shown with black symbols. Red symbols show comparisons to an aragonite standard (PDF# 980000098 [3]) and aragonite parameters reported by others (geogenic and conch from [7, 8, 9]).

After stirring clam powder alone in water, there are no distinguishable changes in the ATR-FTIR spectra; in all cases (left/right, hinge/non-hinge, with/without periostracum, with/without heating), aragonite remains the dominant phase, with no clear evidence of conversion to calcite in any case (Figure 3.6c,d,k,l). However, for sectioned clams that were suspended with purchased calcite (with/without periostracum or with/without heating), some phase conversion from aragonite to calcite is evident in all cases (Figure 3.6e–h,m–p).

3.3.3 Biogenic *vs.* Lab-Synthesized

Since our results show that adding calcite enhances the polymorphic pumping process to make it readily observable in a 1 week time frame, we also investigated other mixed-polymorph scenarios.

For biogenic specimens that already contain mixed polymorphs, the mere co-existence of calcite and aragonite does not guarantee that the polymorphic pumping
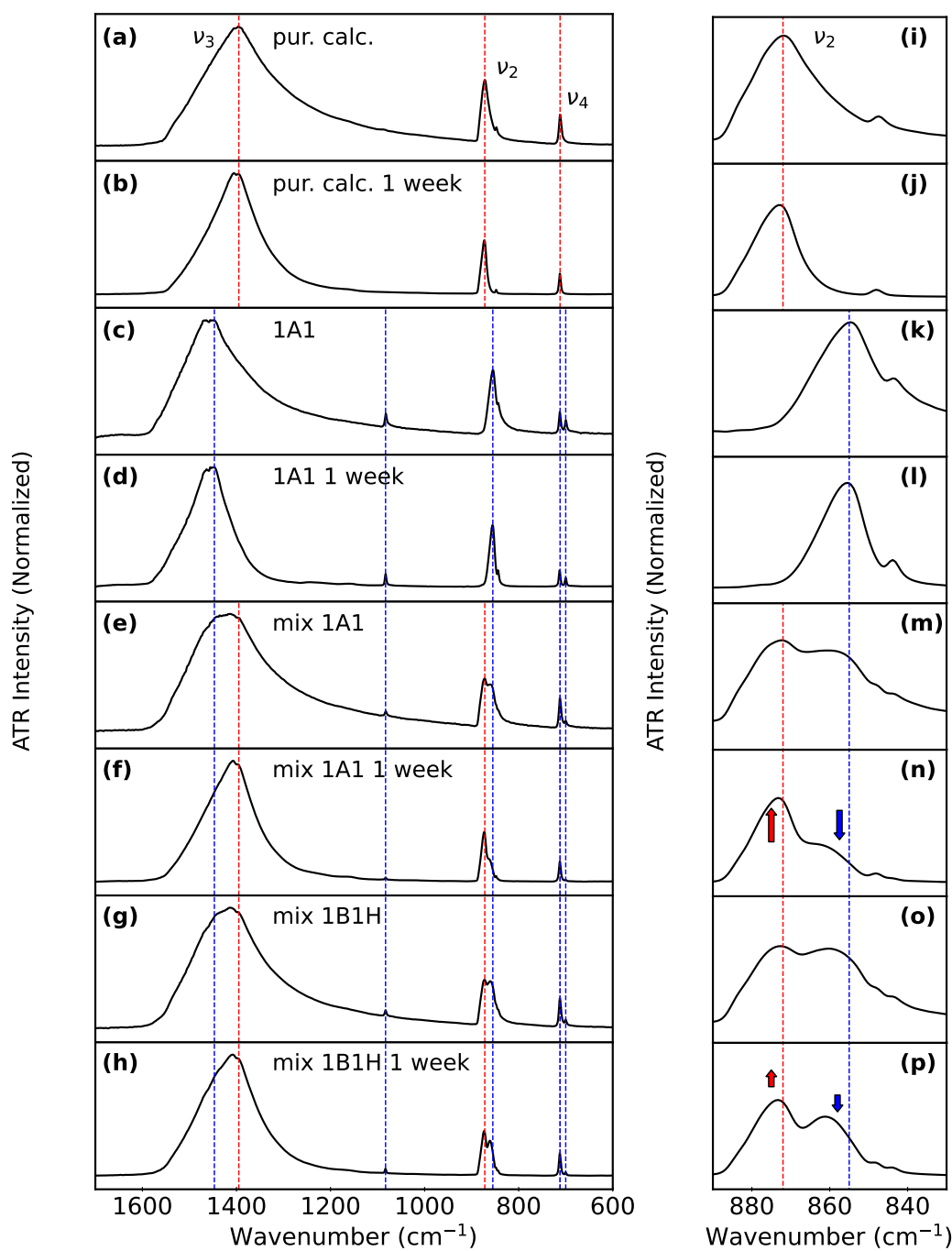
Figure 3.6: Representative ATR-FTIR spectra to compare changes before and after aqueous suspension. The top 4 rows (**a**–**d**) compare the individual starting materials alone in water; the bottom 4 rows (**e**–**h**) compare mixtures of clam and purchased calcite. Panels (**i**–**p**) show zoomed views of the ν_2 region, where the changes in the relative intensities of the aragonite and calcite peaks are easiest to follow. In all panels, blue and red vertical lines show peak positions for standards of aragonite (RRUFFID R040078) and calcite (RRUFFID R040070), respectively [6]. Arrows highlight the peak intensity changes relative to the pre-suspension spectra for calcite (red) and aragonite (blue).

behaviour is noticeable. Figure 3.7 helps to illustrate this point. Figure 3.7a compares ATR-FTIR spectra for heated butter clam powder before and after 1 week of stirring in water. There was no evidence of polymorphic pumping, similar to what is shown in Figure 3.6c–d,k–l for a different (unheated) clam portion. In both cases, the clam spectra show only aragonite after being stirred in water for one week.
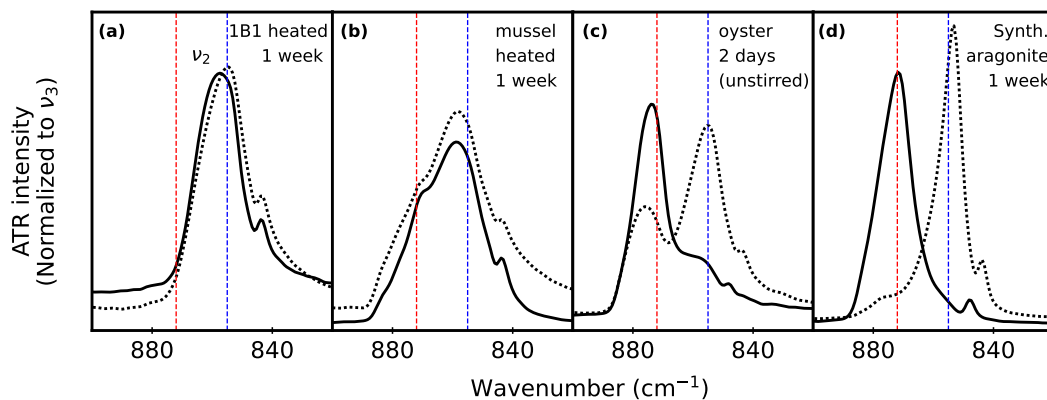
Figure 3.7: Representative ATR-FTIR spectra comparing polymorphic conversion before (dotted line) and after (solid line) aqueous suspension of (**a**) heated clam powder, (**b**) heated blue mussel powder, (**c**) food-grade oyster shell powder, and (**d**) lab-synthesized aragonite. In all panels, blue and red vertical dashed lines show peak positions for standards of aragonite (RRUFFID R040078) and calcite (RRUFFID R040070), respectively. [6].

Blue mussels (Figure 3.7b) contain a noticeable amount of calcite to start with. For these suspension experiments, a whole ground blue mussel valve (heated in the same way as the clams, with a similar 2.8% mass loss after heating) included both $CaCO_3$ polymorphs in the ν_2 region (Figure 3.7b), consistent with reports by others [82]. The aragonite and calcite peaks in the ν_2 region do not show any relative intensity changes after 1 week of stirring, whether using heated or unheated powder.

In contrast, we also tested a live-purchased (food-grade) oyster, whose shell consisted of aragonite with calcite as a sizable secondary phase (Figure 3.7c). For this powdered specimen, it showed significant phase conversion after only 2 days in water, even without stirring.

As another comparison, we were able to observe polymorphic pumping behaviour in lab-synthesized aragonite (Figure 3.7d), wherein a small amount of calcite was present as an unintentional secondary phase from the synthesis procedure. In this case, 1 week of stirring was enough time for the aragonite to dissolve completely, recrystallizing as calcite. This is consistent with earlier reports from our group [33, 12] that confirm this polymorphic pumping behaviour.

To summarize, the tendency toward aragonite dissolution and calcite recrystallization is not the same for all biogenic sources of aragonite and calcite. There are many bivalve species that grow heterogeneous aragonite and calcite distributions within their shells. A polymorph mixture is also possible in specimens in which diagenetic dissolution of aragonite has occurred with reprecipitation as calcite [20]. This means that, even if both aragonite and calcite are present in a specimen, there is no guarantee that polymorphic pumping will happen in similar time frames.

3.4   Discussion

The polymorph conversion (pumping) that we track in this work relies on two factors: (1) a solubility difference between the two starting polymorphs (calcite and aragonite) and (2) recrystallization that occurs as the less soluble polymorph (calcite) [31, 12]. It is a different scenario from direct nucleation from a solution, for which there are many careful studies that document the persistence of multiple $CaCO_3$ polymorphs [34, 87]. To this point, our study demonstrates some experiments where polymorphic pumping occurs within a short (1 week) time span and others where the process is much slower.

Since many biominerals are reported to contain substitutional impurities as well as a variety of polymorphs, it is worth commenting on how each of these factors could influence the thermodynamic polymorph pumping behaviour. We also comment on the possible broader relevance to ocean sediment studies.

3.4.1   Substitutional Impurities

In our samples, we consider lattice constant refinements and elemental analysis information together to assess whether we have evidence for substitutional impurities. Lattice constants and unit cell volumes that are significantly different from those reported for pure $CaCO_3$ could indicate a substitutional impurity: Vegard's law is an empirical linear relation between the unit cell size and substitutional impurity concentration, and it has been usefully applied to many different solid solutions, including $Ca_{1-x}Mg_xCO_3$ [98]. Comparing with representative data for aragonite (Figure 3.5), we notice that our clam unit cell volumes and a value tend to be slightly smaller than the biogenic and geogenic reference values with which we compare. In elemental analyses of the butter clam, the dominant impurity was a very small amount of Sr at 0.19(3) wt%. We note that the elements detected with ICP-OES were not necessarily substitutionally incorporated into the $CaCO_3$ itself. These shells contain a range of macromolecules as a normal part of their structure, some of which would dissolve in the acid dissolution treatment required for the ICP-OES sample preparation.

It is important to note that different apparent solubility constants are not the only way that impurities could influence the dissolution and recrystallization behaviour of aragonite and calcite. Numerous investigations have explored the complex role that the surface incorporation of Sr and Mg, among others, can have on crystal growth rates and surface structures [99, 100, 83, 101, 102]. Other works show that grain structure and other microstructural factors can yield results that are counter to thermodynamic expectations [103, 104]. Earlier work from our group [33, 12] shows that polyphosphate can be incorporated into both aragonite and calcite surfaces, which stalls the surface dissolution process for both polymorphs.

3.4.2   Polymorphism in Bivalves

There are many examples of poorly crystalline carbonates (ACC) in bivalve shells, including oysters [105, 106, 107], blue mussels [108, 109], and hard clams [105]. Other studies have also shown that ACC, whether biogenic [82] or lab-synthesized [33], can crystallize upon mild heating to temperatures that are far below the temperature at which thermal conversion from aragonite to calcite would occur. This suggests that it should not be surprising that we see weak calcite peaks in our butter clam PXRD data after mild heating, even though ACC has not yet been reported for butter clams.

We note that, even though heating can make a difference in the material composition of our butter clam shells, the resulting loss of organic carbon (assessed through TOC measurements) and the formation of a small amount of calcite (visible in PXRD data) did not accelerate the polymorphic pumping (aragonite-to-calcite) process.

There are many reasons why the biogenic and lab-synthesized samples could have different time scales for observing dissolution and recrystallization behaviours, including the presence of organic molecules or other inorganic material that is incorporated within and between layers of the mineralized specimen. Our experimental design with Clam 1 was intentionally geared toward assessing these variables in a few different ways. The overall finding was that the mechanical removal of the periostracum did not alter the time scale of the polymorphic conversion in butter clam to any noticeable degree. Using another method to remove organic material, mild heating to a temperature well below where the thermal transition from aragonite to calcite would be expected, did not accelerate the phase conversion: if anything, it appears to have inhibited it slightly.

3.4.3   Relevance to Ocean Sediment Studies

One context where the time scales for dissolution and crystallization of carbonates are important, but there is much disagreement in the literature, is the long-term stability

of biogenic carbonates in ocean sediments [83, 110]. This is important not only to understand global carbon budgets [110] but also to recognize that more dissolution-prone ocean-based carbonate producers could be under-represented when considering data based on skeletal material contained in ocean sediments [111]. Earlier studies in freshwater have shown that the dissolution kinetics of biogenic calcite and aragonite are not different from their geogenic counterparts [4]. However, the chemistry of ocean water is significantly more complicated, which has led to more variation in the literature values for carbonate solubilities and dissolution rates [83]. In the specific case that we consider here (aqueous aragonite-to-calcite conversion), there have been recent modelling studies based on different geometric shapes of intact marine organisms [31] that point to the potential relevance of this polymorphic change for modelling geochemistry at the ocean floor.

Exploring more realistic ocean-like conditions in laboratory experiments would include other ions [103, 86, 101, 84] as well as different apparent solubility constants [83, 112, 39]. The most similar experiment to ours is a recent study [84] that tracked pH in the pore space as a function of time. This elegant study still needed to make some simplifications relative to a true ocean system, including filtered ocean water and the removal of organic material from the shells. Furthermore, while they could detect aragonite dissolution, it was not feasible for them to confirm that there was a concomitant recrystallization of calcite. Thus, that study highlights both the importance—and challenges—of moving toward studies that are more similar to the ocean sediment environment.

3.5   Conclusions

Our study uses the existing knowledge of microstructural and textural differences among bivalve shells, considering the organic and inorganic portions of such biogenic samples, and follows the behaviour of powdered specimens after suspension in water.

We find the following:

(1) In ultrapure water with stirring, co-suspensions of powdered biogenic bivalves (butter clams or blue mussels) with powdered purchased calcite showed partial aragonite-to-calcite polymorph conversion within a 1-week time frame.

(2) Even small amounts of synthesized calcite in the lab-synthesized aragonite triggered the aragonite-to-calcite phase conversion in ultrapure water; however, the same was not true for small amounts of biogenic calcite in biogenic aragonite under the same conditions.

(3) Heating to remove organics and/or mechanical periostracum removal did not accelerate polymorph conversion (when powdered in an aqueous suspension) within a 1-week time frame.

Our lab-based experiments are one kind of model that makes many simplifications (such as using ultrapure water), but they do respect the complex hierarchical structure of the butter clam by exploring the impact of different portions of the clam shell by comparing results with and without the removal of organic material. They also suggest that different species of bivalves may not undergo phase conversion as rapidly as others, which means that future modelling studies could consider ranges of phase conversion rates, rather than aiming for a single value.

Author Contributions:

Data Availability Statement:

The data presented in this study are available at `https://doi.org/10.5683/SP3/7UXHRF`.

Conflicts of Interest:

The authors declare no conflicts of interest. The funders had no role in the design of the study; in the collection, analyses, or interpretation of data; in the writing of the manuscript; or in the decision to publish the results.

3.6   Supplementary Information

3.6.1   Additional powder X-ray diffraction data collection and analysis details

In this study, our biogenic powders were used in a way that allowed us to track a specific type of dissolution–recrystallization reaction that occurs in water. These biogenic materials are not ideal for detailed powder XRD analyses because they are known to contain different aragonite crystallite morphologies, including lamellar and tabular, as well as small portions of calcite (less than 5%).

The sample volume is low for each biogenic starting sample due to the sample portioning that we needed to perform in order to set up control experiments on each separate shell portion (hinge or non-hinge; with and without periostracum; heating or no heating). Furthermore, each of these portions was tested alone in water and then also in a 1:1 mixture with purchased calcite. Some destructive analyses, such as ICP-OES and total organic carbon determination, also consumed some powder. This portioning was an important part of our experiment, since shells from two different individual clams will have some natural variations.

Despite the small sample volume, PXRD data for the starting materials were of sufficient quality to allow for phase quantification.

As described in the main text, PXRD data were collected at room temperature using an XtaLAB Synergy-S, Dualflex, HyPix-6000HE diffractometer (Rigaku (The Woodlands, TX, USA) with Cu Kα radiation ($\lambda = 1.5406$ Å). The powder samples were loaded in a 0.5 mm borosilicate glass capillary (HR6-112, Hampton Research). The detector distance was set to 86.0 mm. Data acquisition involved a series of 360° $\phi-$scans at ω angles of $-65.792°$, $-23.646°$, $23.802°$, and $65.948°$, with an exposure time of 300 seconds for each image. Data collection and extraction were performed within CrysAlisPro (Rigaku OD, 2024).

Table 3.2: Representative Rietveld refinements for PXRD data shown in Figures 3.8-3.11 for different portions of Clam 2. The refined % amount of each phase (aragonite and calcite) is listed, along with the weighted-profile R factors (R_{wp}) and the expected R factors (R_{exp}). The specimen labels are defined in Table 1 in the main text.

Label	Valve	Hinge?	Periostracum?	Aragonite %	Calcite %	R_{wp} %	R_{exp} %
2B1	right	yes	no	98.6(3)	1.4(3)	8.2	19.5
2B1-H	right	yes	no	96.3(3)	3.8(3)	7.8	15.4
2B2	right	yes	yes	98.8(2)	1.3(2)	7.1	18.2
2B2-H	right	yes	yes	89.5(4)	10.5(4)	1.2	16.9

Representative diffraction images at each of these four ω angles (Figures 3.8-3.11) demonstrate that our PXRD data show smooth rings. Table 3.2 shows Rietveld refinement results for these butter clam portions, demonstrating that these biogenic samples are predominantly aragonite with small amounts of calcite.

Although the PXRD data provided estimates of the calcite–aragonite phase distribution in each starting material, the PXRD data were less useful for the 1:1 calcite–aragonite mixtures used in our aqueous suspension experiments. We attempted polymorph quantification on test mixtures (1:1 mixtures by mass of calcite + aragonite) using whole-pattern fitting (JADE software), but the uncertainties were too large (as high as $\pm$ 25%) to make these analyses meaningful. A representative example is shown in Figure 3.12. This challenge in quantifying the phase compositions in the intentional mixtures could be due to preferential sampling or orientations of one phase due to different particle sizes (hand-ground shells were in the range of 40-120 μm, while the purchased calcite had smaller sizes (5-50 μm)). As described above, obtaining more samples to try different sample geometries or powder preparation conditions was not feasible without compromising the integrity of the aqueous suspension experiments.

Given the concerns about the reliability of PXRD quantification in these intentionally mixed samples for suspension experiments, we do not rely on phase quantification

Figure 3.8: Representative diffraction images (**a**–**d**) at the four different ω angles, and (e) the corresponding diffraction pattern and fit. Rietveld refinements for these data are shown in Table 3.2. All data correspond to a portion of Clam 2, portion B1 (an unheated right hinge with no periostracum).
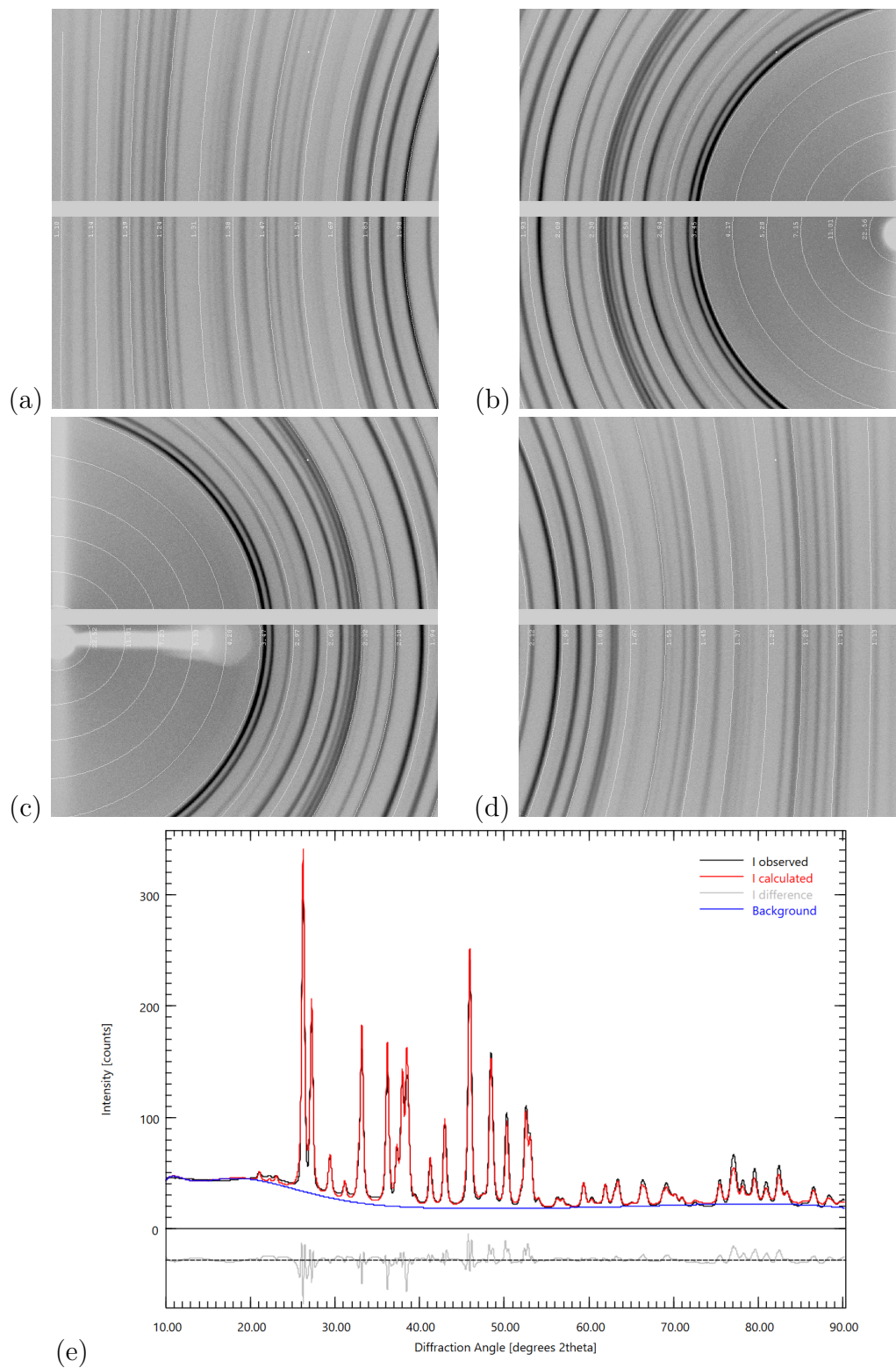
Figure 3.9: Representative diffraction images (**a–d**) at the four different ω angles and (e) the corresponding diffraction pattern and fit. Rietveld refinements for these data are shown in Table 3.2. All data correspond to a portion of Clam 2, portion B1-H (a heated right hinge with no periostracum).
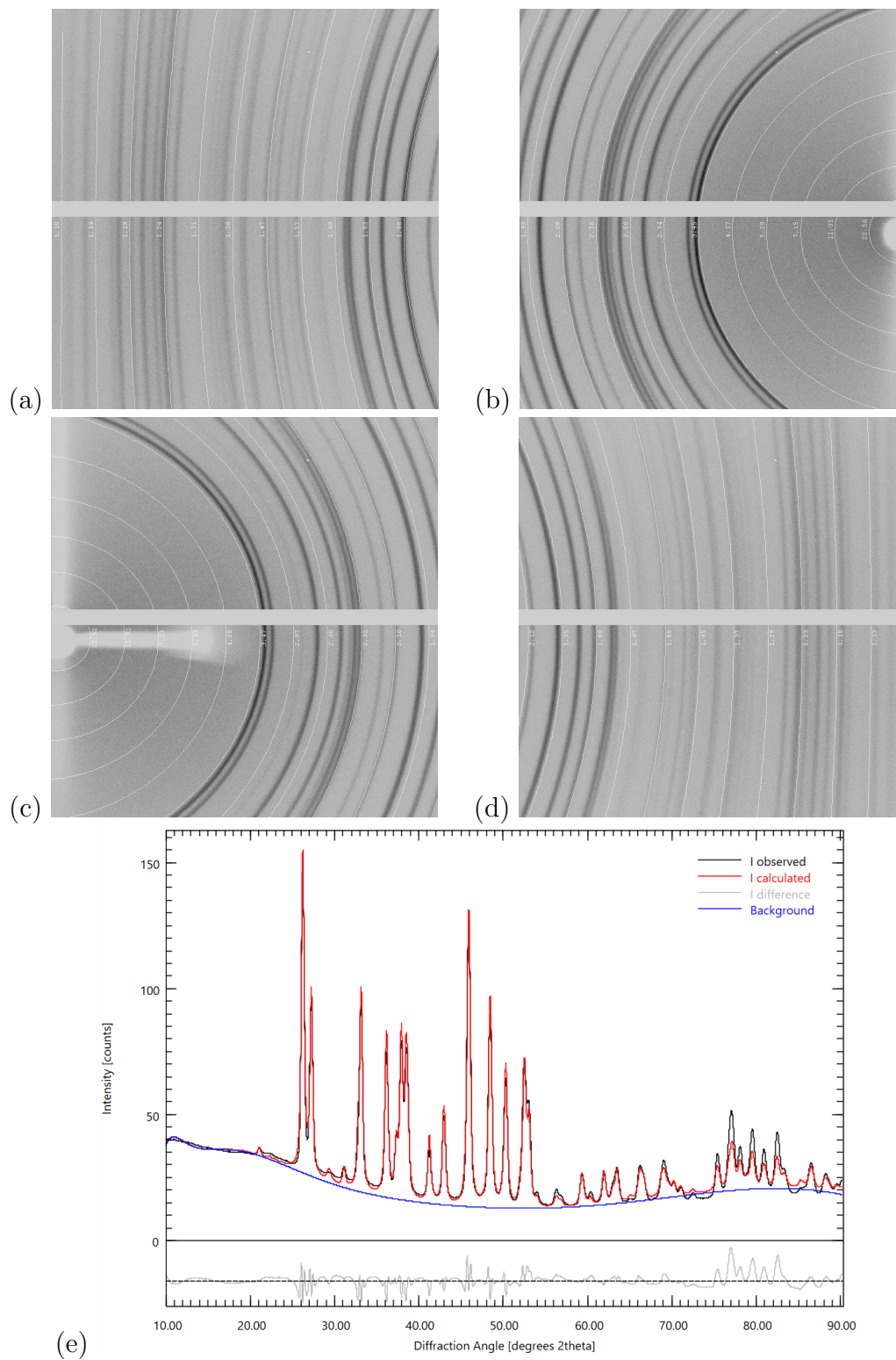
Figure 3.10: Representative diffraction images (**a**–**d**) at the four different ω angles and (**e**) the corresponding diffraction pattern and fit. Rietveld refinements for these data are shown in Table 3.2. All data correspond to a portion of Clam 2, portion B2 (an unheated right hinge with periostracum).
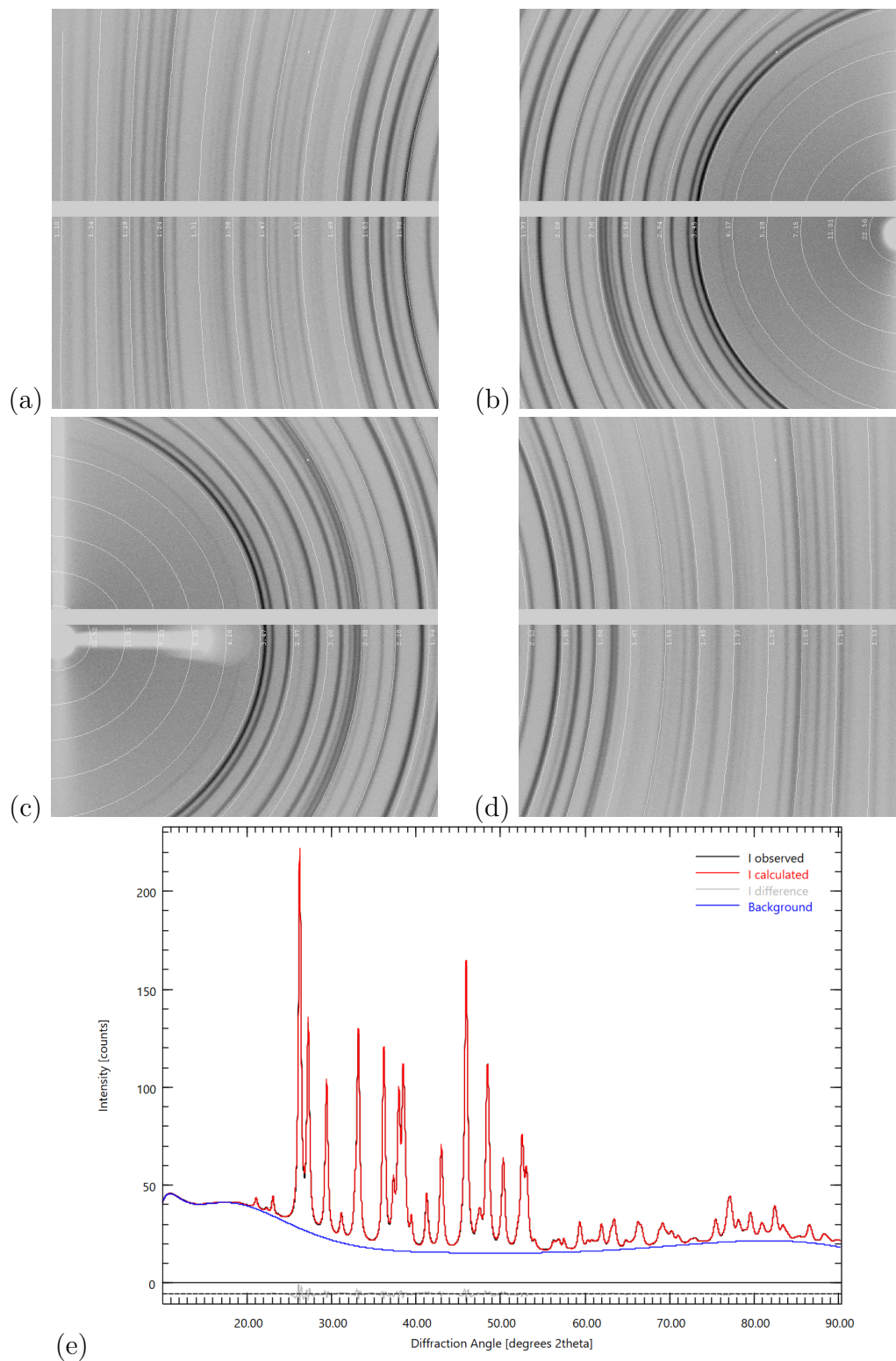
Figure 3.11: Representative diffraction images (**a–d**) at the four different ω angles, and (**e**) the corresponding diffraction pattern and fit. Rietveld refinements for these data are shown in Table 3.2. All data correspond to a portion of Clam 2, portion B2-H (a heated right hinge with periostracum).
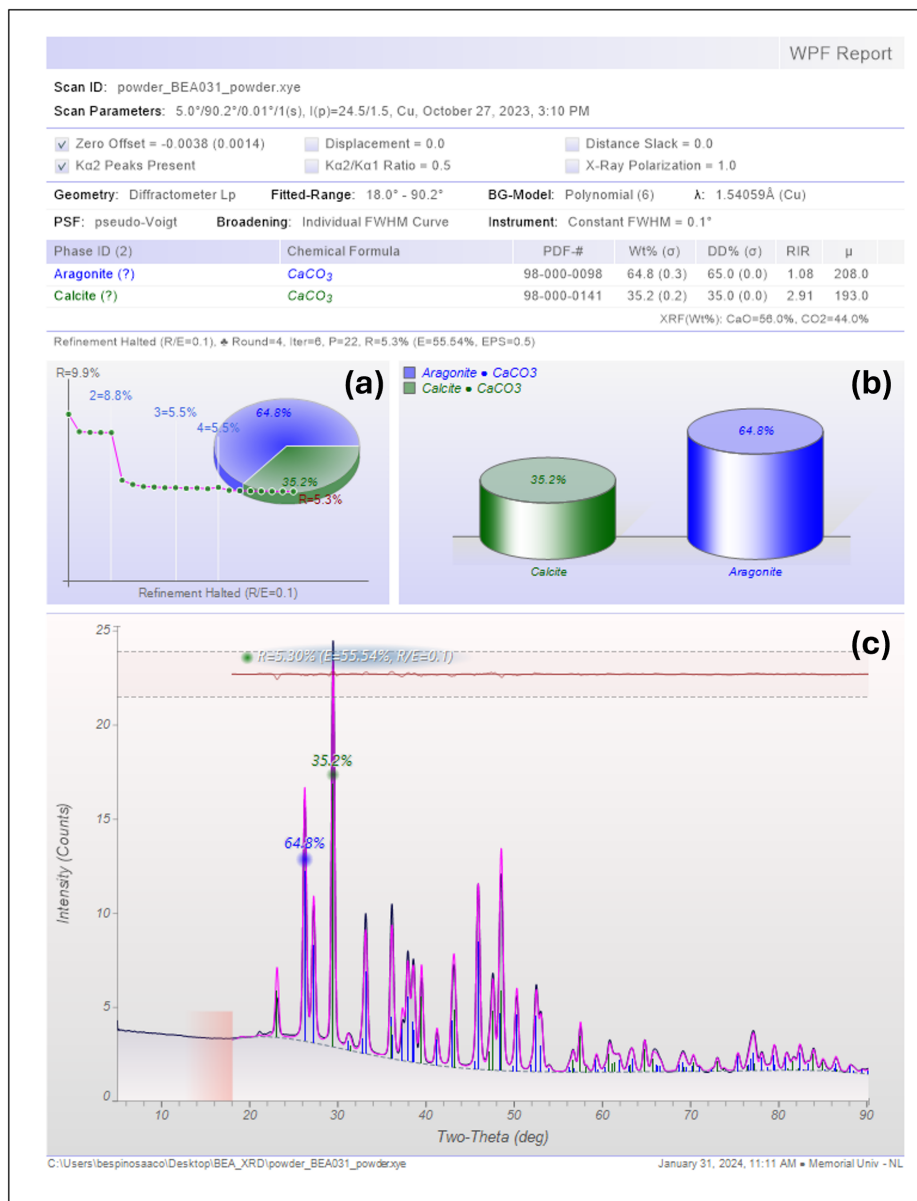
Figure 3.12: A representative screenshot of a whole-pattern fit (WPF) for PXRD data from an intentional mixture of 50% biogenic aragonite (Clam 4) plus 50% purchased calcite. Although the uncertainties in the fits are low, the values extracted from the fits (64.8(3)% aragonite and 35.2(2)% calcite) are far from what we expect of the sample mixture. This suggests that the two types of powder particles may not be equivalently measured, perhaps due to sampling biases due to different particle sizes or orientations during sample loading. (a) shows a pie chart with the proportions of aragonite (blue) and calcite (green). (b) shows a bar chart with the proportions of aragonite (blue and calcite (green). (c) shows the whole pattern fit (pink) compared to the raw data (black), with vertical sticks representing expected peak positions for aragonite (blue) and calcite (green).

or crystallinity information for any of our conclusions. Our shells have complicated phase, morphology, and crystallinity contributions from different layers within the shell. The powder grains that we studied in our aqueous suspension experiments are necessarily complex, formed by grinding these layered shells. Therefore, the PXRD data reflect the complexity and heterogeneity of these biogenic samples. As a result, we do not use these PXRD data to quantify differences before and after the aqueous suspension experiments. Instead, we pair PXRD with FTIR in order to ensure that qualitative trends are consistent with both measurement methods.

3.6.2 Additional infrared spectra comparisons

Figure 3.13 shows representative Attenuated Total Reflectance Fourier Transform Infrared (ATR-FTIR) spectra comparing our clam and purchased calcite data with standards for aragonite and calcite [6]. Purchased calcite has characteristic bands at 1396 cm^{-1} (ν_3), 872 cm^{-1} (ν_2), and 712 cm^{-1} (ν_4), in agreement with the calcite standard (RRUFFID R040070; ν_3 at 1395 cm^{-1}, ν_2 at 872 cm^{-1}, and ν_4 at 712 cm^{-1} [6]). Clam specimens are aragonite, with ν_3 at 1447-1460 cm^{-1}, ν_2 at 857-854 cm^{-1}, ν_4 at 712-713 cm^{-1}, as well as two distinct aragonite bands at 1083 cm^{-1} (ν_1) and 700 cm^{-1} (also ν_4), all of which are consistent with what is reported for aragonite (RRUFFID=R040078 [6]). Additional examples are shown in Figure 3.14, with comparisons among heated samples in Figure 3.15. Comparisons among different mixtures before and after aqueous suspension are shown in Figure 3.16.
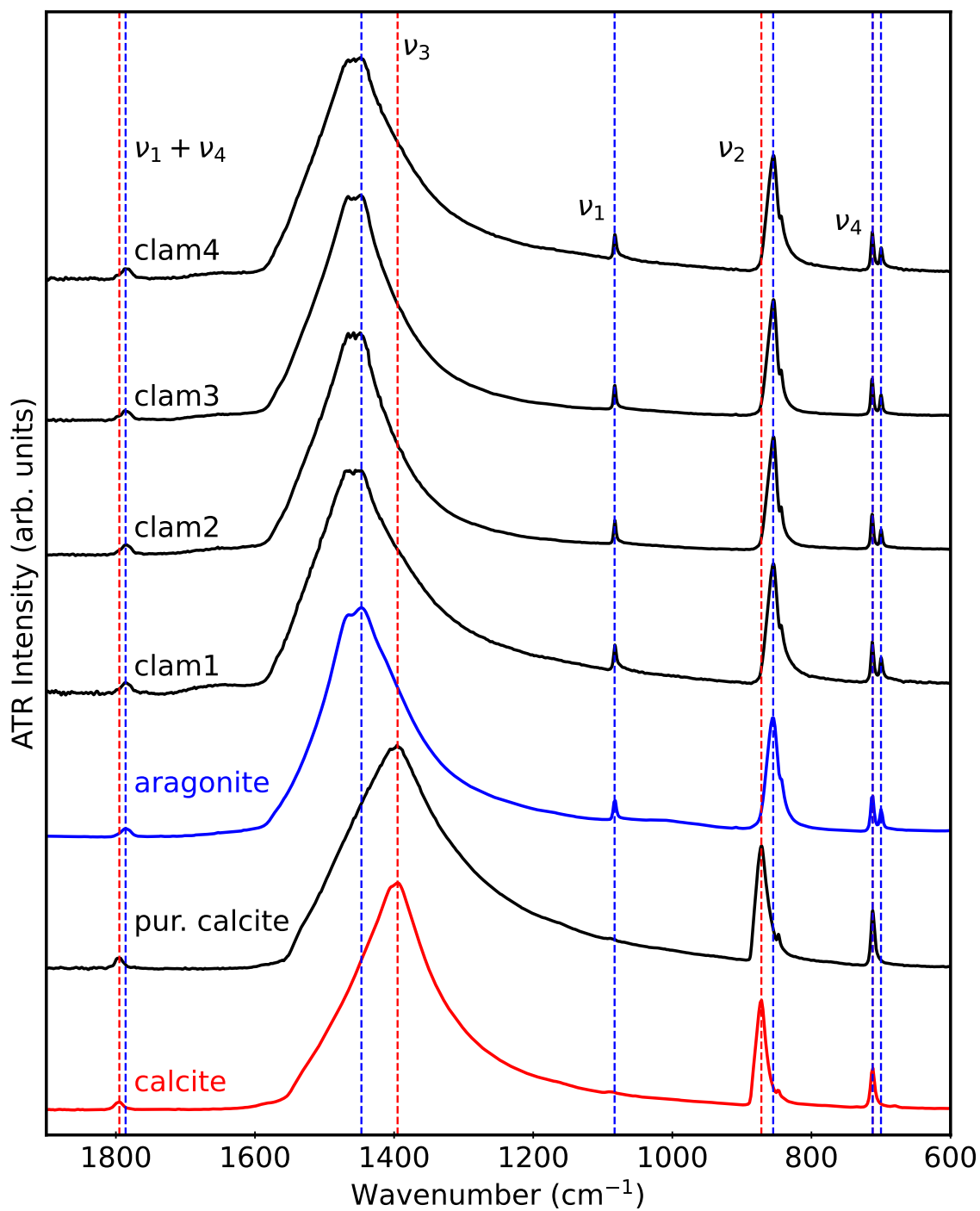
Figure 3.13: Representative ATR-FTIR spectra for clam specimens and purchased calcite (all in black) compared with calcite (RRUFFID R040070, in red) and aragonite (RRUFFID R040078, in blue) standards from the RRUFF database [6]. Labelling conventions for clam samples are described in Table 1 in the main text.
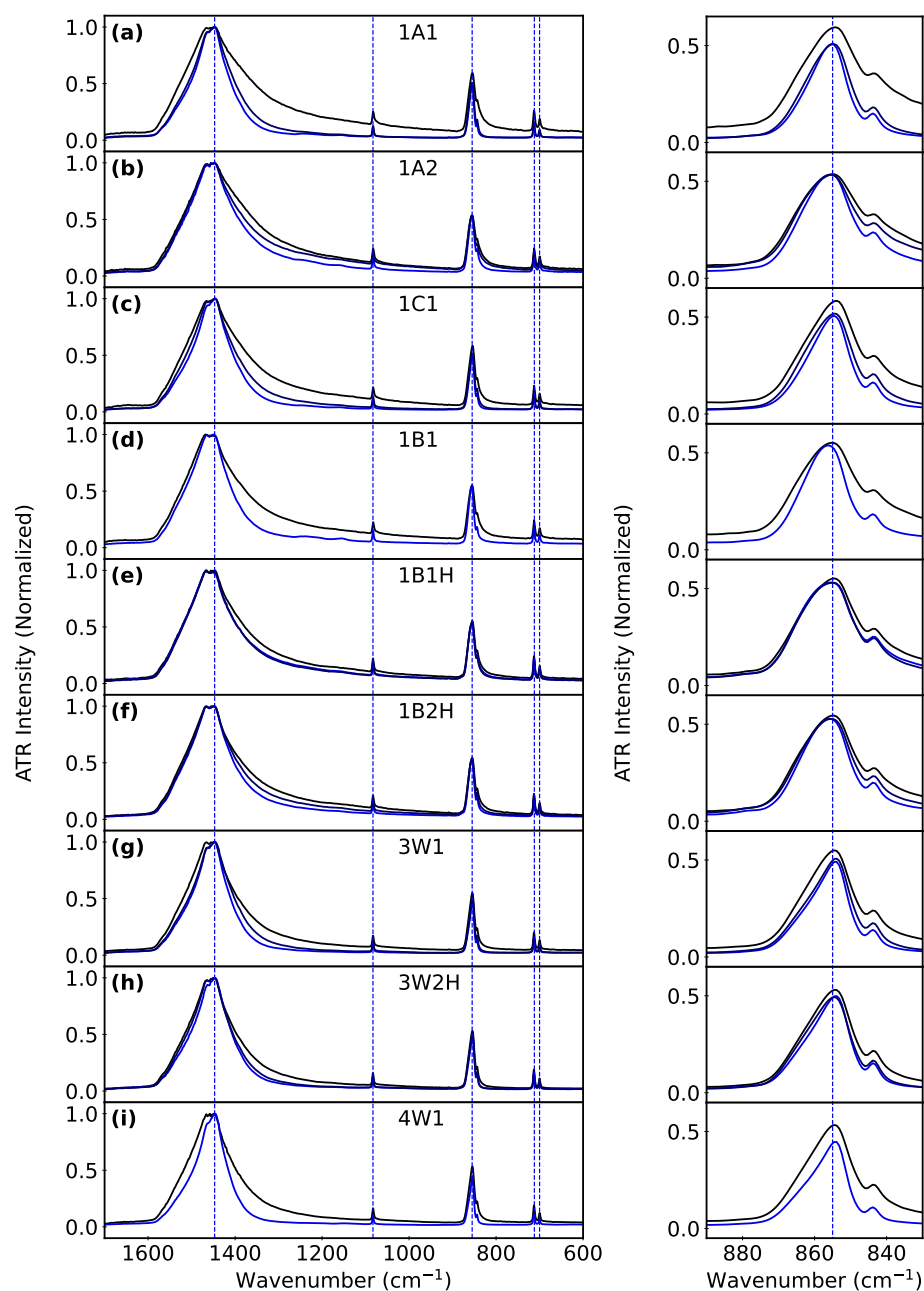
Figure 3.14: Representative ATR-FTIR spectra for clam specimens compared with an aragonite standard (RRUFFID R040078 [6]): each panel (a)-(i) shows three spectra for each specimens: before stirring (black), after two days of stirring (dark blue) and after one week of stirring (light blue) in an aqueous suspension. Vertical blue lines denote the aragonite standard's peak positions. Sample labelling conventions are consistent with those described in Table 1 in the main text: 1A1, 1A2, 1C1, 1B1 refer to different parts of unheated Clam 1; 1B1H, 1B2H refer to different parts of heated Clam 1; 3W1 refers to unheated Clam 3; 3W2H refers to heated Clam 3; 4W1 refers to unheated Clam 4.
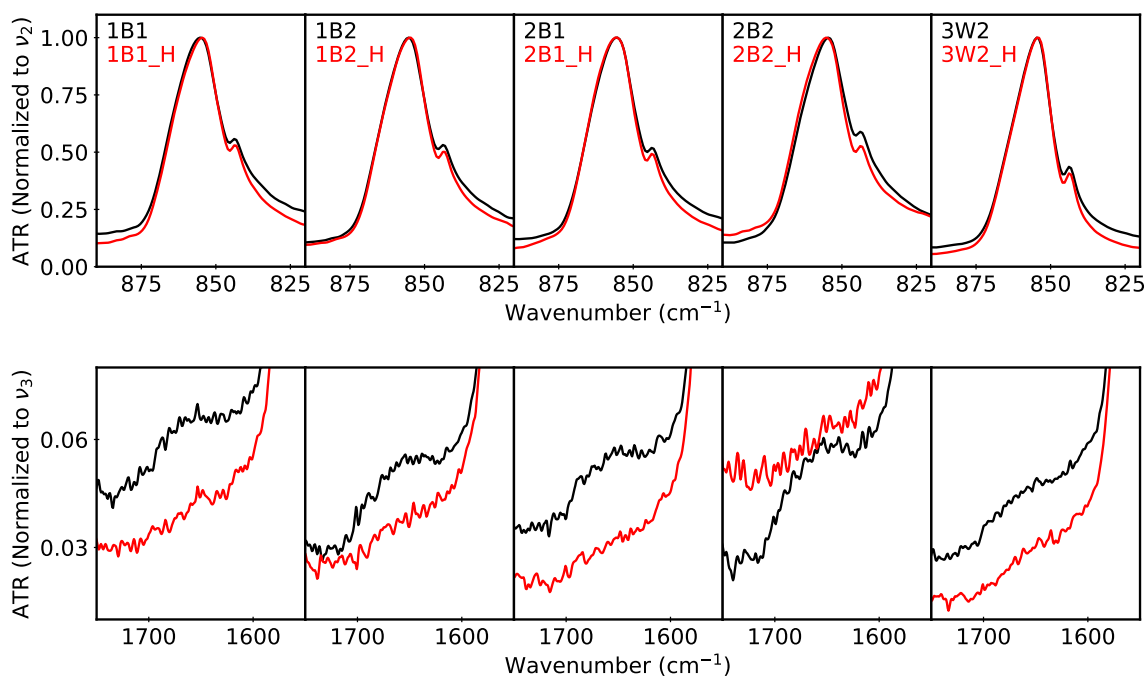
Figure 3.15: Representative ATR-FTIR spectra for different clam specimens before (black) and after (red) heating, emphasizing the ν_2 region (top row) and amine region (bottom row). Sample labelling conventions are described in Table 1 in the main text.
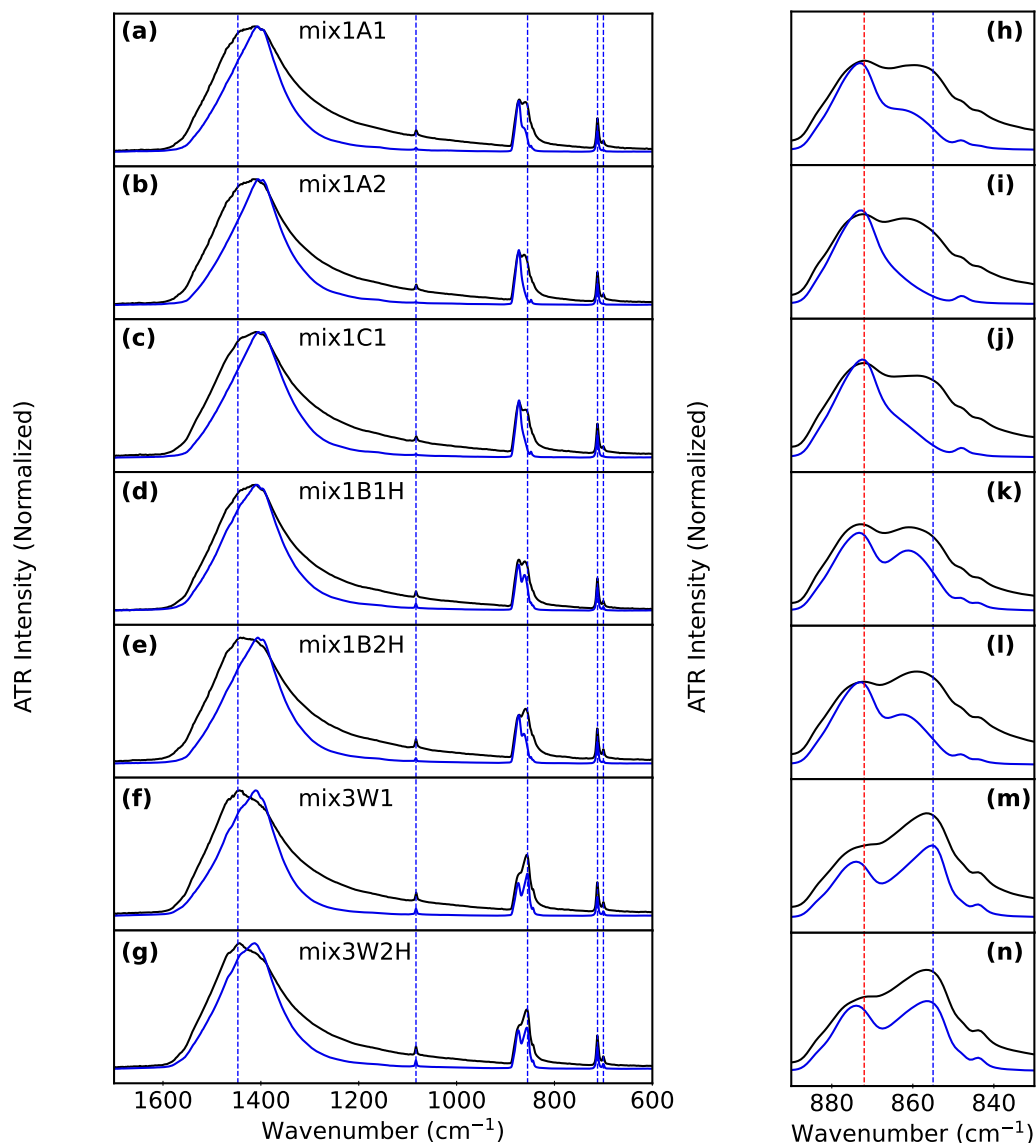
Figure 3.16: Representative ATR-FTIR spectra for 1:1 mixtures of clam powder and purchased calcite before (black) and after (blue) one week of stirring in an aqueous suspension; panels in the left column (**a**–**g**) show full-range spectra, while panels in the right column (**h**–**n**) show zooms in the ν_2 region. The vertical dashed lines show the peak positions for aragonite (blue, RRUFFID R040078) and calcite (red, RRUFFID R040070) standards [6]. Sample labelling conventions are consistent with those described in Table 1 in the main text, with mixtures of purchased calcite and the following clam specimens: mix1A1, mix1A2, mix1C1, mix1B1 refer to different portions of unheated Clam 1; mix1B1H, mix1B2H refer to different portions of heated Clam 1; mix3W1 refers to Clam 3 ; mix3W2H refers to heated Clam 3.

3.6.3 Additional X-ray diffraction data comparisons

Figure 3.17 shows representative powder X-ray diffraction (PXRD) data for our specimens compared with aragonite (PDF 980000098) and calcite (PDF 980000141) [3]. Figure 3.18 shows a zoom that highlights a weak calcite peak that grows after the samples are heated.
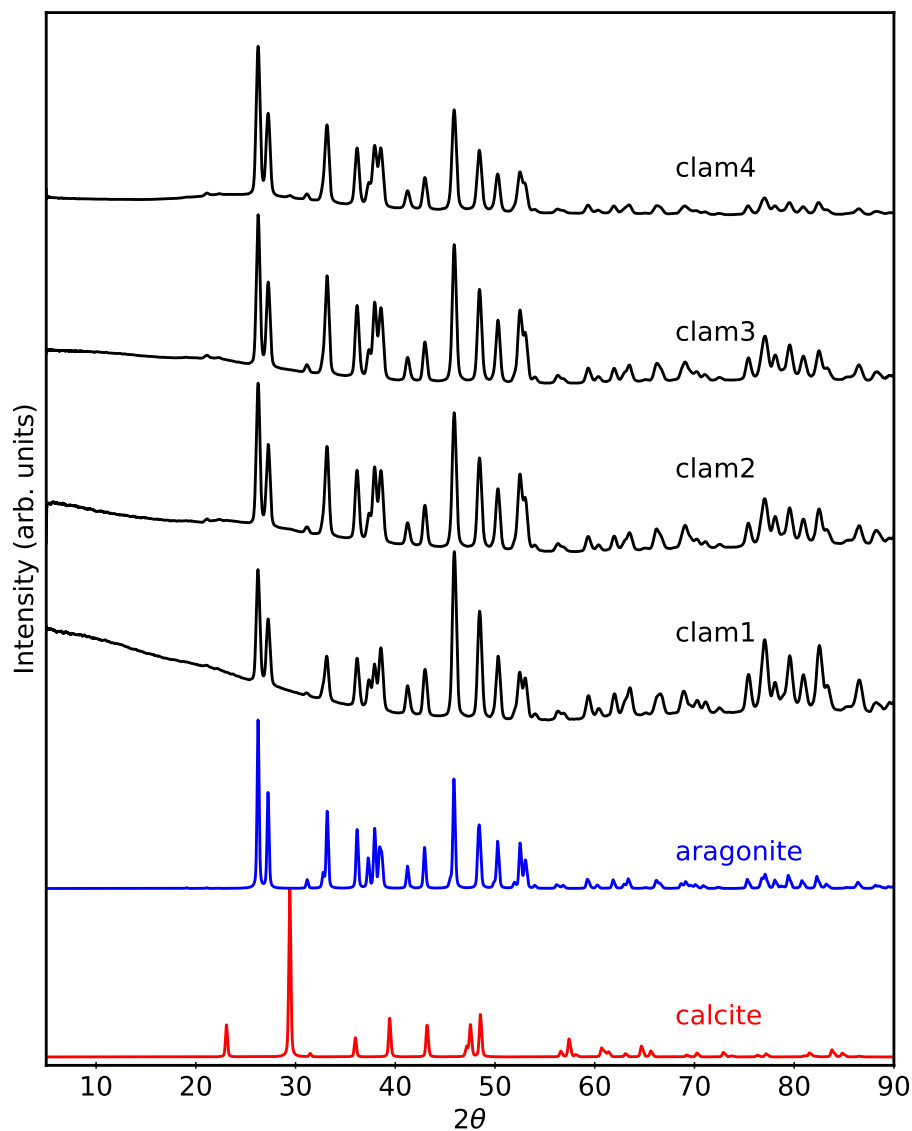
Figure 3.17: Representative PXRD data for clam specimens (black) compared with standards of aragonite (PDF 980000098, in blue) and calcite (PDF 980000141, in red) [3]. The specimen labels are defined in Table 1 in the main text.
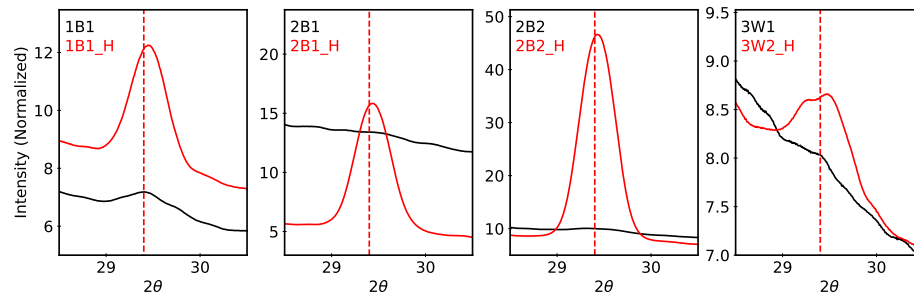
Figure 3.18: Representative PXRD data for clams that emphasize the growth of a weak calcite peak after heating. Data before heating are shown in black; data from heated samples are shown in red. The red vertical line shows the 104 peak position for a calcite standard (PDF 980000141) [3]. The specimen labels are defined in Table 1 in the main text.

Chapter 4

Biogenic and geogenic carbonates aqueous suspensions

This chapter is intended for a broader scope of experiments, still in the carbonate mixture aqueous suspensions. We intend to reproduce some of the results from Chapter 3 and test other mixture configurations with different carbonate sources. In this chapter, clams and Oyster 2 samples were procured by Dr. Meghan Burchell (Department of Archaeology), crabs by student Jake J. Breen (Department of Chemistry), mussels, Oyster 1 and rocks by Dr. Kris M. Poduska (Department of Physics & Physical Oceanography) and coral by Dr. K. C. K. Ma (Department of Ocean Sciences). Dr. Kris M. Poduska helped with theoretical background, methodology, revision and edition.

4.1 Introduction

As discussed earlier, $CaCO_3$ has three polymorphs: vaterite, aragonite and calcite, ordered by their stability, respectively. Knowing that aragonite and calcite are frequently found in a biogenic or geologic context, expanding the experiments of Chapter 3 to other sources seems a reasonable next step to validate its results. The research conducted by B. Gao and K. M. Poduska [33, 11, 12] and Chapter 3 stands as the precedent for the studies carried out in this chapter.

Some takeaways we must keep in mind from previous students' lab-synthesized carbonates and Chapter 3 biogenic mixtures in different solutions from their research are:

- Aragonite mixed with low amounts of calcite produces a dis-rec that increases calcite over time. Having a more even aragonite : calcite starting mixture ratio leads to more aragonite conversion (over the usual 1 week span.)

- Whenever the aragonite powder is suspended in water, there is some dissolution and recrystallization as calcite.

- Stirring triggers more dis-rec than an unstirred suspension monitored for the same one-week period.

- Phosphate compounds prevent aragonite recrystallization into calcite.

- 1 week stirred suspensions of butter clams do not show dis-rec, whereas adding purchased calcite triggers faster phase conversion.

- There are no noticeable differences across butter clam parts.

- Thermal organic removal did not seem to accelerate the process; instead, it might have slowed it down.

In this chapter, we characterize the samples similarly to how we did in the previous chapter. We additionally use ATR-FTIR to qualitatively assess the presence of detectable amounts of inorganic and organic substances in calcium carbonate structure without the necessity of recurring to the other techniques. Mg^{2+} substitution in the calcite structure leads to a shift to higher energies of the ν_4 to 728 cm^{-1} (dolomite) and 750 cm^{-1} (magnesite) [72]. On the other hand, Sr^{2+} substitution in aragonite's structure influences the ν_1 band more visibly, making it shift to a lower wavenumber [65]. Phosphates (PO_4^{3-}), another of the most representative co-molecules in the carbonates structures, have apatites bands around ν_3 1020-1120 cm^{-1}, ν_1 960 cm^{-1} and ν_4 560-600 cm^{-1} [113, 96]. Chitin is a common molecule in the organic matrix of many carbonated shells that shows typical amide and sugar bands (CO, C-OH) around 1650-1550 and 1300-1100 cm^{-1}, respectively [114, 96].

We synthesized aragonite to test our own non-biogenic carbonates polymorphic pump and measure the heating effects performed for butter clam in an organic-free sample. We cover the experiments related to natural polymorphic mixtures like blue mussels and some oyster specimens mentioned in the previous chapter. We repeated the mechanically made suspensions of biogenic aragonites plus purchased calcite with other species. We explore a more realistic scenario where both carbonate sediments are biogenic in origin. We also studied the scenario where the calcite is biogenic, and aragonite is lab synthesized. Finally, we explore the effect dolomite-like rock could have on synthetic aragonite dis-rec.

4.2 Materials

4.2.1 Sample collection and preparation

We have collected various natural samples, from geological to biogenic, to test the dis-rec behaviours. No specific criteria were used for sample collection; some came

from the shore, bottom of the ocean, mainland, or grocery store. Specific sample results will contain where they are from and if we collected them or another research group did. The samples are urchins, grocery oyster shells, dead collected oyster shells, sea snails, mussels, butter clams, coral, crab and dolomite rocks.

In some experiments, synthesized $CaCO_3$ is used as a control. To achieve the phase wanted, we employed a well-established aqueous precipitation reaction to synthesize $CaCO_3$ powder [45]. Sodium carbonate (Na_2CO_3) and calcium chloride ($CaCl_2$) salts (Sigma Aldrich) were dissolved in ultrapure water (Barnstead Nanopure, 18.2 MΩ·cm) to make 60 mM solutions. The carbonate solution (25 mL) was added gently to the chloride solution (25 mL) within 3 minutes while the solution was stirred at 400 rpm. As a result, a fine white calcium carbonate precipitated. The reagent solutions were warmed up to 96 °C to achieve aragonite as the primary polymorph. Purchased $CaCO_3$ (ALFA AESAR 99 %) was used as reference pure calcite in other mixtures.

Every natural sample was first, if needed, cleaned with ultrapure water (Barnstead Nanopure, 18.2 MΩ·cm) and sonicated to eliminate attached dirt and remaining biological materials. Then, they were scraped in different spots to identify the most relevant polymorph by ATR-FTIR. That way, we could separate the natural samples with a single phase from those classified as "natural mixtures". Finally, every sample was hand-ground individually using a mortar and a pestle until a fine powder was obtained. Oysters were exceptionally hard, so before hand-grinding, a portion of the sample was obtained by drilling (1 mm diamond-coated cylindrical drill, Minitor Co. Ltd. model No. 27304, bit No. 835104010). Attempts to grind with stainless steel ball milling were abandoned since it introduced metallic debris to the samples.

Selected samples were heated (alumina crucible in a Thermolyne 114300 furnace) for annealing and/or removing water or organic material. The heating profile was a ramp from 20 to 300 °C at 100 °C/h, holding at 300 °C for 1 hour.

4.2.2 Aqueous treatment

Two kinds of aqueous solution suspensions were investigated: single starting material and artificially made mixed material suspensions. The artificially blended material consisted of powder mixtures of always a 50% - 50% by mass of polymorph X to polymorph Y. The powder mixture was ground to achieve better homogeneity and from where a pinch ($< 5mg$) was subtracted using a spatula for pre-aqueous suspension ATR-FTIR screening. Aqueous suspensions are prepared between the mixture of powders or the naturally occurring mixtures with either water (ultrapure, Barnstead Nanopure, 18.2 MΩ·cm) or tap water in a glass-capped vial. The total powder-to-solution ratio was always maintained at 10 mg/mL, being 100 mg: 10 mL the most repeated setup. The powder-solution suspension was ultrasonicated for 2 minutes. Some suspensions were stirred using a magnetic bar at 400-1000 rpm to study the effects of mass transport. In one set of suspensions, at different chosen periods (1 hour (1h), 3 hours (3h), 2 days (2d), 3 days (3d), 1 week (1w), 3 weeks (3w), 1 month (1m) or 3 months (3m)), we shook the vial and took three 1 mL aliquots of suspension to Eppendorf vials. Then, the Eppendorf vials were centrifuged, the supernatant was returned to the glass vial, and the powder was left to dry before ATR-FTIR. In another set of experiments, instead of subtracting aliquots, the treatment was untouched until the final chosen time, and afterwards, the supernatant was dumped. Finally, the mixed powder was left out to dry for at least a day.

4.3 Characterization parameters

We utilized attenuated total reflectance Fourier transform infrared (ATR-FTIR) spectra obtained using a Bruker Alpha spectrometer with a diamond ATR crystal to evaluate phase purity. This technique is well-suited for distinguishing between different polymorphs. By analyzing the changes in relative peak intensities, we could semi-quantitatively assess the proportions of various phases in multi-phase samples before

and after treatment [72]. The spectra were collected across the mid-infrared (mid-IR) range, spanning from 4000-400 cm^{-1}, 36 scans with a resolution of 2 cm^{-1}. ATR-FTIR measurements have a penetration depth of approximately 1 μm, which implies that the spectra encompass contributions from both the surface and bulk of the samples. Before pouring the mixture into the aqueous treatment, a small portion of the powder was separated to do at least three pre-treatment ATR-FTIR measurements. In the same way, after treatment, the mixture was measured in triplicate. Polymorph assignments were based on comparisons with ATR-FTIR spectral standards (RRUFF project [6]).

Powder X-ray diffraction (PXRD) data for some starting materials were collected at room temperature with a transmission geometry (Rigaku (The Woodlands, TX, USA) XtaLAB Synergy-S X-ray diffractometer, Cu source) using a glass capillary holder. We refined lattice constants for each pattern using whole pattern fitting (JADE 10 software [1]), and compared them with aragonite and calcite unit cells reported in the PDF-2 databases [3]. Due to the relatively small sample volume available for each clam portion, our analyses showed that these PXRD data were unreliable for quantifying the relative amounts of calcite and aragonite in mixed-phase samples.

For elemental analysis (Perkin-Elmer 5300 DV ICP-OES), a subset of powders that were used for the PXRD analyses (where there was sufficient mass remaining) were dissolved in acid (HNO_3:HCl 4:1) for 1 hour, then diluted to 1%. These solutions were then analyzed for the following elements that are commonly found in biogenic aragonite: Ca, Mg, Sr, Ba, Fe.

4.3.1   ATR-FTIR data processing

Most samples can be inspected without needing any special processing, particularly the starting materials. However, when comparing samples before and after solution

suspension, data processing is needed to plot ATR-FTIR spectra more comparably between them. A minimum-maximum normalization is used to compare features across samples and within samples before and after treatment. It is a rapid way to detect peak intensity changes relative to the maximum and differences in bandwidth, symmetry, and peak position. Normalization to a specific vibration band is often preferable to assess the changes in polymorph mixture intensity ratios before and after suspension/heating treatment. This could be done in two regions: the ν_2 (900-820 cm^{-1}) or the ν_4 (730-650 cm^{-1}). In the ν_2 region, we arbitrarily chose aragonite ν_2 as the reference band to normalize so that any intensity ratio change is expressed respectively to the aragonite band. Typically, in this region, bands overlapping commonly result in band shoulders; therefore, the first derivative was used to approximately resolve peak position and intensity. In the ν_4 region, the peak at 700 cm^{-1} was used for normalizing. In some cases, we can use peak intensity ratio versus time to display the relative changes during the experiment duration. This data analysis was performed using a Python script that we wrote.

4.4   Results

4.4.1   Starting samples characterization

ATR-FTIR

ATR-FTIR was used to rapidly characterize and categorize the principal polymorph present in the starting samples. Figure 4.1 shows a normalized representative ATR-FTIR of how we matched band positions to standards spectra from the RRUFF database [6]. Calcite (RRUFFID: R040070) has its characteristic bands at 1795 cm^{-1} ($\nu_1 + \nu_4$), 1395 cm^{-1} (ν_3), 872 cm^{-1} ($\nu_{2\,C}$) and 712 cm^{-1} (ν_4), whereas aragonite (RRUFFID: R040078) has them at at 1786 cm^{-1} ($\nu_1 + \nu_4$), 1447 cm^{-1} (ν_3), 1083 cm^{-1} (ν_1), 855 cm^{-1} ($\nu_{2\,A}$) and 712 cm^{-1} with 700 cm^{-1} (ν_4 pair) (Figure 4.1c) [6]. These

bands are the vibrational modes corresponding to the CO_3^{2-} molecule present in these types of carbonated samples. We have symmetrical stretch (ν_1), out-of-plane bending (ν_2), asymmetric stretch (ν_3) and in-plane bending (ν_4) as the first order internal modes. Then the combination modes $\nu_1 + \nu_4$ and $\nu_1 + \nu_3$ (at ~2514 cm^{-1} not shown in Figure) are also visible. As we can notice, the calcite standard lacks of ν_1 (forbidden by symmetry) and the 700 cm^{-1} ν_{4a} bands. Furthermore, the ν_2 is shifted to higher energies with respect to ν_2 from aragonite, while ν_3 is red-shifted. As an example, the band positions of calcite (red dotted lines) and aragonite (blue dotted lines) confirm that our purchased calcite and synthesized aragonite are indeed calcite and aragonite, respectively (Figure 4.1b). The 4000-2000 cm^{-1} region only contains the weak $\nu_1 + \nu_3$ combination band (~2514), and in some samples, a hump in the 3500-3000 cm^{-1} related to hydration water.

Figure 4.1a shows a natural calcite plus aragonite mixture (Oyster 1) found from scraping the inner part shell of a grocery store oyster. In the graph, the presence of both $\nu_{2\,A}$ and $\nu_{2\,C}$ bands at 855 and 875 cm^{-1}, respectively, is effortlessly recognizable along with 1083 cm^{-1} ν_1 and the 713 cm^{-1} with the 700 cm^{-1} ν_4 pair. This mixture has resulted in an elusive calcite plus aragonite proportion since we have not been able to find it in any other sample at that magnitude. We can say that there are significant amounts of calcite and aragonite by looking at their ν_2 bands intensities [72].

Detecting Mg^{2+} in calcitic crystal structure using ATR-FTIR is also possible. As the Mg% increase in the calcite structure, ν_4, ν_3 and in less extension ν_2 bands shift to higher wavenumber, where theoretically, ν_4 follows the linear trend: ν_4 (cm^{-1}) = 39.40 X_{Mg} + 712.20 (X_{Mg}: Mg molar fraction) [115]. Figure 4.2b Dolomite standard (50% Mg) has a ν_4 blueshifted to 726 cm^{-1} and Magnesite standard (100% Mg) up to 748 cm^{-1} (RRUFFID: R050129, R050443 [6] respectively). Rock1 (Figure 4.2a) is a Mg-present representative spectra showing peaks at 1424 cm^{-1} (ν_3), 877 cm^{-1} (ν_2), 728 cm^{-1} (ν_4), thus closely matching dolomite standard [6]. A slightly blueshifted ν_4 in Rock1 compared to the dolomite standard could indicate a higher than 50% Mg
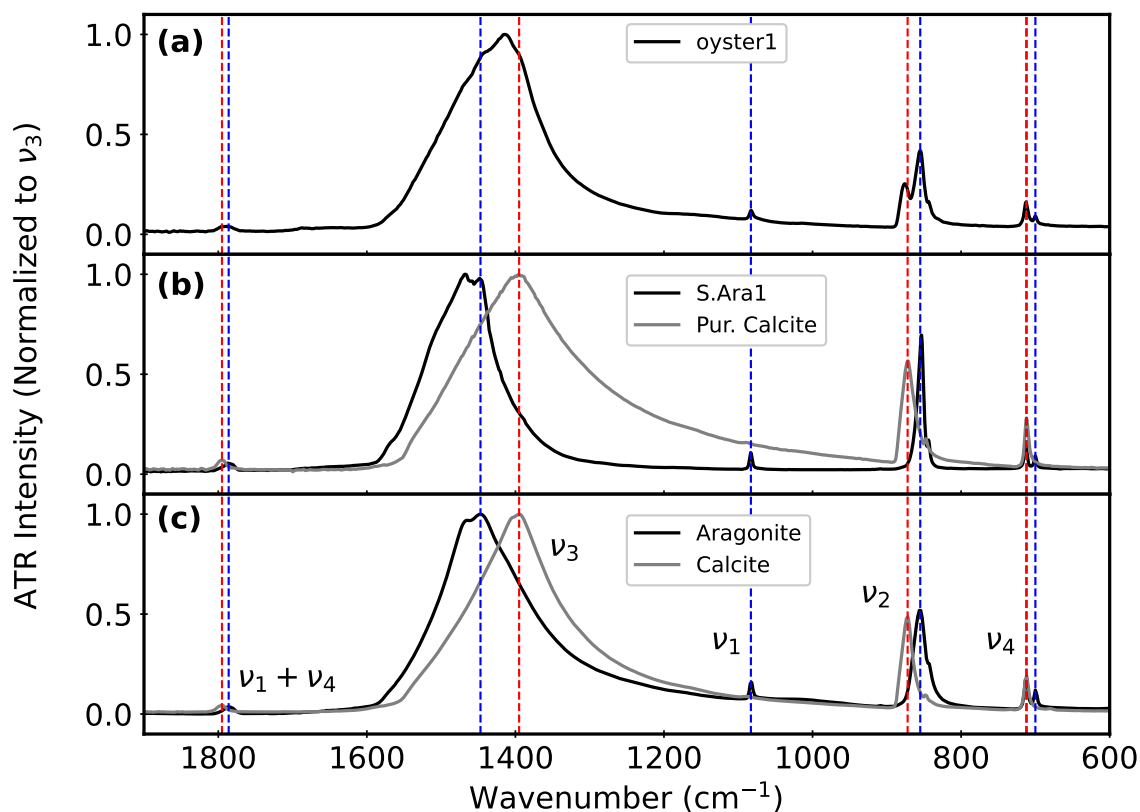
Figure 4.1: (a) Oyster 1 natural mixture (black line). (b) Purchased calcite (Pur. Calcite grey line) and synthesized aragonite (S.Ara1 black line). (c) Database standard spectra of calcite RRUFFID: R040070 (grey line) and aragonite RRUFFID: R040078 (black line). Representative ATR-FTIR normalized spectra. Blue and red vertical dashed lines show peak positions for standards of aragonite (RRUFFID R040078) and calcite (RRUFFID R040070), respectively. [6].

concentration. Rock1 also has a weak overlapped peak at 713 cm^{-1}, which could indicate a lower Mg-calcite secondary phase. Notice that, according to Mg substitution ν_4 linear trend [115], to detect a displacement from the 712 cm^{-1} to 713 cm^{-1}, at least 0.02 moles (0.49wt%) of Mg must be contained in the calcite structure. According to this, biogenic samples like crabs show hints of Mg substitution owing to a broad and displaced ν_4 at 714 cm^{-1} (Figure 4.3c, purple hatched area). Moreover, 1wt% Mg presence in crabs has been detected and described by others [116].
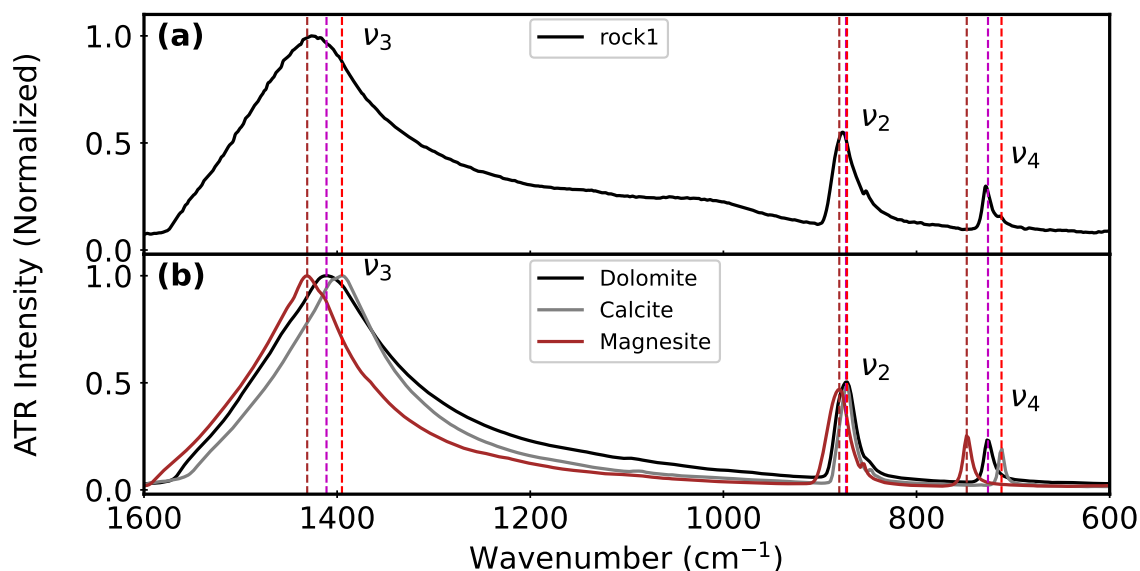
Figure 4.2: (a) Calcite (grey line), dolomite (black line) and magnesite (brown line) standards shows how normal vibrational modes shift to higher wavenumber (RRUF-FID: R040070, R050129, R050443 respectively). (b) Representative spectra of a dolomite sample (rock1 black line). Red, magenta and brown dashed lines represent characteristic band positions of calcite, dolomite and magnesite standards [6].

Biogenic samples usually have organic matrices and phosphates that can be detected by ATR-FTIR, but there is a wide range of organic co-compounds in these biogenic carbonates. Thus, identifying the specific organic molecules could be challenging. Nonetheless, having previous information from literature about the samples can help to at least narrow down what organic families may be present in them. Our butter clams show a hump in 1600 cm^{-1} that could be related to amide/amine protein bands (amide I $\sim$1650 cm^{-1}, amide II $\sim$1545 cm^{-1} [95]) (See Figure 4.3a, grey hatched area). Oyster samples (Oyster 2) also show a hump in the same region that could be related to proteins, but also a bump in 1100-1200 cm^{-1} region related to the polysaccharides present in this type of oyster structures [117, 118] (Figure 4.3b, grey hatched areas). The presence, in the oyster, of a band where the ν_1 would appear is more likely due to substitutional impurities like Mg^{2+} or Sr^{2+} that may allow this forbidden by symmetry vibrational mode than to phosphate compound since there

is no evidence of the ν_4 bands that would exhibit around 600 cm^{-1} [59, 119]. Crab samples do show big organic absorption areas in the 1600 and 1100-1200 cm^{-1} clearly identified as chitin by others (Figure 4.3c, grey hatched areas) [120, 96].
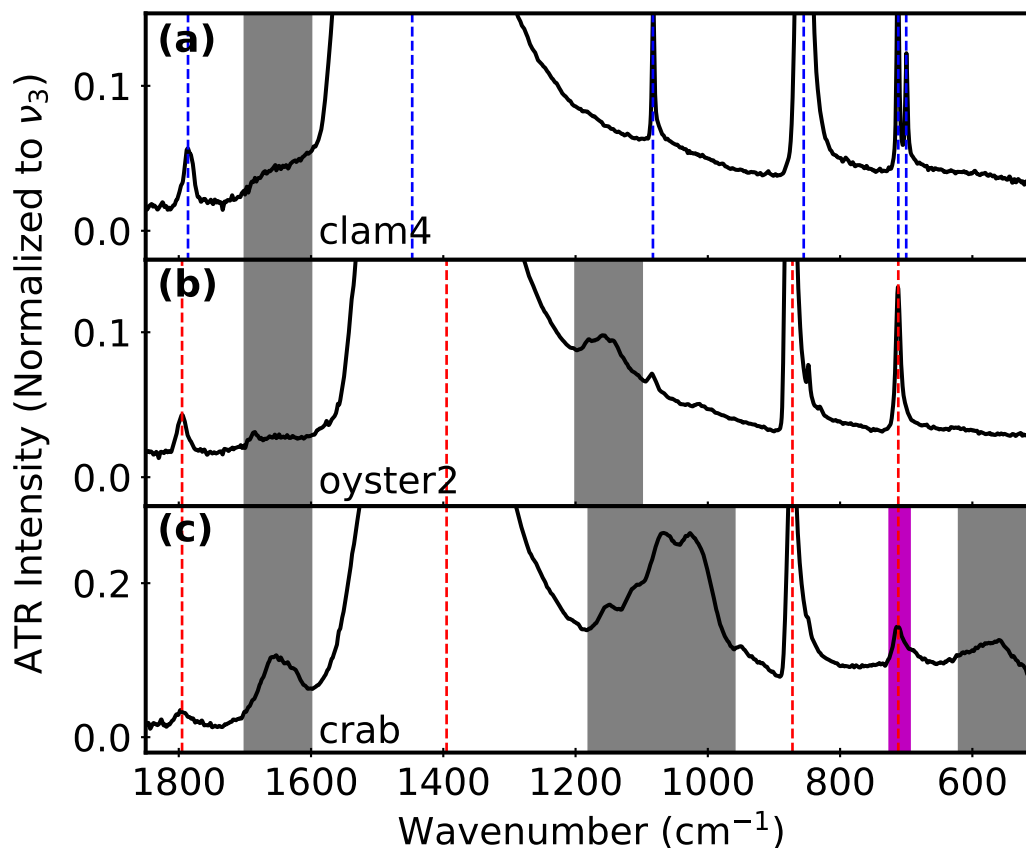
Figure 4.3: Representative normalized ATR-FTIR of Clam 4 (a), Oyster 2 (b) and crab (c). Grey hatched areas represent the organic compounds present in each and are described in the text. Purple hatched area shows ν_4 broadening. Blue and red vertical dashed lines show peak positions for standards of aragonite (RRUFFID R040078) and calcite (RRUFFID R040070), respectively. [6].

Summarizing, the ν_2 region (890-820 cm^{-1}) is what we look at when we are classifying between CaCO$_3$ polymorphs. Whenever we see two bands in this region, we can confirm the presence of both polymorphs. In the same way, we are able to qualitatively compare relative proportion changes before and after treatments by looking at the variations in the intensity ratios. Therefore, in this project, we will focus on the ν_2 region to establish the changes in polymorph ratios. Additionally, we look at

ν_4 and ν_1 to detect possible Mg^{2+} and Sr^{2+}, respectively. If possible, the presence of organic molecules was classified beforehand. Table 4.1 mentions, and Appendix A.1 shows a sample catalogue along with the identified main mineral and noticeable co-compounds.

Table 4.1: Summary of the starting material samples, origin/species, carbonated mineral detected by ATR-FTIR, and principal remarks (or co-compounds present). C: calcite, A: aragonite, D: dolomite.

Sample	Origin/Species	Carbonate mineral	Remarks
Pur. Calcite	Purchased Calcite	C	Reagent ALFA AESAR 99 %
S.Ara1	Synthesized Aragonite	A	IR-pure
S.Ara2	Synthesized Aragonite	A + some C	$\nu_{2\,C}$ weak shoulder
Clam 1	*Saxidomus gigantea*	A	proteins
Clam 2	*Saxidomus gigantea*	A	proteins
Clam 3	*Saxidomus gigantea*	A	proteins
Clam 4	*Saxidomus gigantea*	A	proteins
Coral	*Flabellum alabastrum*	A	proteins & <0.1 Sr^{2+}
Oyster 1	Grocery store	C + A	$\nu_{2\,C}$ & $\nu_{2\,A}$ even peaks
Oyster 2	*Crassostrea gigas*	C	proteins & polysaccharides
mussel1	*Mytilus edulis*	A + C	proteins
mussel2	*Mytilus edulis*	A + C	proteins
crab	*Hyas araneus*	C	chitin & <0.06 Mg $^{+2}$
rock1	Geogenic	D	Mg-calcite traces

PXRD

Powder X-ray diffraction was performed to corroborate the crystal phase of selected starting samples. The tested samples were indexed using JADE 10 software [1], resulting in matching the predominant crystal phase with the polymorphs found by ATR-FTIR (Table 4.1). Figure 4.4 left graph shows representative diffraction patterns of samples (black lines) and how their diffraction lines correspond to the indexed standard pattern from PDF-2 database, aragonite PDF 80000098 (blue solid line) and calcite PDF 980000141 (red solid line) [3]. Contrary to ATR-FTIR, PXRD shows that clams (*Saxidomus gigantea*) have a broad and weak peak in the 2theta region where

calcite's most intense diffraction line (104) would appear (e.g. Clam 4 in the right column of Figure 4.4). Furthermore, using the Whole Pattern Fitting (WPF) tool in JADE 10 software, we were able to assess that the calcite mass percent in clams was too small ($< 2\%$) to be computed by the software. Therefore, ATR-FTIR cannot detect amounts of less than a few percent. Additionally, using the WPF tool, we obtained the cell parameters of the starting materials surveyed by PXRD (Table 4.2). Clam 1 and Clam 2 PXRD were addressed in depth earlier in Chapter 3.
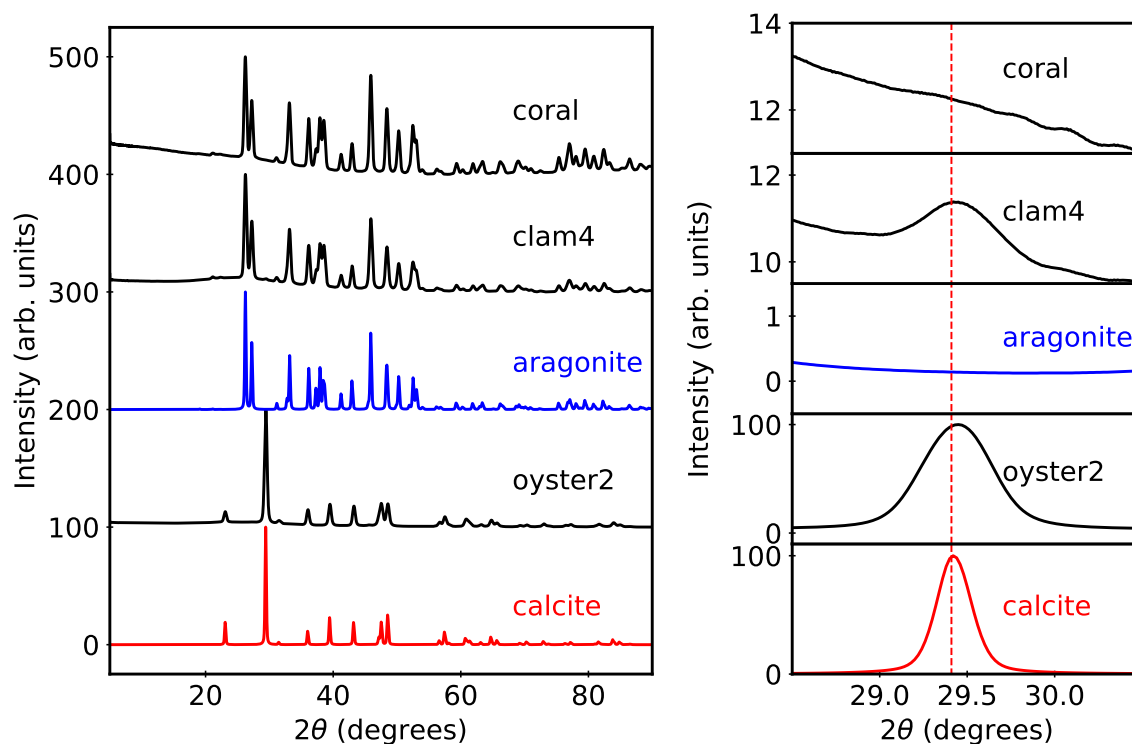
Figure 4.4: Left column shows representative PXRD data of coral, Clam 4 and Oyster 2 starting samples (black solid lines). Blue and red patterns show data for standards of aragonite (PDF 980000098) and calcite (PDF 980000141), respectively [3]. The right column panel shows a zoomed area where the strongest calcite line (104) from the calcite standard appears; the red vertical line shows the peak position for this line. Clams (e.g. Clam 4) zoomed diffraction pattern shows a slight peak where a calcite line (104) would appear, whereas other aragonitic biogenic samples (e.g. coral) do not show any calcite sign.

Table 4.2: Cell parameters summary of the samples studied by PXRD resolved using WPF tool in JADE 10 [1]. Clam 1 and Clam 2 cell parameters were reported in Chapter 3.

Sample	$\mathbf{V}$ ($\mathring{A}^3$)	$\mathbf{a}$ ($\mathring{A}$)	$\mathbf{b}$ ($\mathring{A}$)	$\mathbf{c}$ ($\mathring{A}$)
PDF 80000098	226.97	4.9616	7.9705	5.7394
coral	226.88(3)	4.9588(3)	7.9645(5)	5.7447(3)
Clam 3	226.54(5)	4.9585(7)	7.958(2)	5.7413(8)
Clam 4	226.78(2)	4.9593(2)	7.9620(3)	5.7433(2)
PDF 980000141	367.78	4.9890	4.9890	17.0620
Oyster 2	366.51(8)	4.9813(6)	4.9813(6)	17.056(2)

ICP-OES

We noticed some deviations in the cell parameters of our selected samples that were different from the standards, for which we wanted to investigate the presence of substitutional minerals by studying the elemental analysis (ICP-OES Table 4.3). As explained in the mineral subsection of Chapter 1, Mg^{2+} in calcite structure tends to contract the crystal cell. The calcitic Oyster 2 has a 0.15 wt% that if assuming all belongs to the carbonate mineral rather than to the organic matrix, the molar fraction in calcite would be 0.006 mol of Mg^{2+}. This could explain the slight contraction in the cell volume. However, to achieve a cell volume reduction down to 362.48(4) $\mathring{A}^3$, ten times (0.06) Mg^{2+} mol fraction should be present in the cell as for urchin carbonates with formula $Ca_{0.94}Mg_{0.06}CO_3$ [121]. Both aragonitic samples have lower cell parameters with respect to the reference, and since the effect of Sr^{2+} in the aragonite structure is to expand the cell volume rather than reduce it [63], we may infer that the Sr^{2+} is forming part of the organic matrix rather than the mineral. Mg^{2+} substitution in aragonitic orthorhombic structure is energetically difficult [34]; therefore, we assume it is present in the organic matrix. Iron and barium are in low concentrations with big standard deviations impeding driving meaningful conclusions from them.

Table 4.3: Elemental analysis results from ICP-OES measurements, listed in weight percent with uncertainty estimates in parentheses. Samples listed here are the same for those whose PXRD data is shown in Figure 4.4.

Element	Oyster 2 (wt%)	Clam 4 (wt%)	Coral (wt%)
Ca	37.4(3)	37.2(4)	35.3(5)
Mg	0.15(3)	0.010(1)	0.077(8)
Sr	0.07(4)	0.19(3)	0.84(4)
Fe	0.00(3)	0.007(3)	0.020(5)
Ba	0.0(3)	0.01(6)	0.0(1)

4.4.2 Sample heating

Heating of the initial samples was conducted purposely at a temperature (300 °C) lower than the thermodynamic transformation of aragonite to calcite ($\sim$468 °C) [122]. Although small percentages of calcite transformation in biogenic aragonites have been reported at slightly lower temperatures ($\sim$280 °C) but larger heating times [123], we are prioritizing burning out as much organic matrix as possible rather than having a collateral minority phase. We tested our heating regime with a selected set of examples, some of which were studied more in-depth in the previous chapter (Clam 1, Clam 2, Clam 3). As a baseline control, our synthesized aragonite (S.Ara1) was thermally treated, and no evidence of calcite increase was spotted under the ATR-FTIR in the ν_2 region, and as expected from clean synthesized aragonite, no unplanned protein bands should appear in the 1600 cm^{-1}(See Figure 4.5a,b). However, we cannot rule out calcite's presence entirely after heating due to ATR-FTIR limits, but we can say that if it is present, it is in less than a few percent (as explained in the PXRD section).

Blue mussels (mussel1) consisting of a natural mixture of calcite and aragonite lost 2.8% mass, and the powder's colour changed from light purple to white (Appendix A.2) after the thermal treatment. This mass loss is a combination of hydration water and organic compounds in the biomineral matrix. Moreover, ATR-FTIR spectra indicate a reduction in the wide peak around 1600 cm^{-1} (Figure 4.5d) [95, 96]. This
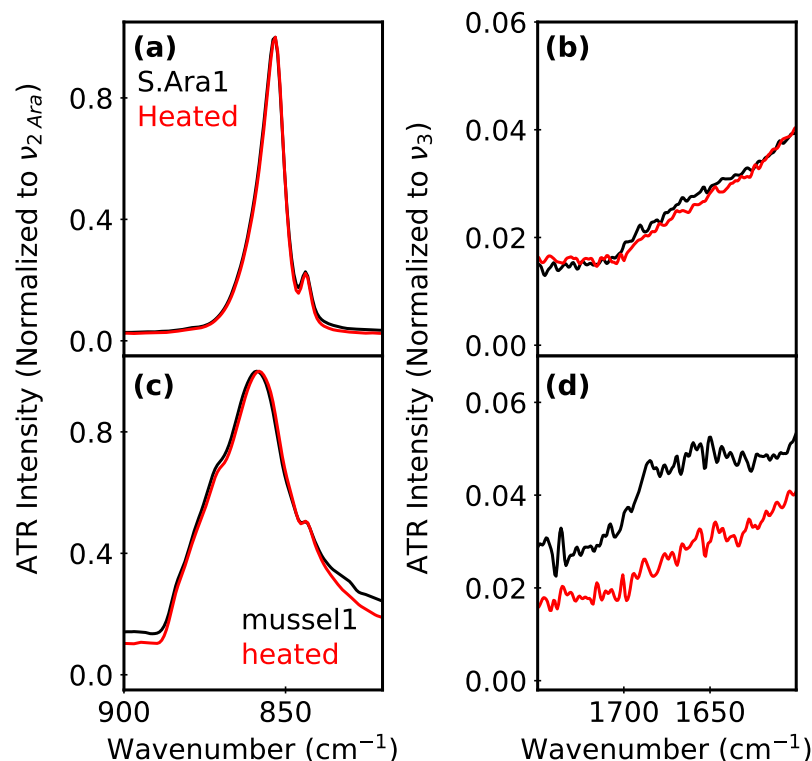
Figure 4.5: ATR-FTIR of thermally treated samples before (black solid lines) and after treatment (red solid line). (a,c) Show the spectra of ν_2 region normalized to the aragonite band of synthesized aragonite (S.Ara1) and blue mussel (mussel1), respectively. No ATR-FTIR detectable ν_2 calcite grows as a result of the treatment. (b,d) Show the spectra in the protein region (1750-1600 cm^{-1}). No protein is present in S.Ara1 (b), and a visible reduction is seen in mussel1 (d).

area typically features peaks from amides and water, suggesting that such changes are likely due to decreased protein content. No evidence of increasing calcite-to-aragonite ratio is detected as was not for the synthesized aragonite either (Figure 4.5c).

4.4.3   Aqueous suspensions: single-solid behaviour

Although the ATR-FTIR of synthesized aragonite alone in water suspension was explored by our team in previous studies [124], we repeated these experiments with our synthesized aragonites to have a baseline comparison for our thereafter mixtures. Synthesized aragonite (S.Ara2) with an unintentionally low amount of calcite (a shoulder

around 875 cm^{-1}) showed an increase in the calcite-to-aragonite ν_2 intensity ratio when suspended in water during 3 months (Figure 4.6a). This aragonite-to-calcite transformation (polymorphic pump) was tracked by ATR-FTIR screening of subtracted aliquots at different times. This behaviour followed what is expected according to calcite and aragonite thermodynamic solubility constants and resembled what was discovered by others [124, 11, 12, 31]. It is noticeable that between 1 and 3 months, this conversion seems to occur at a slower pace. When this multiphase CaCO$_3$ is exposed to moderate stirring (400 rpm) during a week, almost complete polymorphic pump can be affirmed by the acute reduction of the ν_2 aragonite band at 853 cm^{-1} while the ν_2 calcite band at 873 cm^{-1} increases (Figure 4.6b). The disappearance of the ν_1 and 700 cm^{-1} ν_4 bands give more confirmation of this (Appendix A.3). This rapid conversion is expected as increased mass diffusion generally favours both dissolution and recrystallization. When our "pure" (under the ATR-FTIR) synthesized aragonite (S.Ara1) is suspended and stirred (1000rpm) in water for a week, fast and complete transformation is also observed. Meanwhile, the same aragonite under the same water suspension conditions, but pre-heated, does not show calcite as a majoritarian phase in the same timeframe (Figure 4.6c,d). On the contrary, the heated sample still shows a predominant aragonitic phase. Our heated sample behaves more like the synthesized aragonite studied by Gao [124], although still at a faster transformation rate. A slower pumping could be related to a solid with fewer dislocations and/or imperfections after annealing. Hence, it is reasonable to infer that our as-synthesized aragonite (S.Ara1) is less ordered than the heated one, and as a consequence, dissolution proceeds faster [42, 20]. Additionally, S.Ara1 could have some small percent of collateral calcite that cannot be detected by ATR-FTIR. At the end of each synthesized aragonite suspension, the pH of the remaining supernatant is always in the 8.4-8.6 range.
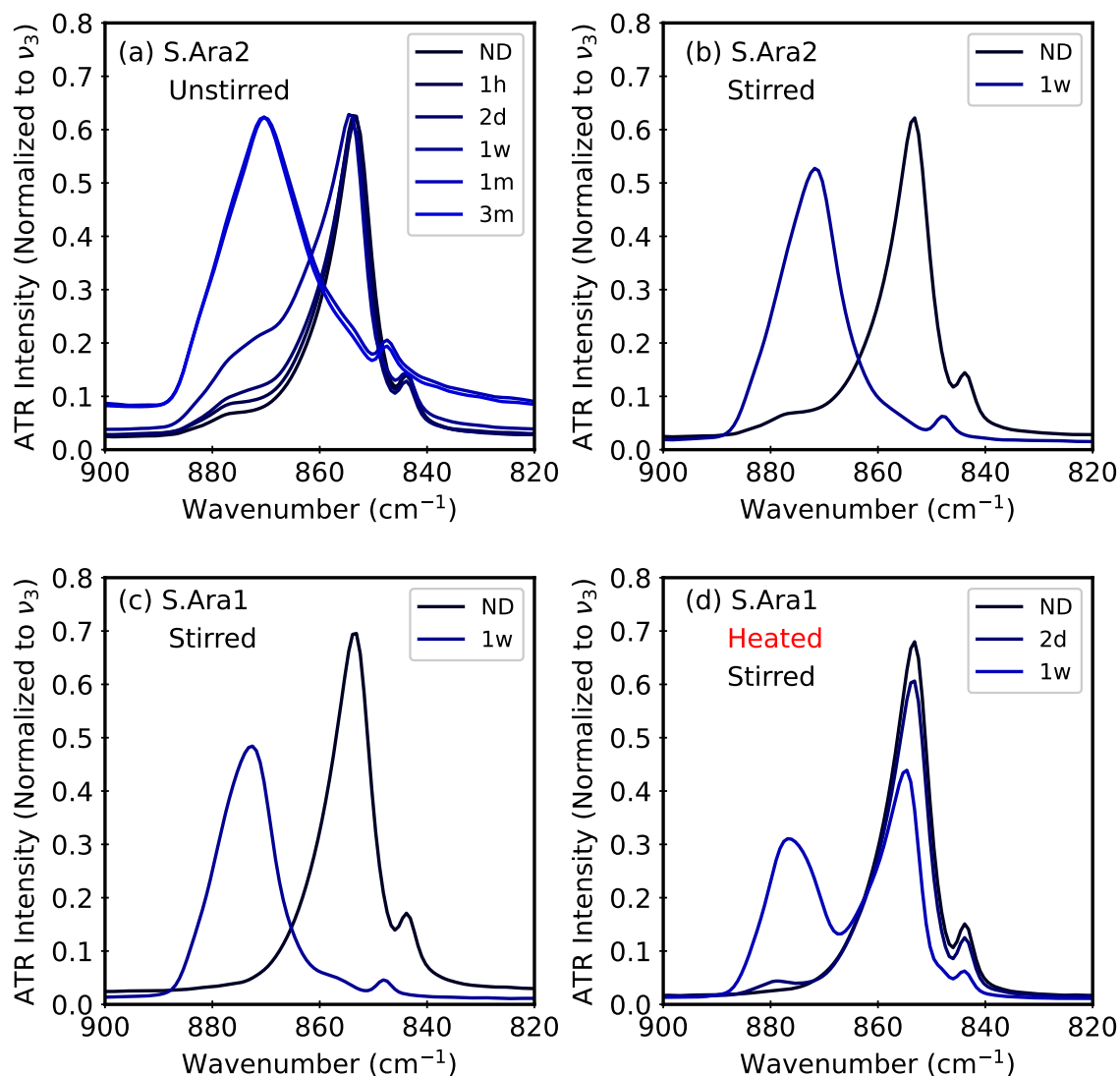
Figure 4.6: ATR-FTIR of the ν_2 region changes for synthesized aragonites water suspensions.(a) unstirred water suspension of S.Ara2 spectra over a 3-month time span. (b) Stirred water suspension of S.Ara2 in a 1-week span. (c,d) Stirred suspension of S.Ara1 and S.Ara heated for 1 week. Acronyms mean water suspension not done (ND), and after 1 hour (1h), 2 days (2d), 1 week (1w), 1 month (1m) or 3 months (3m).

The results of these single-material suspensions in water for biogenic samples diverge greatly from the synthesized aragonite. The grocery oyster shell (Oyster 1) resulted in the only natural aragonite plus calcite mixture that showed phase transition, even in a short time period (2 days) and without necessitating stirring (Figure 4.7a,f).

This result was extremely difficult to repeat since spotting such a visible mixture in oysters proved to be unachievable. Besides that sample, none of the other biogenic aragonites or biogenic natural mixtures described in Table 4.1 show any phase conversion when stirred in water over a week. Clam 4 (Figure 4.7b) does not show ν_2 calcite band naturally, but the PXRD proved (Figure 4.4) that this sample does have a small peak where calcite's strongest peak would appear. Unlike S.Ara1, stirring Clam 4 in water suspension for 1 week does not lead to polymorphic pumping (Figure 4.7b,g). Moreover, having a possible small percentage of calcite in its structure does not trigger the aragonite-to-calcite transformation. Blue mussels have $CaCO_3$ polymorphic mixtures naturally present [88, 82] as can be seen in Figure 4.7g,h. We would expect that some amount of change (increase) in the calcite-aragonite $\nu_{2\,Cal}/\nu_{2\,Ara}$ ratio should occur. We suspected that the organic matrix could have some effect in avoiding the dissolution of aragonite and recrystallization as calcite. However, the heated blue mussel (Figure 4.7d,i) shows more of the same behaviour (no change). After 1 week of stirring experiments, the supernatant pH values were 8.3-8.5, which is similar to the range of values expected according to the literature [11, 94].

The only visual change for the biogenic powders that had been suspended in water is that the ATR-FTIR peaks appear to sharpen, changing the relative intensities of the aragonite peaks in a consistent way, with the 1400 cm^{-1} peak sharpening more than the 860 cm^{-1} peak, which, in turn, sharpens more than the 712/700 cm^{-1} peaks (Figure 4.7b,c,d). We note that this is not unique to biogenic samples since, as a comparison, our purchased calcite experiences the same change in band shape (Figure 4.7e,k). Recent reports based on lab-synthesized samples show similar spectral effects [33, 12]. Other studies have attributed this sharpening to optical effects related to smaller particle sizes (in ATR-FTIR spectra) [125] or changes in scattering effects related to particle shape and proximity [70].
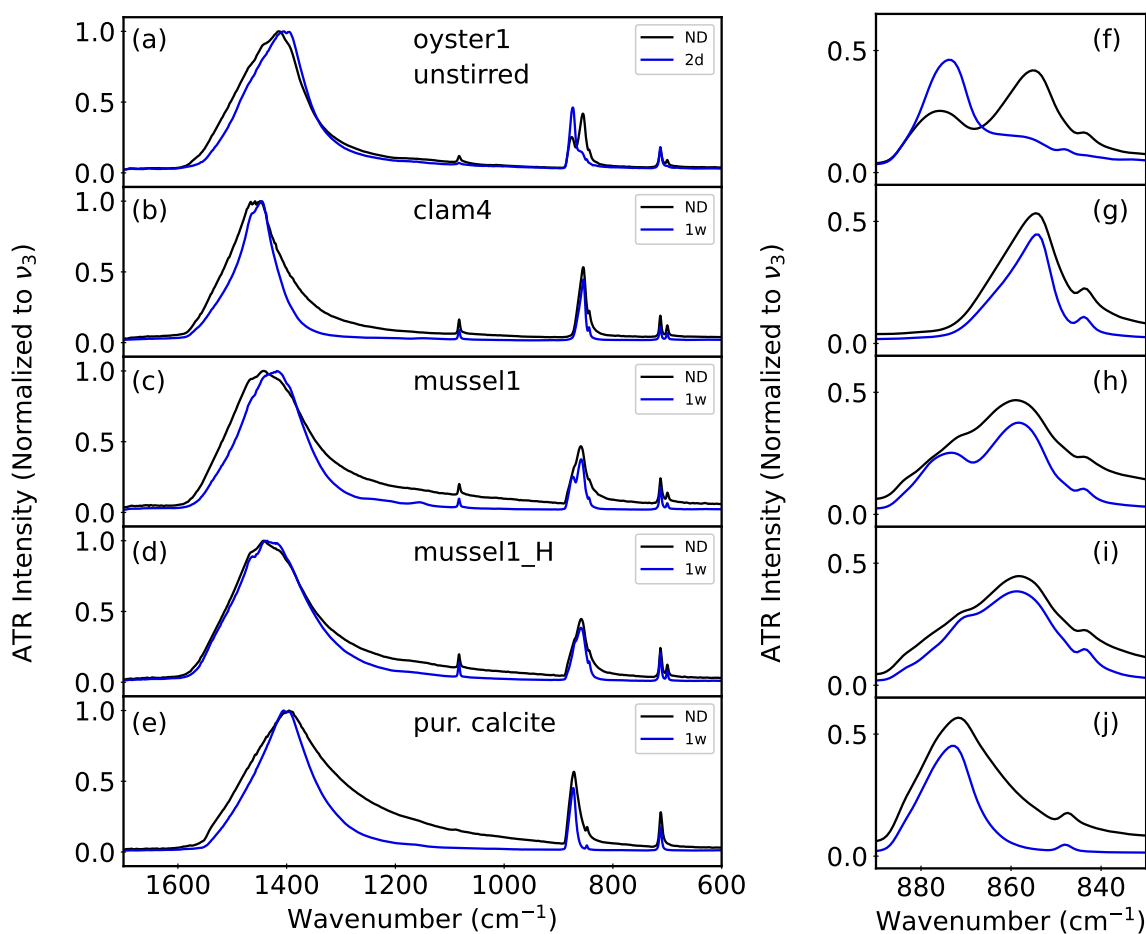
Figure 4.7: Single-solid water suspensions ATR-FTIR. The left column shows a wider wavenumber range, and the right column shows the ν_2 interest zone. (a,f) Grocery oyster (Oyster 1) unstirred before (ND) and after 2 days (2d). (b,g) Clam 4, (c,h) mussel1, (d,i) mussel1 heated and (e,j) purchased calcite before (ND) and after 1 week (1w) of stirred (1000rpm) water suspension.

4.4.4 Aqueous suspensions: polymorphic made mixtures

Long-term unstirred mixed suspensions

After testing the biogenic samples individually, we decided to mechanically make a 50%-50% mixture by mass of a biogenic aragonite sample plus a calcite-like material (either purchased calcite or biogenic calcite) and test them in unstirred suspension.

Gao 2022 [33] proved that when both $CaCO_3$ polymorphs are present in the same suspension, the 1:1 calcite-aragonite mixed proportion resulted in the one that showed the most noticeable rapid transformation from aragonite to calcite [124]. Furthermore, he used solid-state Nuclear Magnetic Resonance (ssNMR) to confirm the increase in the ν_2 calcite band in ATR-FTIR as a result of C-13 enriched aragonite recrystallizing as C-13 calcite. Table 4.4 summarizes the mixtures prepared for the unstirred experiments. To better visualize the change in the ν_2 calcite relative to the ν_2 aragonite, we normalized each spectrum such that $\nu_{2\,Ara} = 1$ and then we plotted the $\nu_{2\,Cal}$ intensity value against suspension time (Figure 4.8). Since every spectrum was recorded in triplicate, the error bars represent the standard deviation.

None of the unstirred mixtures showed a qualitatively big polymorphic pumping over the course of 1 month, whereas S.Ara2 (red dashed line) showed an almost complete conversion in the same time span. Mix1 and mix2 are purchased calcite plus Clam 4 or coral, respectively (solid triangles and squares). Although they show some recrystallization as calcite in the first instances, after a month, we cannot ensure that a noticeable transformation has occurred. In fact, they both look as if they have retroceded or stabilized. Mix3 (open squares) and mix4 (open triangles) are both mixtures of Clam 4 and Oyster 2 in order to test a more realistic mixture. Mix4 was suspended in tap water. These sample mixtures are rather interesting because instead of showing some transformation to calcite, they are steadily decreasing, or for what is the same, aragonite is increasing slowly.

Suspended mixtures with stirring

After not seeing a substantial change in the unstirred suspension of mixed polymorphs, we took a step further to push the polymorphic pumping. Stirring has shown to be a straightforward way of pushing total conversion in our synthesized aragonites (See Figure 4.6b,c). Although starting biogenic aragonite material did not show any indication of phase conversion, adding purchased calcite and stirring gives results
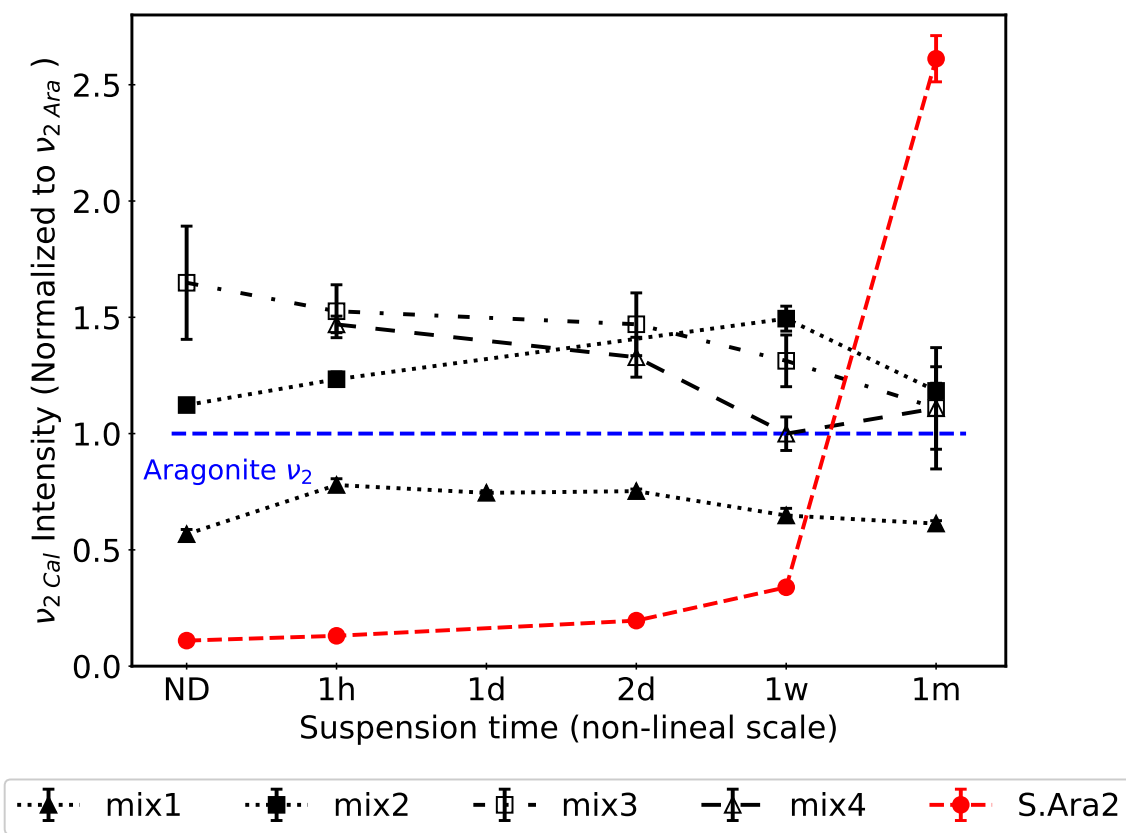
Figure 4.8: ATR-FTIR spectra of ν_2 calcite intensity change respective to ν_2 aragonite of diverse unstirred suspended mixtures. The Blue dashed horizontal line represents ν_2 aragonite with intensity equal to 1. The red plot represents the ν_2 calcite of synthesized aragonite (S.Ara2) as a baseline comparison. Mix1 to mix4 compositions are described in Table 4.4. Error bars are standard deviations, and markers represent the median.

ranging from some calcite to substantial transformation. Clam 3, either as ground or heated, showed such little increase in calcite that we cannot ensure is qualitatively significant using ATR-FTIR (Figure 4.9a,b,f,g). However, other biogenic aragonites plus purchased calcite (mix7, mix8, mix9) exhibited a polymorphic pump after 1 week of intense stirring (1000 rpm) suspension. In Figure 4.9 right panel, ν_2 aragonite normalized infrared spectra of coral (h) and mussel1 (i) mixed with purchased calcite show relatively large aragonite-to-calcite conversion. The heated mussel1 (j) also manifests some transformation, but relatively less than the unheated sample. It is noticeable that a natural mixture such as mussel1 does not show transformation on

its own, nor after organic removal through heating. However, adding pure purchased calcite triggered the dissolution and recrystallization of the mussel1 aragonite phase. The heated mussel, which has a reduced organic matrix (Figure 4.5d), does not show a significant difference in completing the conversion; in fact, it appears to delay the process.
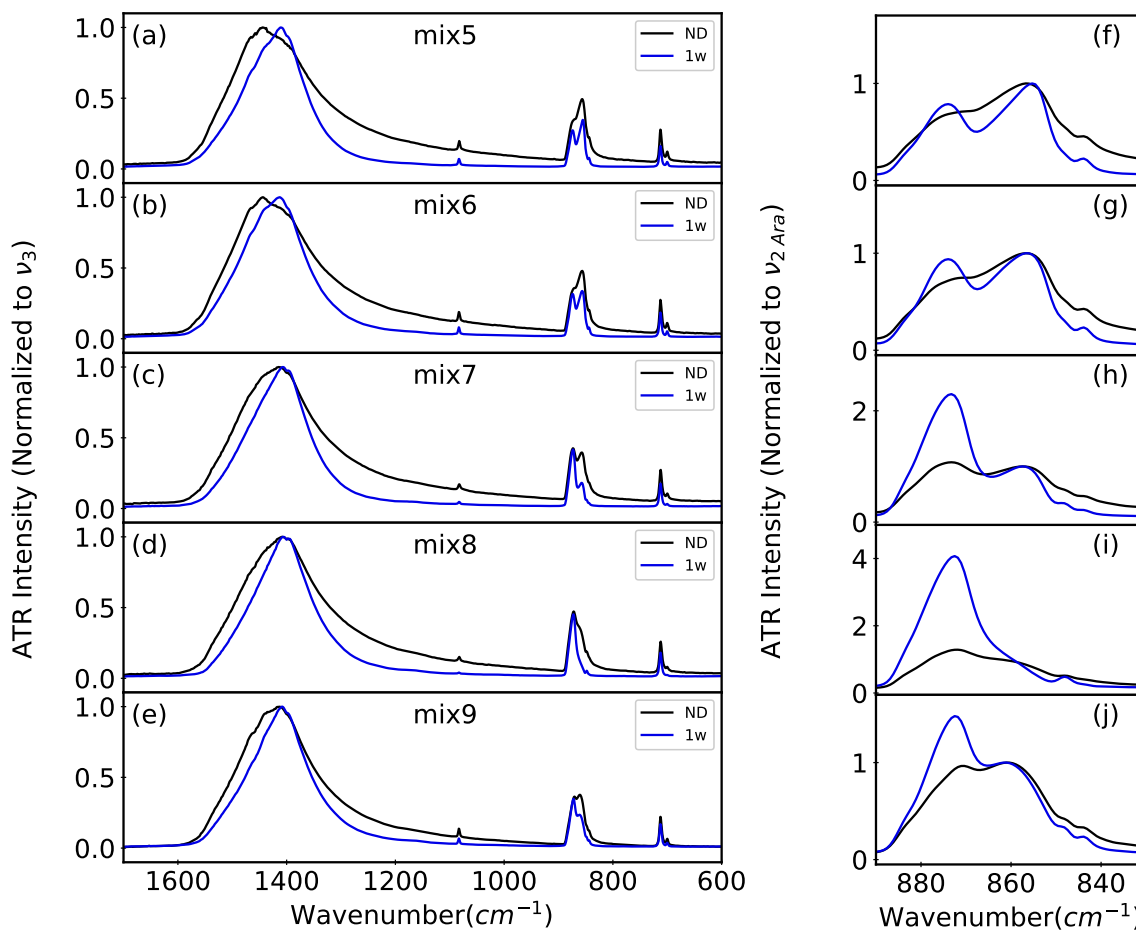
Figure 4.9: Purchased calcite plus biogenic aragonite mixtures in water suspension with stirring. Mixture constituents are described in Table 4.4. Left column panels (a-e) are normalized to the maximum absorption band ν_3. Right column panels (f-j) are zoomed in the ν_2 region and normalized to ν_2 aragonite to visualize relative calcite change.

On the other hand, we see that the result may vary when testing the effects of biogenic calcites in synthesized aragonite (S.Ara2) dissolution and recrystallization as

calcite. Oyster 2 mixture with S.Ara2 (mix10) does not impede calcite from growing (Figure 4.10a). When we compare the bands present in the S.Ara2 (blue dotted lines) and the mix10 (blue solid line) after 1 week of stirring, we can say that no visible aragonite bands are left, except for a tiny presence of the ν_1 that belonged originally to the oyster sample (Figure 4.3b). With this result, it appears unlikely that the organics are leaching out of the oyster, given that the presence of the powdered oyster in suspension with the lab-synthesized aragonite did not alter the expected polymorphic pumping behaviour. The only difference between the resulting calcite in mix10 and in S.Ara2 is the lower ν_2 intensity relative to ν_3 in comparison. This difference could be attributed to the differences in particle shape, proximity or size [125, 70]. When using a more complex biogenic calcite as it could be crab as the counterpart for the synthesized aragonite (S.Ara2), we notice a slower transformation rate (Figure 4.10b). After one week of stirring this combination (mix11), aragonite remains being the majority phase. Additionally, the contour of the chitin-related bands (1600 and 1100-1200 cm^{-1}) is more pronounced after stirring.

As we did in the unstirred suspensions, more naturally possible mixture trials between biogenic aragonites (Clam 3, Clam 4) and biogenic calcites (Oyster 2) with stirring were tested (mix12, mix13 in Table 4.4 and Figure 4.10c,d). Contrary to the mixtures with purchased calcite, where calcite transformation is unmistakable (mix7, mix8, mix9) and some with a slight increase (mix5,mix6), biogenic calcite mixed with its biogenic counterpart (mix12, mix13) does not seem to show a noticeable change to calcite crystallization. If anything, there is a slight decrease in calcite. In fact, an exploratory PXRD test of mix12 unequivocally shows that both polymorphs are largely present after 1 week of stirred suspension (Appendix A.4). Although our PXRD data quality has its limitations, as explained in Section 2.1.2 when mix12 data was assessed using JADE10 [1] and QUALX2.0 [126] software, both resulted in a mostly even proportion percent of aragonite and calcite phase (53:47 and 50.3:49.7 aragonite:calcite, respectively). Mix13 (Clam 3 + Oyster 2) shows an even more noticeable calcite
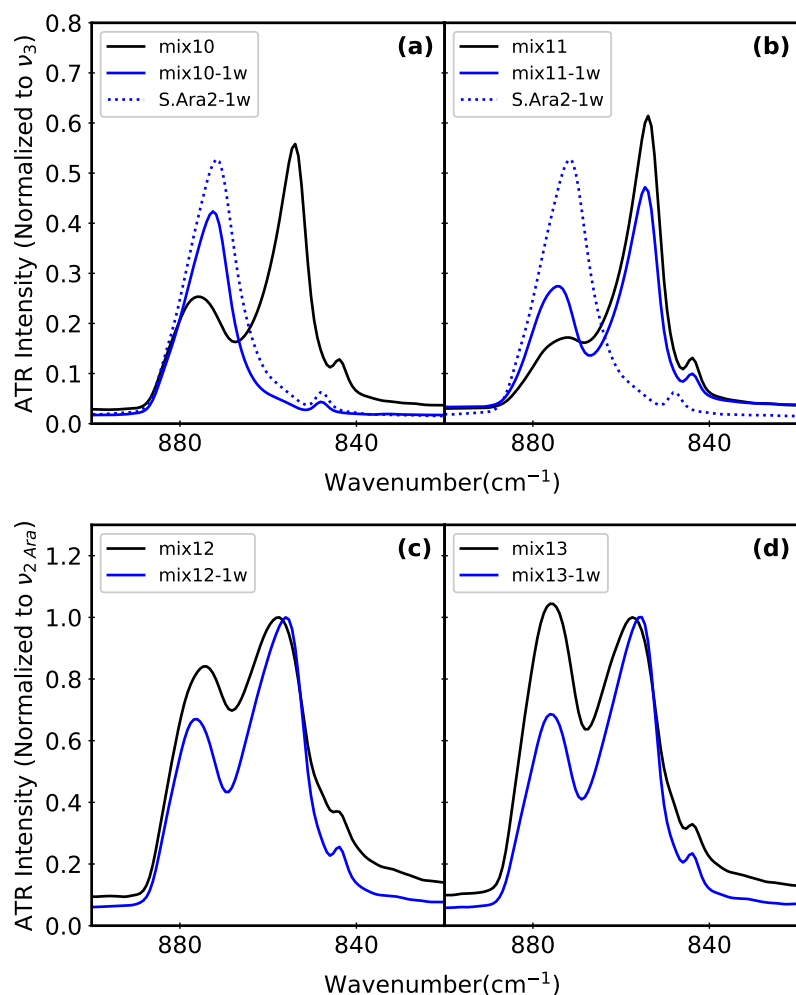
Figure 4.10: ATR-FTIR of synthesized aragonite plus biogenic calcite (a,b) and biogenic calcite plus biogenic aragonite (c,d) mixture suspensions. Mix10 - mix13 compositions are described in Table 4.4.

decrease, which could mean the same as an aragonite ν_2 band increase.

Aragonite-like plus dolomite mixture behaviour

Exploratory tests of the effect other carbonates could have in the aragonite-to-calcite polymorph transformation were also studied in this project (mix14, mix15 Table 4.4). Rock1, previously identified as Dolomite with some Mg-Calcite traces, was mixed with synthesized aragonite (S.Ara1) and/or butter clam (Clam 3).
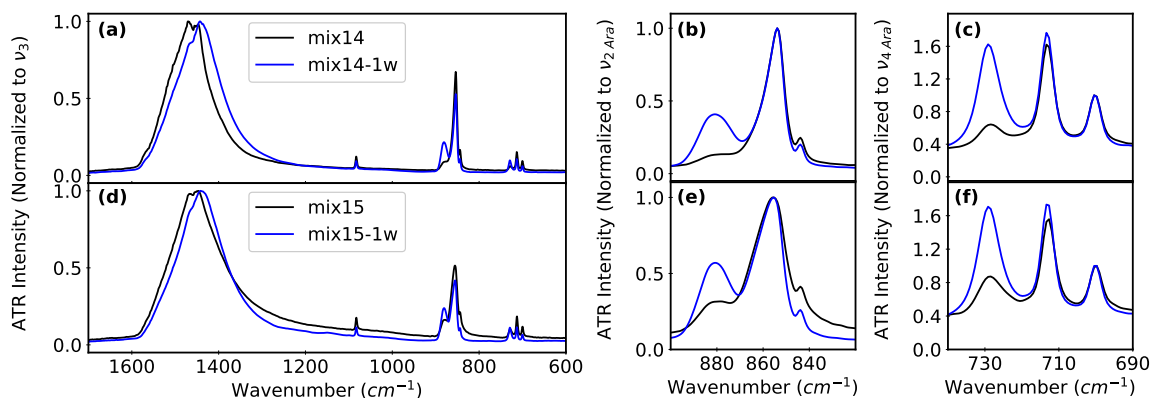
Figure 4.11: ATR-FTIR of dolomite-like plus aragonite-like water suspensions. (a) Mix14 is made with synthesized aragonite, and (b) mix15 is made with butter clam (Clam 3).

When rock1 was added to S.Ara2 (mix14), the expected complete polymorph pumping that usually happens with single S.Ara1 is partially inhibited (Figure 4.11a-c). After 1 week of stirring, there was a partial growth of the ν_2 band at 881 cm^{-1} of around one-third relative to ν_2 aragonite (Figure 4.11b). We comment that this rising band is displaced left 4 cm^{-1} from the reported dolomite and even farther from the 872 cm^{-1} ν_2 calcite (RRUFFID: R050129, R040070 [6]). An inspection of the ν_4 region with all the bands normalized to the aragonite 700 cm^{-1} ν_4 band (Figure 4.11c) exhibits an intensity increase in the 729 cm^{-1} ν_4 band from rock1 rather than in the 712 cm^{-1} ν_4 from calcite. Only a slight increase in 712 cm^{-1} is visible when comparing to the dissolving 700 cm^{-1} aragonite ν_4. We do not have enough arguments to justify that aragonite is transforming to dolomite, but we can say there is a conversion, and it does not appear to be moving toward a calcite phase. The butter clam and the dolomite rock trials displayed similar conduct (Figure 4.11d-f).

Table 4.4: Summary table of the mixtures prepared for aqueous suspension. The mixtures resulted from combining 50:50 mg of the starting materials described in Table 4.1 and 10 mL of solution. The "Change" column gives a qualitative overview of the changes seen under ATR-FTIR.

Label	Combine	Stirring (rpm)	Time	Change in calcite
mix1	Clam 4 + pur.calcite	no	1 month	stable
mix2	coral + pur.calcite	no	1 month	stable
mix3	Clam 4 + Oyster 2	no	1 month	slightly less
mix4	Clam 4 + Oyster 2* *tap water	no	1 month	slightly less
mix5	Clam 3 + pur.calcite	400	1 week	slightly more
mix6	Clam 3_H + pur.calcite	400	1 week	slightly more
mix7	coral + pur.calcite	1000	1 week	much more
mix8	mussel1 + pur.calcite	1000	1 week	substantially more
mix9	mussel1_H + pur.calcite	1000	1 week	more
mix10	S.Ara2 + Oyster 2	400	1 week	complete
mix11	S.Ara2 + crab	400	1 week	slightly more
mix12	Clam 4 + Oyster 2	400	1 week	stable to less
mix13	Clam 3 + Oyster 2	1000	1 week	less
mix14	S.Ara1 + rock1	1000	1 week	more Mg-calcite
mix15	Clam 3 + rock1	1000	1 week	more Mg-calcite

4.5 Discussion

4.5.1 Starting materials structure

A selected group of diverse biogenic $CaCO_3$ were analyzed and classified using ATR-FTIR in order to find correlations between their structural properties and the aragonite dissolution and recrystallization as calcite that would be expected according to these carbonates thermodynamic constants [27]. Most of the biogenic and geogenic samples ATR-FTIR that we tested matched with the polymorphs that are reported in the literature for those species [71, 25, 127, 88]. We effectively set apart aragonite from calcite biominerals by identifying the presence of both ν_1 and 700 cm^{-1} ν_4 along

with a red-shifted ν_2 with respect to calcite's ν_2 [33, 6]. Although polymorphic natural mixtures have been well explained, the different phases are often spread unevenly within the main mineral phase [108, 109, 82, 105]. As we always mechanically ground the solid, effectively homogeneously diluting secondary solid phases, we generally detected the vibrational bands of the majoritarian polymorph. Nevertheless, we were able to spot and analyze some natural mixtures like oysters and blue mussels (Figure 4.1a and 4.5c) when two close and overlapping ν_2 bands are present. Meanwhile, butter clams ATR-FTIR showed only aragonite, and PXRD analysis (Clam 4 Figure 4.4) unveiled traces of a secondary phase that appears where calcite's strongest diffraction line would emerge [3]. The same was not true for the aragonitic-like coral.

Authors have effectively detected common cations like Mg^{2+} and Sr^{2+} in $CaCO_3$ infrared by tracking ν_4 and ν_1 shift respectively [115, 128]. Oyster 2 cell parameters are smaller than the reported for calcites [3], and it has some Mg^{2+} content according to ICP-OES (Table 4.2, 4.3). However, that Mg^{2+} content is insufficient to justify such cell contraction compared to other synthesized and biogenic Mg-calcites [47, 121]. Furthermore, the ν_4 band is not even 713 cm^{-1} from which we can say not much Mg^{2+} has been inserted in the crystal structure [115]. Still, the presence of the ν_1 band when no signs of aragonite are present in the PXRD indicates that some slight amount of substitutional cations are present [59]. Our aragonitic-like biominerals have low concentrations of Mg^{2+} that we could infer are out of the aragonitic structure since Mg^{2+} incorporation in is unlikely [34, 20], and it has been found often in the organic matrix [24]. On the other hand, Sr concentration is larger in comparison but still less than 1 wt%. Sr^{2+} inclusion in the aragonitic cell tends to expand it rather than, as we witness, contracting it [63, 62]. Nonetheless, the wider and red-shifted ν_1 in coral could be an indication of at least some Sr^{2+} in the structure [65] (Appendix A.5). The most feasible reason for both crystal structures' contraction is the presence of defects, disorder and dislocations typically found in these biogenic carbonates [7, 8].

Heating is widely used for burning out the organics in carbonated minerals [129,

130]. After treating the blue mussel, we effectively identified an amide-related band reduction after heating (Figure 4.5d). The loss on ignition mass (LOI), a commonly used measurement to estimate the organic reduction in carbonates [129, 131], was around 2.8%. We recognize that part of this mass could be hydration water, but most organics should still burn out. Some persistent organics may remain in the biomineral structure [25], but experiments in this thesis conducted for clams showed that they have a negligible percentage. At the same time, we did not detect an increase in calcite due to this treatment for either synthesized aragonite or blue mussels.

4.5.2 Aqueous suspensions

Synthesized aragonites show the expected polymorphic pump when suspended in water. One of our obtained aragonites unintentionally contaminated with a secondary calcite phase exhibits how the progression of this dissolution recrystallization occurs (Figure 4.6a). Moreover, it is noticeable that the calcite crystallization jumps after 1 week of suspension, as shown in Figure 4.8 and then is followed by a stabilization of up to 3 months. This aligns with Gao's [124] results since he reported that 50:50 in mass polymorphic mixture showed the most rapid transformation, whereas extremely uneven phase proportions slowed it. Thus, when the phase proportion becomes even, the aragonite-to-calcite transformation explodes. Stirring synthesized aragonites drives the dissolution recrystallization forward. Heating, on the contrary, reduces the conversion pace because of decreased dislocation density after annealing, which correlates with carbonates' lower dissolution rates [20]. This expected polymorphic pump was not the same for biogenic aragonites. When water suspensions of single biogenic carbonates were stirred, no recrystallization as calcite was spotted (Figure 4.7g-i). No signs of calcite increase are visible even when clams have some low percent calcite in PXRD or large-extent natural polymorphic mixtures and/or organic-removed blue mussels have been stirred in water suspension. The basic pH (8.4-8.6) of the after-suspension supernatants and longer-term pH studies of butter

clams (Appendix A.6) indicate that aragonite dissolution is happening. Therefore, it is not unthinkable to say that calcite precipitation and growth have been inhibited or delayed in these short timeframes. In fact, sulphates and orthophosphates likely present in trace concentration (otherwise could be detected by ATR-FTIR and PXRD) are known to have a strong precipitation-inhibiting effect on calcite [66, 20]. According to Blusenberg and Plummer, biogenic aragonite has low ppm concentrations of sulphates [66]. That leaves phosphates or the heating persistent organics as inhibitor candidates, as proved by our group in synthetic samples [12, 33]. The only exception from all the biological carbonates suspended in water that showed phase conversion was an elusive natural mixture spotted in a grocery oyster (Figure 4.7a).

Unstirred mechanically made mixtures aimed to boost the biogenic aragonite dissolution recrystallization artificially did not show transformation when compared to synthesized aragonite or previous group experiments [11, 124], at most the calcite ν_2 band decreased in some cases (Figure 4.8). However, stirred mixtures had diverse results (Table 4.4). Whenever purchased calcite is added to biogenic aragonites, we notice a polymorphic pump (mix5-mix9). The extension of that transformation varies among mixtures from slightly to substantially more calcite (increased ν_2 band). This may indicate different conversion speeds across different species, which are either related to dissolution or precipitation rate differences. When comparing heated versus unheated samples plus purchased calcite, we did not witness a substantial acceleration as obeying the diminished organic matrix; in fact, we observed a similar effect to the heated synthesized aragonite (a slower transformation). Surprisingly, if both polymorphs are of biological origin, like oyster and clams mixture (mix12, mix13 Table 4.4 and Figure 4.10c,d), the dissolution recrystallization reaction seems to proceed backward towards aragonite crystallization. This behaviour is harder to verify with ATR-FTIR since the aragonite band increase could be confused with a calcite band decrease because of particle size or morphology changes [125, 70]. Also, Mg^{2+} content in oysters is nowhere near 15-20 mol% necessary to make biogenic magnesian calcite

more soluble than aragonite [53, 54, 56]. The PXRD does confirm that after 1 week, large amounts of both polymorphs are still present.

The studies between synthesized aragonite and biogenic calcites show that meanwhile, Oyster 2 does not impede the complete transformation of the contaminated synthesized aragonite; crab does reduce the transformation ratio such that aragonite is still the main phase after suspension (Figure 4.10a,b). This indicates that nothing is leaching out of the oysters, whereas the complexity of crab organic and mineral compounds could partially inhibit the polymorphic pump. Geogenic dolomite displayed a similar retarding effect on synthesized and biogenic aragonite (Figure 4.11). This result shows that even though dolomite ($R\bar{3}$) has the same crystal structure type as calcite ($R\bar{3}C$), calcite growth is not smooth on dolomite's surface. Additionally, the fact that some transformation is seen for the mixture with butter clam once again suggests that aragonite dissolution is not the controlling reaction (Figure 4.11b). Impressively, the transformation that proceeds for these dolomite-aragonite-like mixtures does not seem to generate pure calcite. When looking closer at the ν_4 region, the band that increases is 729 cm^{-1} related to dolomite rather than calcite 712 cm^{-1} peaks. ATR-FTIR alone is not powerful enough to confirm that dolomite is being formed out of aragonite recrystallization. A more realistic situation is the precipitation of a Mg-calcite, taking advantage of any extra Mg^{2+} atoms that do not form part of the dolomite structure.

4.5.3   Phosphates and organic matrix possible influence

The effect of phosphates and the organic matrix in biogenic calcite and aragonite dissolution and crystallization cannot be discussed without describing inhibition processes. Inhibition mechanisms do not follow a definitive pathway, but theoretically, they can be described as how reversible the adsorption on the surface dislocations that serve as the limiting step in both dissolution and crystallization reactions is. Some

models argue that the Langmuir reversible isotherm rein on the solid surface, whereas others describe the adsorption as consecutive steps of irreversibly attached impurities that slow the process until an increased supersaturation surpasses that impurity layer and resume's reactants migration to the active sites [20]. If the concentration of impurities increases, the inhibition will increase correspondingly. In many of the previously explained cases, they can also be addressed as inhibition processes.

Ocean water is supersaturated relative to both calcite and aragonite; therefore, according to their low solubility constant, massive inorganic precipitation should be thermodynamically spontaneous. However, most of the $CaCO_3$ found in the ocean is biomineralized by sea organisms. While the other factors mentioned in previous subsections influencing calcite and aragonite dissolution and crystallization have an impact on the behaviour of either polymorph, the lack of larger inorganic precipitation to relieve supersaturation and/or the persistence of less stable aragonite over long-time spans cannot be explained by them. For example, supersaturation with respect to calcite can be largely explained due to high Mg^{2+} in ocean water, which promotes aragonite precipitation instead, but then aragonite supersaturation is not explained [34]. Thus, organic matter has been proven to be a better candidate for such phenomena. Two processes could explain the effect of organic molecules: (1) an organic coating layer that physically isolates $CaCO_3$ and (2) targeted obstruction of the active sites where dissolution and crystallization occur [20].

The influence of organic matter in $CaCO_3$ polymorph precipitation highly depends on the organic compound present. Inhibition of precipitation is linked to Ca^{2+}-active organic group complex formation, and it is directly proportional to the concentration of the organics. Also, the organic compounds that favour calcite come along with a slower precipitation rate [132]. Many organic groups present in the ocean have been linked to calcite nucleation inhibition: citrates, stearate, and sodium glycerophosphate, among others [133]. More recently, dissolved organic matter (DOM) has been found to slow the precipitation rates at low salinity (freshwater conditions) to control

polymorph formation and crystal defects [134]. Aragonite precipitation in the presence of a wide range of organic compounds was studied by Berner et al. [135]. They found that some molecules have little, some weak, and others have strong inhibition when comparing the ratio of precipitation to organic-free solution. Aromatic acids (gallic acid, mellitic acid) and humic and fulvic substances are among those strong organic inhibitors.

Morse et al. [136] declared that dissolution inhibition of natural carbonate has been correlated to organic physical isolation rather than other adsorption processes. Others have proven that acidic amino acid adsorption causes aragonite to calcite transformation inhibition by forming an adsorbed layer [137]. However, neutral and basic amino acids speed up the dis-rec transformation. Studies of carbonate mineral diagenesis suggest that the organics mentioned have more significance in inhibiting its crystallization than its dissolution [20]. More recently, other authors [138] have shown that DOM is the main cause of calcite dissolution inhibition in seawater conditions. Moreover, when they used lab-controlled seawater, they found that the dissolution rate was still faster by a factor of 4 compared to in situ ocean experiments. When they added DOM as oxalic acid and d-glucose, their lab-controlled seawater matched the ocean rate. On the other hand, soluble reactive phosphate did not seem to affect calcite dissolution in seawater pH. However, orthophosphate uptake strongly inhibits the crystallization of both calcite and aragonite by attaching to carbonate surface in seawater conditions. Still, the uptake of phosphates is greater for aragonite than calcite [139]. Additionally, when analyzing aragonite to calcite transformation in ultrapure water, Gao et al. [33, 12] did find an inhibition of this transformation that would otherwise occur in orthophosphate and polyphosphate-free distilled water. In summary, DOM and phosphates as a whole have variable effects on carbonate dissolution and in the case of DOM, the effect is organic compound-specific. However, most authors agree that they are highly correlated to precipitation and/or crystallization inhibition.

4.6 Conclusions

Clams and coral samples are biogenic aragonites with a low content of other minerals. In clams, an ATR-FTIR undetectable calcite phase can be spotted with PXRD; however, its concentration is small. Oysters and crabs can be classified as calcites. Blue mussels are polymorphic mixtures. All biogenic samples exhibit organic-related infrared bands. Our geogenic rock sample was categorized as dolomite. Heating shows a decrease in the organic-related bands, and there is no infrared detectable increase in the calcite phase.

The dissolution and recrystallization of synthetic aragonites to calcite were once again tracked using ATR-FTIR. Complete recrystallization is achievable when stirring synthetic aragonites, even if no calcite is detectable under the ATR-FTIR. Heating reduces the transformation ratio of 1 week stirred synthesized aragonite suspension.

The biogenic aragonite samples studied did not show aragonite to calcite transformation, even when calcite is present in both clams and blue mussels (more extended). Organic reduction by heating did not accelerate the process either.

Unlike synthesized aragonite, long-term unstirred experiments with mechanically added calcite-like phase do not show a polymorphic pump.

Polymorphic mixtures of biogenic aragonites with purchased calcite did exhibit calcite growth but in different extensions. Organic removed biominerals did not experience an accelerated process, rather the contrary.

Combinations of both biogenic polymorphs do not show any calcite increase, if anything, a disputable decrease.

Oyster organics do not impede calcite growth from synthetic aragonite with a secondary calcitic phase, while crabs decelerate the same transformation.

Similarly, the proportion of aragonite transformation is significantly diminished when synthesized aragonite is added to a dolomite-like rock sample. The conversion

ratio is comparable for butter clam plus dolomite rock, which means biogenic aragonite dissolution is possible.

In summary, due to the increased pH, biogenic aragonite dissolution is feasible in every situation. On the other hand, calcite crystallization depends on the origin. When biogenic calcite was the only template for crystallization, the polymorphic pump did not necessarily proceed. Actually, in most cases, no transformation is seen.

Chapter 5

Conclusions

5.1 Summary of thesis work

Calcium carbonate ($CaCO_3$) most common polymorphs, aragonite and calcite, undergo phase conversion, "polymorphic pump", in undersaturated water suspensions. We studied how biogenic aragonite's expected dissolution-recrystallization process occurs in water compared to the synthetic material. Chapter 3 is an in-depth study of butter clam structure and water suspension behaviour, where the differences across separate shell sections were tested and found to have little dissimilarities. Chapter 4 expanded the experimentation to a larger set of samples and combinations to extrapolate the results from the previous chapter. We mainly used ATR-FTIR to track the effects of dissolution-recrystallization as previously proved by our group [124, 11, 12]. We retested the stability of synthetic aragonite in a water solution, finding conditions in which complete recrystallization as calcite is achieved in one week. The thermal annealing of my synthetic aragonite makes the material approach the stability accomplished by my predecessor. We both witnessed accelerated transformation when calcite was present either as an unintended secondary phase or a mechanically made mixture.

This research takes a step further to track the stability of biogenic aragonites either alone or mixed with their counterparts. We decided to make the mixtures 50%-50% by mass of polymorph to follow the faster-proven conversion pace for synthetic-like material mixtures. Our results indicate that contrary to their synthetic peer, the biogenic aragonite specimens studied do not show any infrared detectable conversion in the studied timeframes. Furthermore, neither perfectly aragonite coral, aragonite-like butter clams with traces of secondary phase calcite, blue mussels with undeniably large amounts of calcite, nor mechanically made mixtures of calcite-like oysters with clams showed calcite growth. However, recrystallization is observed when pure purchased calcite is added to clams, corals, or blue mussels. Mechanically or thermic removal of the organic did not accelerate the process either. All this suggests three things: (1) the lack of organics does not promote the dissolution and recrystallization of the biogenic aragonites studied, (2) biogenic aragonite dissolves and recrystallizes in the presence of pure calcite, but still conversion extent differs across aragonite sources and (3) generally if the calcite crystallization seed is from natural origin the calcite growth seems inhibited or delayed in one-week long experiments.

To further see if the biogenic calcite was impeding calcite crystallization, we took calcite-like oysters and crabs and mixed them with the synthetic aragonite that had an undesired calcitic secondary phase. Neither biogenic calcite stopped the dissolution-recrystallization of synthetic aragonite, although it was slower in the crab experiment. This suggests that calcite recrystallization struggles in biogenic calcites but not because of compounds leaching out of the calcitic shells and inhibiting aragonite from dissolving.

Finally, we tested the stability of aragonite in the presence of a dolomite-like sample. We once again saw aragonite dissolution in both synthetic and biogenic aragonite, but recrystallization did not proceed completely, and we are dubious that the conversion was not directly to calcite but rather to a Mg-calcite material. Nevertheless,

future analysis must be conducted in this line of research. We recognize that the polymorphic pump investigated in this thesis may proceed in longer time frames and that we used undersaturated pure water solutions, so these experiments can not be taken as the final result in the natural context. We recommend using this methodology to test other co-compounds and, every time, increase the complexity of the experiment up to the real ocean-like scenarios.

5.2   Relevance and future work

5.2.1   Relevance for ocean carbonate interactions

This research focuses on tracking the aragonite-to-calcite dissolution-recrystallization of naturally occurring carbonates using ATR-FTIR. We also tried correlating the co-elements in the starting materials with the observed polymorphic pumping. Idealistically, in undersaturated solutions, aragonite should recrystallize as calcite. Gao et al. have successfully tracked this process using ATR-FTIR and studied phosphates' inhibitor effect [11, 12]. Additionally, Sulpis et al. have made simulations of how aragonite dissolution could be buffering ocean acidification and protecting calcite dissolution [31]. Recently, Van de Mortel et al. conducted an experiment with a similar goal to ours but using close-to-real seawater solution scenarios [84]. Van de Mortel implies that if both polymorphs dissolve, the total alkalinity should be higher than that for a single polymorph. Since they did not see a change in the total alkalinity before and after the polymorph mixture, they suggested that it could only be explained by aragonite dissolution with equally proportional inhibited calcite dissolution, which must be accompanied by 1-day-long calcite precipitation. Our direct measurements in biogenic aragonite plus biogenic calcite indicate this could not be necessarily true in all cases and could actually be that no transformation is seen. Still, they needed to make simplifications relative to a true ocean system: filtered ocean water, organic

material removed from the shells, and others. In contrast, we used a more facile setup to advance from a simple to a complex approach.

We are aware that some companies are actively using calcium carbonates, dolomites, calcium oxides and other reagents to enhance and buffer water pH in river and basin water areas. Moreover, according to the findings of this thesis, they will need to account for the aragonite-like sediment dissolution-recrystallization that will happen differently in the short term, depending on the carbonate counterpart they decide to use.

Appendix A

Biogenic and geogenic carbonates aqueous suspensions

Figure A.1 shows representative Attenuated Total Reflectance Fourier-Transform Infrared (ATR-FTIR) spectra comparing our mussels, synthesized aragonites, oysters, and purchased calcite data with standards for aragonite and calcite [6]. Purchased calcite and Oyster 2 have characteristic bands at 1396 cm^{-1} (ν_3), 872 cm^{-1} (ν_2) and 712 cm^{-1} (ν_4), in agreement with (calcite RRUFFID=R040070 ν_3 at 1395 cm^{-1}, ν_2 at 872 cm^{-1}, and ν_4 at 712 cm^{-1} [6]). Additionally, Oyster 2 presents a bump at 1446-1460 cm^{-1} most likely related to the polysaccharides [117, 118] and a weak ν_1 at 1085 cm^{-1} that appear when substitutionals impurities are present [59, 119]. Synthesized aragonite 1 is aragonite, with ν_3 at 1446-1460 cm^{-1}, ν_2 at 854 cm^{-1}, ν_4 at 712 cm^{-1}, as well as two distinct aragonite bands at 1083 cm^{-1} (ν_1) and 700 cm^{-1} (also ν_4), all of which are consistent with what is reported for aragonite (RRUFFID=R040078 [6]). Mussels, Oyster 1 specimens and synthesized aragonite 2 are a natural mixture of aragonite and calcite, evidenced in the broad ν_3 1400-1460 cm^{-1} and the presence of both ν_2 bands from calcite and aragonite. Mussels and synthesized aragonite have the calcite ν_2 band as a shoulder at 875-870 cm^{-1}. Oyster 1 has a well defined ν_2 band at 875 cm^{-1}. Figure A.2 photographs highlights the decoloration

effect heating has on mussels' loss of organic matrix. Figure A.3 shows interest band range spectra of how synthesized aragonite undergoes dissolution-recrystallization before and after water suspension. A PXRD corroboration of the no-dissolution-recrystallization of mixture between the calcite-like Oyster 2 and the aragonite-like Clam 4 mixture after 1-week long stirred water suspension is shown in Figure A.4. Figure A.5 shows that coral samples match the bands reported for aragonite (RRUF-FID=R040078 [6]), but the broader ν_1 band is an indication of substitutional Sr^{2+} [65]. Figure A.6 tracks the pH behaviour of clam and purchased calcite suspension over 3 days of measurement. It compares the similar trend and final suspension pH to that obtained when simulating the same mass calcite suspension when reaching equilibrium with atmospheric CO_2.
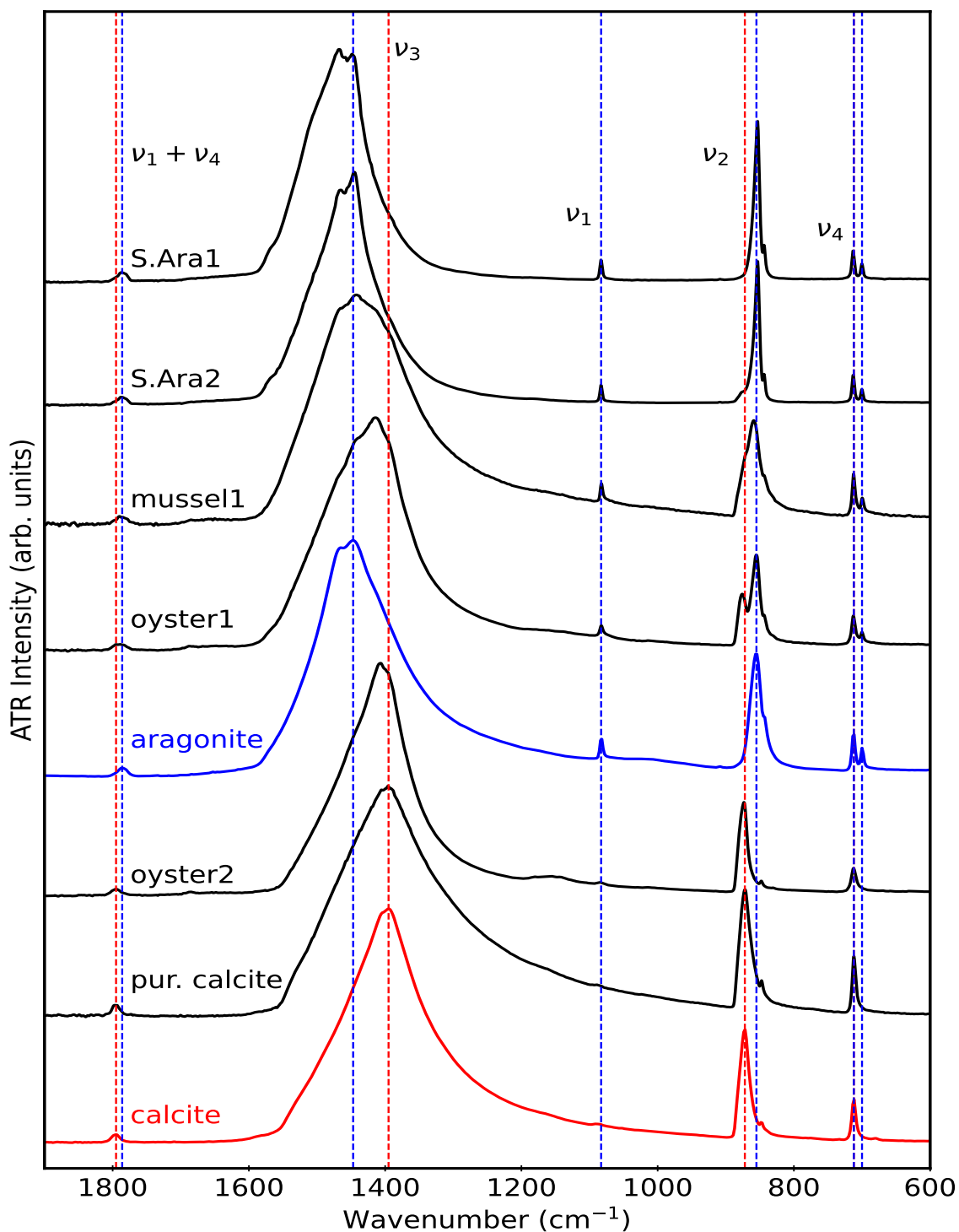
Figure A.1: Representative ATR-FTIR spectra for oysters, blue mussels, synthesized aragonites and purchased calcite (all in black) compared with calcite (RRUFFID R040070, in red) and aragonite (RRUFFID R040078, in blue) standards from the RRUFF database [6]. Labelling conventions are described in Table 4.1 of the main text.
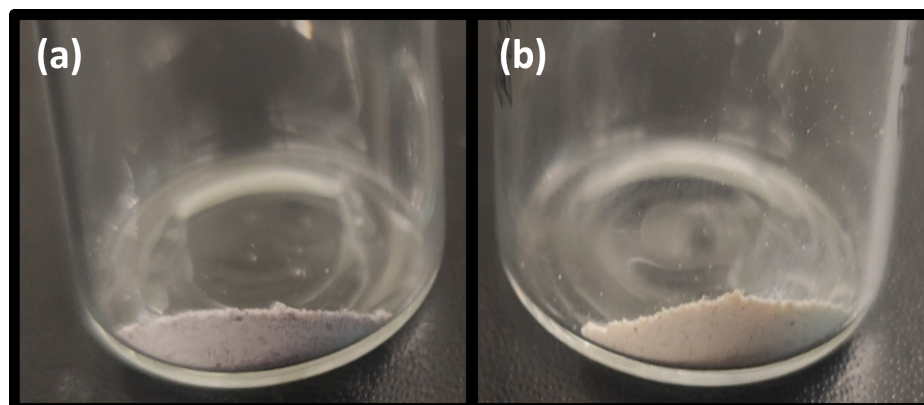
Figure A.2: Representative photographs of ground blue mussel before (a) and after heating (b). Heating shows a decoloration from light purple to white after treatment.
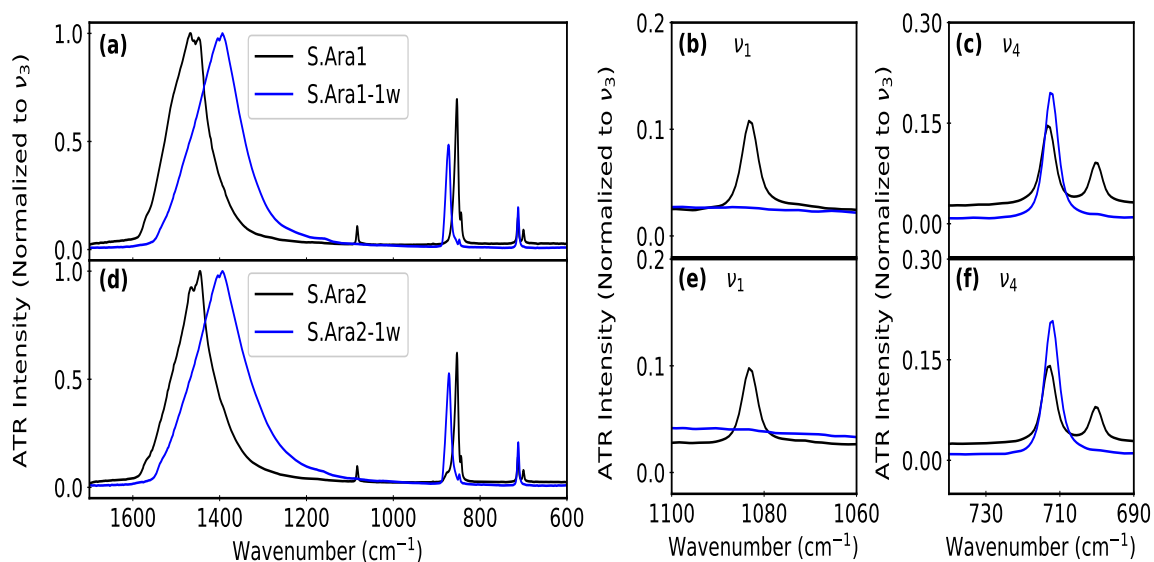
Figure A.3: Representative ATR-FTIR spectra of the synthesized aragonite 1 (S.Ara1) (a) and 2 (S.Ara2) (b) before (black line) and after one week of stirring (blue line). (a,b) the ν_2 aragonitic band at 855 cm^{-1} decreased and the calcitic band at 873 cm^{-1} increased after water suspension. ν_1 (b,e) and 700 cm^{-1} ν_4 band (c,f) disappearance confirm aragonite dissolution and recrystallization as calcite.
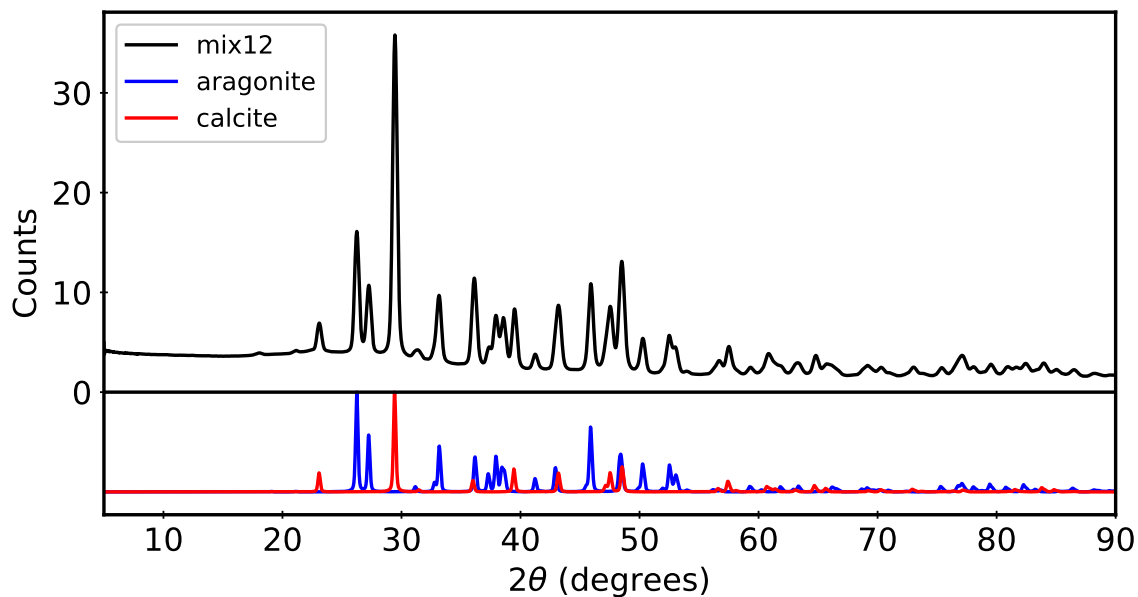
Figure A.4: Mix12 X-ray diffraction pattern of Oyster 2 plus butter Clam 4 1-week stirred suspension (black line). Aragonite (PDF 980000098, in blue) and calcite (PDF 980000141, in red) [3]. The pattern shows large amounts of aragonite after the water treatment.
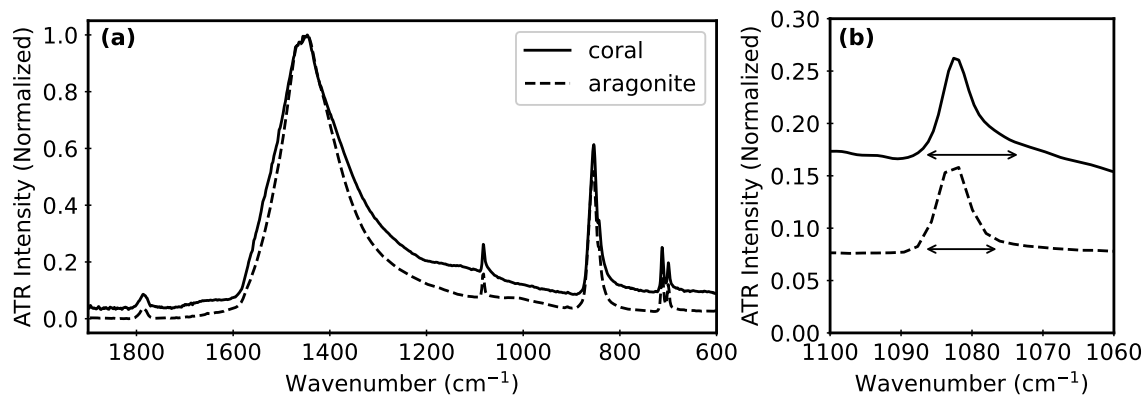
Figure A.5: (a) Representative ATR-FTIR of coral (solid line) compared to aragonite (RRUFFID R040078, dashed line) standard from the RRUFF database [6]. (b) Zoom in the ν_1 region that shows broader bands for coral than for aragonite standard.
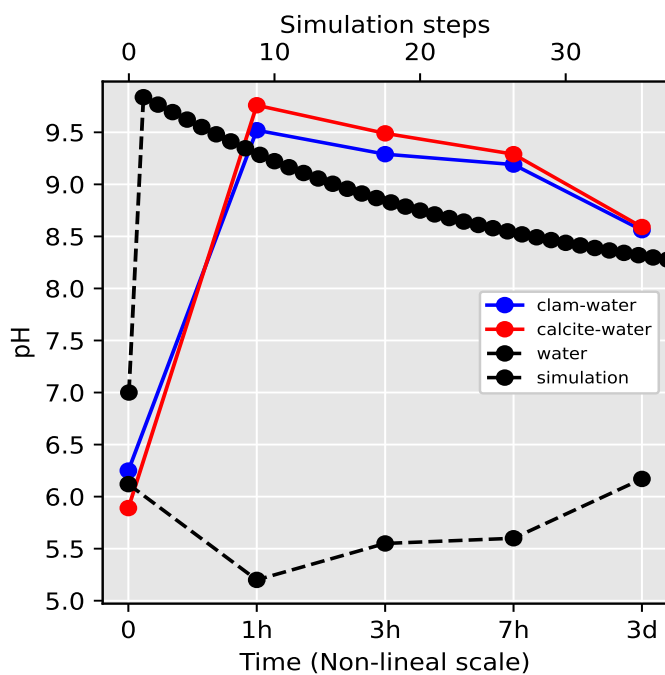
Figure A.6: pH evolution of aragonitic butter clam (blue), purchased calcite (red) and ultrapure water (solid black) on a 3-day time span. Simulated calcite pH evolution (transparent grey) through a series of steps is also included. The simulation was performed using PHREEQC for a calcite suspension that reach equilibrium with CO_2 dissolution [10].

Bibliography

[1] JADE 10; Materials Data: Livermore, CA. 2019.

[2] K. Momma and F. Izumi, "*VESTA3* for three-dimensional visualization of crystal, volumetric and morphology data," *J. Appl. Crystallogr.*, vol. 44, pp. 1272–1276, Dec 2011.

[3] S. Gates-Rector and T. Blanton, "The powder diffraction file: a quality materials characterization database," *Powder. Diffr.*, vol. 34, no. 4, pp. 352–360, 2019. Aragonite PDF# 980000098. Calcite PDF# 980000141.

[4] P. Cubillas, S. Köhler, M. Prieto, C. Chaïrat, and E. H. Oelkers, "Experimental determination of the dissolution rates of calcite, aragonite, and bivalves," *Chem. Geol.*, pp. 59–77, 2005.

[5] Available online: `https://commons.wikimedia.org/wiki/File:Clam_(PSF) .jpg`. (Accessed on 21 March 2024).

[6] B. Lafuente, R. T. Downs, H. Yang, N. Stone, T. Armbruster, R. M. Danisi, *et al.*, "The power of databases: the rruff project," *Highlights in mineralogical crystallography*, vol. 1, p. 25, 2015. Calcite_R040070-1. Aragonite_R040078-1. Dolomite_R050129. Magnesite_R050443.

[7] B. Pokroy, J. Fieramosca, R. Von Dreele, A. Fitch, E. Caspi, and E. Zolotoyabko, "Atomic structure of biogenic aragonite," *Chem. Mater.*, vol. 19, no. 13, pp. 3244–3251, 2007.

[8] B. Pokroy, A. Fitch, and E. Zolotoyabko, "Structure of biogenic aragonite ($CaCO_3$)," *Cryst. Growth. Des.*, vol. 7, no. 9, pp. 1580–1583, 2007.

[9] E. N. Caspi, B. Pokroy, P. Lee, J. Quintana, and E. Zolotoyabko, "On the structure of aragonite," *Acta. Crystallogr. B*, vol. 61, no. 2, pp. 129–132, 2005.

[10] S. R. Charlton and D. L. Parkhurst, "Modules based on the geochemical model phreeqc for use in scripting and programming languages," *Comput. Geosci.*, vol. 37, pp. 1653–1663, 2011.

[11] B. Gao and K. M. Poduska, "Tracking amorphous calcium carbonate crystallization products with far-infrared spectroscopy," *Minerals*, vol. 13, no. 1, p. 110, 2023.

[12] B. Gao, S. Kababya, K. M. Poduska, and A. Schmidt, "Surface passivation by embedment of polyphosphate inhibits the aragonite-to-calcite thermodynamic pump," *J. Am. Chem. Soc.*, pp. 1–4, 2023.

[13] D. Archer, M. Eby, V. Brovkin, A. Ridgwell, L. Cao, U. Mikolajewicz, K. Caldeira, K. Matsumoto, G. Munhoven, A. Montenegro, *et al.*, "Atmospheric lifetime of fossil fuel carbon dioxide," *Annu. Rev. Earth. Pl. Sc.*, vol. 37, pp. 117–134, 2009.

[14] C. Baird, *Environmental chemistry.* New York: W.H. Freeman, 5th ed. ed., 2012.

[15] T. Takahashi, R. A. Feely, R. F. Weiss, R. H. Wanninkhof, D. W. Chipman, S. C. Sutherland, and T. T. Takahashi, "Global air-sea flux of CO_2: An estimate based on measurements of sea–air pCO_2 difference," *Proc. Natl. Acad. Sci.*, vol. 94, no. 16, pp. 8292–8299, 1997.

[16] P. Halloran, B. Booth, C. Jones, F. Lambert, D. McNeall, I. Totterdell, and C. Völker, "The mechanisms of north atlantic CO_2 uptake in a large earth system model ensemble," *Biogeosciences*, vol. 12, no. 14, pp. 4497–4508, 2015.

[17] Y. Huang, A. J. Fassbender, and S. M. Bushinsky, "Biogenic carbon pool production maintains the southern ocean carbon sink," *Proc. Natl. Acad. Sci.*, vol. 120, no. 18, p. e2217909120, 2023.

[18] N. Hanken, K. Bjørlykke, and J. K. Nielsen, "Carbonate sediments," *Petrol. Geosci.*, pp. 151–216, 2015.

[19] A. V. Turchyn, H. J. Bradbury, K. Walker, and X. Sun, "Controls on the precipitation of carbonate minerals within marine sediments," *Front. Earth. Sci.*, vol. 9, p. 618311, 2021.

[20] J. W. Morse, R. S. Arvidson, and A. Lüttge, "Calcium carbonate formation and dissolution," *Chem. Rev.*, vol. 107, pp. 342–381, 2007.

[21] D. Jacob, A. Soldati, R. Wirth, J. Huth, U. Wehrmeister, and W. Hofmeister, "Nanostructure, composition and mechanisms of bivalve shell growth," *Geochim. Cosmochim. Ac.*, vol. 72, no. 22, pp. 5401–5415, 2008.

[22] S. M. de Paula and M. Silveira, "Studies on molluscan shells: contributions from microscopic and analytical methods," *Micron*, vol. 40, no. 7, pp. 669–690, 2009.

[23] N. Bianco-Stein, I. Polishchuk, A. Lang, L. Portal, C. Dejoie, A. Katsman, and B. Pokroy, "High-mg calcite nanoparticles within a low-mg calcite matrix: A widespread phenomenon in biomineralization," *Proc. Natl. Acad. Sci.*, vol. 119, no. 16, p. e2120177119, 2022.

[24] B. R. Schoene, Z. Zhang, D. Jacob, D. P. Gillikin, T. Tütken, D. Garbe-Schönberg, T. McConnaughey, and A. Soldati, "Effect of organic matrices on the determination of the trace element chemistry (Mg, Sr, Mg/Ca, Sr/Ca) of aragonitic bivalve shells (*Arctica islandica*)—comparison of ICP-OES and LA-ICP-MS data," *Geochem. J.*, vol. 44, no. 1, pp. 23–37, 2010.

[25] Y. Dauphin, A. D. Ball, H. Castillo-Michel, C. Chevallard, J. Cuif, B. Farre, S. Pouvreau, and M. Salomé, "In situ distribution and characterization of the organic content of the oyster shell crassostrea gigas (mollusca, bivalvia)," *Micron*, vol. 44, pp. 373–383, 2013.

[26] C. P. Glover and S. M. Kidwell, "Influence of organic matrix on the post-mortem destruction of molluscan shells," *J. Geol.*, vol. 101, no. 6, pp. 729–747, 1993.

[27] L. N. Plummer and E. Busenberg, "The solubilities of calcite, aragonite and vaterite in CO_2-H_2O solutions between 0 and 90 °C, and an evaluation of the aqueous model for the system $CaCO_3$-CO_2-H_2O," *Geochim. Cosmochim. Ac.*, vol. 46, no. 6, pp. 1011–1040, 1982.

[28] J. Bischoff and W. Fyfe, "Catalysis, inhibition, and the calcite-aragonite problem;[part] 1, the aragonite-calcite transformation," *Am. J. Sci.*, vol. 266, no. 2, pp. 65–79, 1968.

[29] O. Aumont, C. Éthé, A. Tagliabue, L. Bopp, and M. Gehlen, "Pisces-v2: an ocean biogeochemical model for carbon and ecosystem studies," *Geosci. Model. Dev.*, vol. 8, no. 2, pp. 1375–1509, 2015.

[30] T. Ilyina, K. D. Six, J. Segschneider, E. Maier-Reimer, H. Li, and I. Núñez-Riboni, "Global ocean biogeochemistry model hamocc: Model architecture and performance as component of the mpi-earth system model in different cmip5 experimental realizations," *J. Adv. Model. Earth Sy.*, vol. 5, no. 2, pp. 287–315, 2013.

[31] O. Sulpis, P. Agrawal, M. Wolthers, G. Munhoven, M. Walker, and J. J. Middleburg, "Aragonite dissolution protects calcite at the seafloor," *Nat. Commun.*, pp. 1104:1–8, 2022.

[32] H. van de Mortel, L. Delaigue, M. Humphreys, J. Middelburg, S. Ossebaar, K. Bakker, J. T. Alexandre, A. van Leeuwen-Tolboom, M. Wolthers, and O. Sulpis, "Laboratory observation of the buffering effect of aragonite dissolution at the seafloor," *J. Geophys. Res-Biogeo.*, vol. 129, no. 2, p. e2023JG007581, 2024.

[33] B. Gao and K. M. Poduska, "Comparing polyphosphate and orthophosphate treatments of solution-precipitated aragonite powders," *Solids*, vol. 3, no. 4, pp. 684–696, 2022.

[34] W. Sun, S. Jayaraman, W. Chen, K. A. Persson, and G. Ceder, "Nucleation of metastable aragonite $CaCO_3$ in seawater," *Proc. Natl. Acad. Sci.*, vol. 112, no. 11, pp. 3199–3204, 2015.

[35] R. H. Petrucci, F. G. Herring, J. D. Madura, and B. Carey, *General Chemistry: Principles and Modern Applications*. Pearson, 2017.

[36] J. W. Morse, *Chapter 7. The Kinetics of Calcium Carbonate Dissolution and Precipitation*, pp. 227–264. Berlin, Boston: De Gruyter, 1983.

[37] L. Brečević and A. E. Nielsen, "Solubility of amorphous calcium carbonate," *J. Cryst. Growth*, vol. 98, no. 3, pp. 504–510, 1989.

[38] J. W. Morse, A. Mucci, and F. J. Millero, "The solubility of calcite and aragonite in seawater of 35%. salinity at 25 °C and atmospheric pressure," *Geochim. Cosmochim. Ac.*, vol. 44, no. 1, pp. 85–94, 1980.

[39] A. Y. Bychkov, P. Bénézeth, O. Pokrovsky, Y. V. Shvarov, A. Castillo, and J. Schott, "Experimental determination of calcite solubility and the stability of aqueous ca–and na–carbonate and–bicarbonate complexes at 100-160 °C and 1-50 bar pCO_2 using in situ ph measurements," *Geochim. Cosmochim. Ac.*, vol. 290, pp. 352–365, 2020.

[40] B. Coto, C. Martos, J. L. Peña, R. Rodríguez, and G. Pastor, "Effects in the solubility of $CaCO_3$: Experimental study and model description," *Fluid Phase Equilibr.*, vol. 324, pp. 1–7, 2012.

[41] L. N. Plummer, T. M. L. Wigley, and D. L. Parkhurst, "The kinetics of calcite dissolution in CO_2-water systems at 5 degrees to 60 degrees °C and 0.0 to 1.0 atm CO_2," *Am. J. Sci.*, vol. 278, no. 2, pp. 179–216, 1978.

[42] J. W. Morse and R. S. Arvidson, "The dissolution kinetics of major sedimentary carbonate minerals," *Earth-Sci. Rev.*, vol. 58, no. 1-2, pp. 51–84, 2002.

[43] C. Batchelor-McAuley, M. Yang, R. E. M. Rickaby, and R. G. Compton, "Calcium carbonate dissolution from the laboratory to the ocean: Kinetics and mechanism," *Chem. Eur. J.*, vol. 28, p. e202202290, 2022.

[44] K. Sawada, "The mechanisms of crystallization and transformation of calcium carbonates," *Pure Appl. Chem.*, vol. 69, no. 5, pp. 921–928, 1997.

[45] M. Ma, Y. Wang, X. Cao, W. Lu, and Y. Guo, "Temperature and supersaturation as key parameters controlling the spontaneous precipitation of calcium carbonate with distinct physicochemical properties from pure aqueous solutions," *Cryst. Growth. Des.*, vol. 19, pp. 6972–6988, 2019.

[46] S. Yoshioka, S. Ohde, Y. Kitano, and N. Kanamori, "Behaviour of magnesium and strontium during the transformation of coral aragonite to calcite in aquatic environments," *Marine Chem.*, vol. 18, pp. 35–48, 1986.

[47] J. R. Goldsmith, D. L. Graf, and H. C. Heard, "Lattice constants of the calcium magnesium carbonates," *Am. Mineral*, vol. 46, pp. 453–459, 04 1961.

[48] B. Xu, M. B. Toffolo, L. Regev, E. Boaretto, and K. M. Poduska, "Structural differences in archaeologically relevant calcite," *Anal. Methods*, vol. 7, no. 21, pp. 9304–9309, 2015.

[49] W. Mejri, A. Korchef, M. Tlili, and M. Ben-Amor, "Effects of temperature on precipitation kinetics and microstructure of calcium carbonate in the presence of magnesium and sulphate ions," *Desalin.*, vol. 52, no. 25-27, pp. 4863–4870, 2014.

[50] M. Boon, W. D. A. Rickard, A. L. Rohl, and F. Jones, "Stabilization of aragonite: role of Mg^{2+} and other impurity ions," *Cryst. Growth Des.*, vol. 20, no. 8, pp. 5006–5017, 2020.

[51] L. C. Foster, A. A. Finch, N. Allison, C. Andersson, and L. J. Clarke, "Mg in aragonitic bivalve shells: Seasonal variations and mode of incorporation in *Arctica islandica*," *Chem. Geol.*, vol. 254, no. 1-2, pp. 113–119, 2008.

[52] C. Poulain, D. P. Gillikin, J. Thébault, J. Munaron, M. Bohn, R. Robert, Y. Paulet, and A. Lorrain, "An evaluation of Mg/Ca, Sr/Ca, and Ba/Ca ratios as environmental proxies in aragonite bivalve shells," *Chem. Geol.*, vol. 396, pp. 42–50, 2015.

[53] W. D. Bischoff, F. T. Mackenzie, and F. C. Bishop, "Stabilities of synthetic magnesian calcites in aqueous solution: Comparison with biogenic materials," *Geochim. Cosmochim. Ac.*, vol. 51, no. 6, pp. 1413–1423, 1987.

[54] W. D. Bischoff, M. A. Bertram, F. T. Mackenzie, and F. C. Bishop, "Diagenetic stabilization pathways of magnesian calcites," *Carbonate. Evaporite.*, vol. 8, p. 82–89, 1993.

[55] L. N. Plummer and F. T. Mackenzie, "Predicting mineral solubility from rate data; application to the dissolution of magnesian calcites," *Am. J. Sci.*, vol. 274, no. 1, pp. 61–83, 1974.

[56] E. Busenberg and L. N. Plummer, "Thermodynamics of magnesian calcite solid-solutions at 25 °C and 1 atm total pressure," *Geochim. Cosmochim. Ac.*, vol. 53, no. 6, pp. 1189–1208, 1989.

[57] W. K. Park, S. Ko, S. W. Lee, K. Cho, J. Ahn, and C. Han, "Effects of magnesium chloride and organic additives on the synthesis of aragonite precipitated calcium carbonate," *J. Cryst. Growth*, vol. 310, no. 10, pp. 2593–2601, 2008.

[58] B. Purgstaller, V. Mavromatis, A. Immenhauser, and M. Dietzel, "Transformation of Mg-bearing amorphous calcium carbonate to Mg-calcite - In situ monitoring," *Geochim. Cosmochim. Ac.*, vol. 174, pp. 180–195, 2016.

[59] B. Purgstaller, F. Konrad, M. Dietzel, A. Immenhauser, and V. Mavromatis, "Control of Mg^{2+}/Ca^{2+} activity ratio on the formation of crystalline carbonate minerals via an amorphous precursor," *Cryst. Growth Des*, vol. 17, no. 3, pp. 1069–1078, 2017.

[60] J. D. Rodriguez-Blanco, S. Shaw, P. Bots, T. Roncal-Herrero, and L. G. Benning, "The role of Mg in the crystallization of monohydrocalcite," *Geochim. Cosmochim. Ac.*, vol. 127, pp. 204–220, 2014.

[61] A. Mucci and J. W. Morse, "The incorporation of Mg^{2+} and Sr^{2+} into calcite overgrowths: influences of growth rate and solution composition," *Geochim. Cosmochim. Ac.*, vol. 47, no. 2, pp. 217–233, 1983.

[62] X. Wang, Z. Wang, X. Zhu, D. Liu, Y. Miao, and Y. Ye, "X-ray diffraction and spectroscopic study of $Sr_xCa_{1-x}CO_3$: Implications for equilibrium Sr^{2+} incorporation and carbon/oxygen isotope fractionation in aragonite," *Geochim. Cosmochim. Ac.*, vol. 309, pp. 112–134, 2021.

[63] S. M. Antao and I. Hassan, "The orthorhombic structure of $CaCO_3$, $SrCO_3$, $PbCO_3$ and $BaCO_3$: Linear structural trends," *Canad. Mineral.*, vol. 47, no. 5, pp. 1245–1255, 2009.

[64] L. N. Plummer and E. Busenberg, "Thermodynamics of aragonite-strontianite solid solutions: Results from stoichiometric solubility at 25 and 76 °C," *Geochim. Cosmochim. Ac.*, vol. 51, no. 6, pp. 1393–1411, 1987.

[65] C. B. Tovani, T. M. Oliveira, A. Gloter, and A. P. Ramos, "Sr^{2+}-substituted $CaCO_3$ nanorods: impact on the structure and bioactivity," *Cryst. Growth Des.*, vol. 18, no. 5, pp. 2932–2940, 2018.

[66] E. Busenberg and L. N. Plummer, "Kinetic and thermodynamic factors controlling the distribution of SO_3^{2-} and Na^+ in calcites and selected aragonites," *Geochim. Cosmochim. Ac.*, vol. 49, no. 3, pp. 713–725, 1985.

[67] K. M. Poduska, B. Espinosa Acosta, J. J. Breen, and M. Burchell, "Replication Data for "Biogenic Calcium Carbonate: Phase Conversion in Aqueous Suspensions"," 2024. `https://doi.org/10.5683/SP3/7UXHRF`,Borealis, V1, UNF:6:DA12hLA7JKekgEyOovmiuQ== [fileUNF].

[68] J. B. Lambert, "Organic structural spectroscopy," 2014.

[69] J. D. Schuttlefield and V. H. Grassian, "ATR–FTIR spectroscopy in the undergraduate chemistry laboratory. Part I: Fundamentals and examples," *J. Chem. Educ.*, vol. 85, no. 2, p. 279, 2008.

[70] K. M. Poduska, L. Regev, F. Berna, E. Mintz, I. Milevski, H. Khalaily, S. Weiner, and E. Boaretto, "Plaster characterization at the ppnb site of yiftahel (israel) including the use of 14C: Implications for plaster production, preservation, and dating," *Radiocarbon*, vol. 54, no. 3-4, pp. 887–896, 2012.

[71] M. Dusseault, *Investigating variability in marine mollusk carbonates using infrared spectroscopy and radiocarbon analysis.* PhD thesis, Memorial University of Newfoundland, 2021. https://research.library.mun.ca/15212/.

[72] D. G. Henry, J. S. Watson, and C. M. John, "Assessing and calibrating the ATR–FTIR approach as a carbonate rock characterization tool," *Sediment. Geol.*, vol. 347, pp. 36–52, 2017.

[73] F. Bosch-Reig, J. V. Gimeno-Adelantado, F. Bosch-Mossi, and A. Doménech-Carbó, "Quantification of minerals from ATR–FTIR spectra with spectral interferences using the mrc method," *Spectrochim. Acta A*, vol. 181, pp. 7–12, 2017.

[74] A. Doménech-Carbó, F. Bosch-Reig, and N. Montoya, "ATR–FTIR and xrd quantification of solid mixtures using the asymptotic constant ratio (ACR) methods. application to geological samples of sodium and potassium feldspars," *Spectrochim. Acta A*, vol. 236, p. 118328, 2020.

[75] M. T. Weller, *Inorganic materials chemistry.* Oxford University Press Oxford, 1994.

[76] T. Ryan, "The development of instrumentation for thin-film x-ray diffraction," 2001.

[77] S. T. Silk and S. Z. Lewin, "X-ray diffraction analysis of the calcium carbonate polymorphs," *Advances in X-ray Analysis*, vol. 14, pp. 29–37, 1970.

[78] J. Nölte, *ICP Emission Spectrometry: a practical guide.* John Wiley & Sons, 2021.

[79] B. Espinosa-Acosta, J. J. Breen, M. Burchell, and K. M. Poduska, "Biogenic calcium carbonate: Phase conversion in aqueous suspensions," *Minerals*, vol. 14, no. 7, p. 682, 2024.

[80] D. Jacob, A. Soldati, R. Wirth, J. Huth, U. Wehrmeister, and W. Hofmeister, "Nanostructure, composition and mechanisms of bivalve shell growth," *Geochim. Cosmochim. Ac.*, vol. 72, no. 22, pp. 5401–5415, 2008.

[81] S. M. de Paula and M. Silveira, "Studies on molluscan shells: contributions from microscopic and analytical methods," *Micron*, vol. 40, no. 7, pp. 669–690, 2009.

[82] J. N. Murphy, C. M. Schneider, L. K. Mailänder, Q. Lepillet, K. Hawboldt, and F. M. Kerton, "Wealth from waste: Blue mussels (mylitus edulis) offer up a sustainable source of natural and synthetic nacre," *Green Chem.*, vol. 21, no. 14, pp. 3920–3929, 2019.

[83] J. F. Adkins, J. D. Naviaux, A. V. Subhas, S. Dong, and W. M. Berelson, "The dissolution rate of $CaCO_3$ in the ocean," *Annu. Rev. Mar. Sci.*, pp. 57–80, 2021.

[84] H. van de Mortel, L. Delaigue, M. P. Humphreys, J. J. Middelburg, S. Ossebaar, K. Bakker, J. P. T. Alexandre, A. W. E. van Leeuwen-Tolboom, M. Wolthers, and O. Sulpis, "Laboratory observation of the buffering effect of aragonite dissolution at the seafloor," *J. Geophys Research: Biogeosciences*, vol. 129, p. e2023JG007581, 2024.

[85] K. B. Krauskopf and D. K. Bird, "Solution-Mineral equilibria Part 1: Carbonates," *Introduction of Geochemistry*, pp. 61–83, 1995.

[86] O. Sulpis, C. Lix, A. Mucci, and B. P. Boudreau, "Calcite dissolution kinetics at the sediment-water interface in natural seawater," *Mar. Chem.*, pp. 70–83, 2017.

[87] G. Zhang, J. Morales, and J. M. García-Ruiz, "Growth behaviour of silica/carbonate nanocrystalline composites of calcite and aragonite," *J. Mater. Chem. B*, vol. 5, pp. 1658–1663, 2017.

[88] C. Triunfo, S. Gartner, C. Marchini, S. Fermani, G. Maoloni, S. Goffredo, J. Gomez-Morales, H. Colfen, and G. Falini, "Recovering and exploiting aragonite and calcite single crystals with biologically controlled shapes from mussel shells," *ACS omega*, vol. 7, no. 48, pp. 43992–43999, 2022.

[89] V. Louis, L. Besseau, and F. Lartaud, "Step in time: Biomineralisation of bivalve's shell," *Front. Mar. Sci.*, vol. 9, p. 906085, 2022.

[90] B. R. Schöne, E. Dunca, J. Fiebig, and M. Pfeiffer, "Mutvei's solution: an ideal agent for resolving microgrowth structures of biogenic carbonates," *Palaeogeogr. Palaeocl.*, vol. 228, no. 1-2, pp. 149–166, 2005.

[91] D. P. Gillikin, A. Lorrain, J. Navez, J. W. Taylor, L. André, E. Keppens, W. Baeyens, and F. Dehairs, "Strong biological controls on Sr/Ca ratios in aragonitic marine bivalve shells," *Geochem. Geophy. Geosy.*, vol. 6, no. 5, 2005.

[92] H. Ulens, *The potentials of Saxidomus giganteus as a paleoclimate proxy.* PhD thesis, M. Sc. thesis. Gent University, Belgium, 2003.

[93] N. Hallmann, M. Burchell, B. R. Schöne, G. V. Irvine, and D. Maxwell, "High-resolution sclerochronological analysis of the bivalve mollusk *Saxidomus gigantea* from alaska and british columbia: techniques for revealing environmental archives and archaeological seasonality," *J. Archaeol. Sci.*, vol. 36, pp. 2353–2364, 2009.

[94] C. L. Christ, P. B. Hostetler, and R. M. Siebert, "Stabilities of calcite and aragonite," *Jour. Res. USGS*, vol. 2, no. 2, pp. 175–184, 1974.

[95] H. Yang, S. Yang, J. Kong, A. Dong, and S. Yu, "Obtaining information about protein secondary structures in aqueous solution using fourier transform ir spectroscopy," *Nat. Protoc.*, vol. 10, no. 3, pp. 382–396, 2015.

[96] Kimmel Center for Archaeological Science (Weizmann Institute of Science), "Infrared standards library," 2021. `https://centers.weizmann.ac.il/kimmel-arch/infrared-spectra-library`. (Accessed on 28 June 2024).

[97] P. Forjanes, M. S. Roda, M. Greiner, E. Griesshaber, N. A. Lagos, S. Veintemillas-Verdaguer, J. M. Astilleros, L. Fernández-Díaz, and W. W. Schmahl, "Long-term experimental diagenesis of aragonitic biocarbonates: From organic matter loss to abiogenic calcite formation," *Biogeosciences*, vol. 2021, pp. 1–53, 2021.

[98] K. E. Chave, "A solid solution between calcite and dolomite," *J. Geol.*, vol. 60, no. 2, pp. 190–192, 1952.

[99] L. E. Wasylenki, P. M. Dove, D. S. Wilson, and J. J. De Yoreo, "Nanoscale effects of strontium on calcite growth: An in situ AFM study in the absence of vital effects," *Geochim. Cosmochim. Ac.*, vol. 69, p. 3017–3027, 2005.

[100] J. Astilleros, L. Fernández-Díaz, and A. Putnis, "The role of magnesium in the growth of calcite: An AFM study," *Chem. Geo.*, vol. 271, p. 52–58, 2010.

[101] M. S. Hashim and S. E. Kaczmarek, "The transformation of aragonite to calcite in the presence of magnesium: Implications for marine diagenesis," *Earth Planet. Sci. Lett.*, vol. 574, p. 117166, 2021.

[102] J. V. Mills, H. A. Barnhart, D. J. DePaolo, and L. N. Lammers, "New insights into Mn^{2+} and Mg^{2+} inhibition of calcite growth," *Geochim. Cosmochim. Ac.*, vol. 334, pp. 338–367, 2022.

[103] L. M. Walter and J. W. Morse, "The dissolution kinetics of shallow marine carbonates in seawater: A laboratory study," *Geochim. Cosmochim. Ac.*, vol. 49, pp. 1503–1513, 1985.

[104] J. Astilleros, C. Pina, L. Fernández-Díaz, and A. Putnis, "Metastable phenomena on calcite 101-4 surfaces growing from Sr^{2+}–Ca^{2+}–CO_3^{2+} aqueous solutions," *Chem. Geo.*, vol. 193, p. 93–107, 2003.

[105] I. M. Weiss, N. Tuross, L. Addadi, and S. Weiner, "Mollusc larval shell formation: amorphous calcium carbonate is a precursor phase for aragonite," *J. Exp. Zool.*, vol. 293, no. 5, pp. 478–491, 2002.

[106] J. Huang, C. Liu, L. Xie, and R. Zhang, "Amorphous calcium carbonate: a precursor phase for aragonite in shell disease of the pearl oyster," *Biochem. Bioph. Res. Co.*, vol. 497, no. 1, pp. 102–107, 2018.

[107] T. A. Grünewald, S. Checchia, H. Dicko, G. Le Moullac, M. Sham Koua, J. Vidal-Dupiol, J. Duboisset, J. Nouet, O. Grauby, M. Di Michiel, *et al.*, "Structure of an amorphous calcium carbonate phase involved in the formation of *Pinctada margaritifera* shells," *Proc. Natl. Acad. Sci.*, vol. 119, no. 45, p. e2212616119, 2022.

[108] S. C. Fitzer, P. Chung, F. Maccherozzi, S. S. Dhesi, N. A. Kamenos, V. R. Phoenix, and M. Cusack, "Biomineral shell formation under ocean acidification: a shift from order to chaos," *Sci. Rep.*, vol. 6, no. 1, p. 21076, 2016.

[109] K. Ramesh, M. Y. Hu, J. Thomsen, M. Bleich, and F. Melzner, "Mussel larvae modify calcifying fluid carbonate chemistry to promote calcification," *Nat. Commun.*, vol. 8, no. 1, p. 1709, 2017.

[110] R. A. Simmer, E. J. Jansen, K. J. Patterson, and J. L. Schnoor, "Climate change and the sea: A major disruption in steady state and the master variables," *ACS Environ. Au.*, vol. 3, pp. 195–208, 2023.

[111] G. Castellan, L. Angeletti, S. Canese, C. Mazzoli, P. Montagna, S. Schiaparelli, and M. Taviani, "Visual imaging of benthic carbonate-mixed factories in the ross sea region marine protected area, antarctica," *Minerals*, vol. 11, no. 8, 2021.

[112] E. Hadjittofis, S. M. Vargas, J. D. Litster, and K. L. Sedransk Campbell, "The role of surface energy in the apparent solubility of two different calcite crystal habits," *Proc. R. Soc. A*, vol. 477, p. 20210200, 2021.

[113] A. Massit, A. El Yacoubi, A. Kholtei, and B. C. El Idrissi, "Xrd and ftir analysis of magnesium substituted tricalcium calcium phosphate using a wet precipitation method," *Biointerface Res. Appl. Chem*, vol. 11, pp. 8034–8042, 2021.

[114] O. B. A. Agbaje, I. B. Shir, D. B. Zax, A. Schmidt, and D. E. Jacob, "Biomacromolecules within bivalve shells: Is chitin abundant?," *Acta Biomater.*, vol. 80, pp. 176–187, 2018.

[115] M. E. Böttcher, P. Gehlken, and D. F. Steele, "Characterization of inorganic and biogenic magnesian calcites by fourier transform infrared spectroscopy," *Solid State Ionics*, vol. 101, pp. 1379–1385, 1997.

[116] D. T. Hopkins, S. MacQuarrie, and K. A. Hawboldt, "Removal of copper from sulfate solutions using biochar derived from crab processing by-product," *J. Environ. Manage.*, vol. 303, p. 114270, 2022.

[117] B. Marie, I. Zanella-Cléon, N. Guichard, M. Becchi, and F. Marin, "Novel proteins from the calcifying shell matrix of the pacific oyster crassostrea gigas," *Mar. Biotechnol.*, vol. 13, pp. 1159–1168, 2011.

[118] T. Hong, J. Yin, S. Nie, and M. Xie, "Applications of infrared spectroscopy in polysaccharide structural analysis: Progress, challenge and perspective," *Food Chem.*, vol. 12, p. 100168, 2021.

[119] C. Rey, O. Marsan, C. Combes, C. Drouet, D. Grossin, and S. Sarda, *Characterization of Calcium Phosphates Using Vibrational Spectroscopies*, pp. 229–266. Berlin, Heidelberg: Springer Berlin Heidelberg, 2014.

[120] M. Kaya, M. Mujtaba, H. Ehrlich, A. M. Salaberria, T. Baran, C. T. Amemiya, R. Galli, L. Akyuz, I. Sargin, and J. Labidi, "On chemistry of γ-chitin," *Carbohyd. Polym.*, vol. 176, pp. 177–186, 2017.

[121] J. Paquette and R. J. Reeder, "Single-crystal x-ray structure refinements of two biogenic magnesian calcite crystals," *Am. Mineral.*, vol. 75, no. 9-10, pp. 1151–1158, 1990.

[122] S. M. Antao and I. Hassan, "Temperature dependence of the structural parameters in the transformation of aragonite to calcite, as determined from in situ synchrotron powder x-ray-diffraction data," *Canad. Mineral.*, vol. 48, no. 5, pp. 1225–1236, 2010.

[123] D. Wardecki, R. Przeniosło, and M. Brunelli, "Internal pressure in annealed biogenic aragonite," *CrystEngComm*, vol. 10, no. 10, pp. 1450–1453, 2008.

[124] B. Gao, *Detection and control of calcium carbonate formation and phase conversion: laboratory and field work*. PhD thesis, Memorial University of Newfoundland, 2022.

[125] B. Udvardi, I. J. Kovács, T. Fancsik, P. Kónya, M. Bátori, F. Stercel, G. Falus, and Z. Szalai, "Effects of particle size on the attenuated total reflection spectrum of minerals," *Appl. Spectrosc.*, vol. 71, no. 6, pp. 1157–1168, 2017.

[126] A. Altomare, N. Corriero, C. Cuocci, A. Falcicchio, A. Moliterni, and R. Rizzi, "*QUALX2.0*: a qualitative phase analysis software using the freely available database POW COD," *J. Appl. Crystallogr.*, vol. 48, pp. 598–603, Apr 2015.

[127] T. Van de Flierdt, L. F. Robinson, and J. F. Adkins, "Deep-sea coral aragonite as a recorder for the neodymium isotopic composition of seawater," *Geochim. Cosmochim. Ac.*, vol. 74, no. 21, pp. 6014–6032, 2010.

[128] J. M. Alia, Y. D. De Mera, H. G. M. Edwards, P. G. Martín, and S. L. Andrés, "FT-Raman and infrared spectroscopic study of aragonite-strontianite ($Ca_xSr_{1-x}CO_3$) solid solution," *Spectrochim. Acta A*, vol. 53, no. 13, pp. 2347–2362, 1997.

[129] N. Asikin-Mijan, Y. Taufiq-Yap, and H. Lee, "Synthesis of clamshell derived $Ca(OH)_2$ nano-particles via simple surfactant-hydration treatment," *Chem. Eng. J.*, vol. 262, pp. 1043–1051, 2015.

[130] D. Cree and A. Rutter, "Sustainable bio-inspired limestone eggshell powder for potential industrialized applications," *ACS Sustain. Chem. Eng.*, vol. 3, no. 5, pp. 941–949, 2015.

[131] E. E. Schulte, B. G. Hopkins, and F. R. Magdoff, "Estimation of soil organic matter byweight loss-on-ignition. soil organic matter: Analysis and interpretation. madison, wi," in *Soil Sci. Soc. Am.*, no. 46, 1996.

[132] Y. Kitano and D. W. Hood, "Calcium carbonate crystal forms formed from sea water by inorganic processes," *J. Oceanogr. Soc. Japan*, vol. 18, no. 3, pp. 141–145, 1962.

[133] R. M. Pytkowicz, "Rates of inorganic calcium carbonate nucleation," *J. Geol.*, vol. 73, no. 1, pp. 196–199, 1965.

[134] D. Zhang, Q. Lin, N. Xue, P. Zhu, Z. Wang, W. Wang, Q. Ji, L. Dong, K. Yan, J. Wu, *et al.*, "The kinetics, thermodynamics and mineral crystallography of $CaCO_3$ precipitation by dissolved organic matter and salinity," *Sci. Total Environ.*, vol. 673, pp. 546–552, 2019.

[135] R. A. Berner, J. T. Westrich, R. Graber, J. Smith, and C. S. Martens, "Inhibition of aragonite precipitation from supersaturated seawater; a laboratory and field study," *Am. J. Sci.*, vol. 278, no. 6, pp. 816–837, 1978.

[136] J. W. Morse, "Dissolution kinetics of calcium carbonate in sea water; vi, the near-equilibrium dissolution kinetics of calcium carbonate-rich deep sea sediments," *Am. J. Sci.*, vol. 278, no. 3, pp. 344–353, 1978.

[137] T. A. Jackson and J. L. Bischoff, "The influence of amino acids on the kinetics of the recrystallization of aragonite to calcite," *J. Geol.*, vol. 79, no. 4, pp. 493–497, 1971.

[138] J. D. Naviaux, A. V. Subhas, S. Dong, N. E. Rollins, X. Liu, R. H. Byrne, W. M. Berelson, and J. F. Adkins, "Calcite dissolution rates in seawater: Lab vs. in-situ measurements and inhibition by organic matter," *Mar. Chem.*, vol. 215, p. 103684, 2019.

[139] J. de Kanel and J. W. Morse, "The chemistry of orthophosphate uptake from seawater on to calcite and aragonite," *Geochim. Cosmochim. Ac.*, vol. 42, no. 9, pp. 1335–1340, 1978.